Transport properties in electrically conductive polymeric materials

Edward Robert Holland

Transport Properties In Electrically Conductive Polymeric Materials

by

Edward Robert Holland

A thesis submitted to the faculty of science,

Durham University for the degree of Ph.D.

Department of Physics
University of Durham
November 1995

Abstract

Measurements on free standing films of the conductive polymer polyaniline (PANi) have revealed that charge transport within this material depends upon the level of intermolecular order. This factor is found to depend upon the method of sample preparation. PANi protonated by immersion of solid emeraldine base in aqueous methane sulphonic acid has low conductivity, 30-40 Scm^{-1}. This can be enhanced, up to 250 Scm^{-1}, if films are stretch oriented prior to protonation. Stretched samples have an electrical conductivity anisotropy factor of order 7 at 300 K, also revealed in their thermopower over the range 100 - 300 K. The behaviour of electrical conductivity with temperature is commensurate with charge transport in a disordered system. Protonation of PANi dissolved in meta cresol by addition of camphor sulphonic acid (CSA) yields material with conductivity of 250-300 Scm^{-1}. Variation of the acid concentration has revealed a transition to a metallic response in conductivity (near 300 K) when 20-30% of polymer nitrogen sites are protonated. This character extends to progressively lower temperatures as protonation is increased to 60%. The metallic nature of this material is evident in the linear temperature dependence of thermopower and is ascribed to the presence of crystalline regions within the polymer film, as revealed by an independent x-ray analysis

The role of molecular order upon the properties of thin films of 3[2(S2-methylbutoxy)ethyl]-polythiophene has been investigated. Starting with polymer dissolved in 'good' solvent, quantities of nonsolvent lead to reorganisation of the sidechain groups when added. This promotes an increase in effective conjugation length which can be transferred to the solid state by the spin coating process as indicated by spectroscopic studies. With these films acting as the active layer in a field effect transistor the charge carrier mobility can be measured. It is found that as molecular order increases, mobility decreases from 10^{-5} $cm^2V^{-1}s^{-1}$ to 710^{-8} $cm^2V^{-1}s^{-1}$. This is ascribed to increased interchain separation and effects due to macroscopic aggregate grain boundaries.

Declaration

The material in this thesis has not been submitted for examination for any other degree, or part thereof at the University of Durham or any other institution. The material in this thesis is the work of the author except where formally acknowledged by reference.

Acknowledgements

In the three year period as a research student at Durham I have been fortunate to have the support of academic and technical staff alike. I should therefore like to thank the following people for their invaluable help.

My supervisor, Dr. A.P. Monkman, for answering my many questions, and for providing a constant source of encouragement when things got really bad, and for tolerating some very poor jokes.

Phil Adams and Paul Laughlin for their constant efforts to supply countless samples for my experiments.

All the physics department technical staff and the mechanical and electronics workshop staff for their advice and help in operating, designing (and repairing) numerous gadgets.

Thanks are also due to Dr. D.M. de Leeuw, my industrial supervisor, to Philips Research Laboratories for their contribution to my C.A.S.E sponsorship award and to the EPSRC for the funding of my research.

Finally I should like to thank my parents for their unerring support of all my endeavours.

"Soldier Freddy

Was never ready,

But Soldier Neddy,

Unlike Freddy,

Was always ready,

and steady,

Thats why,

When Soldier Neddy

Is outside-Buckingham Palace-on-guard-in-the-

pouring-wind-and-rain-

being-steady-and-ready

Freddy-

is home in beddy"

Spike Milligan.

Contents

List Of Figures

List Of Figures (continued)

List Of Tables

Preface

Electrically conductive polymers have become an area of intense research activity. These materials hold some considerable promise for future applications as a versatile group of new electronic materials. The findings and conclusions presented in this thesis are based on research into the fundamental electrical properties of two particular polymeric systems; polyaniline and a substituted polythiophene.

The first chapter of this volume includes a review of some principles and theories which detail the important aspects of conjugated polymers, with regard to the electronic structure and bonding of the polymer chain. Particular attention is given to the emeraldine form of polyaniline (PANi) and its transition to conductive behaviour upon protonation with acid species. The synthesis and processing steps involved in the production of PANi-NMP and PANi-CSA, in the form of conductive, free standing films are described.

Chapter two contains a review of the electrical transport mechanisms within disordered and non crystalline materials, with reference to the typical behaviour observed in polymer species such as polyaniline and polyacetylene. The minimum metallic criterion and the factors that contribute to charge carrier localisation in a disordered system are considered. The charge transport mechanisms which ensue in a disordered conductor are then discussed, e.g. variable range hopping and fluctuation induced tunnelling. Also included in this chapter is a description of the origin of thermoelectricity in metallic conductors, and also disordered conductors in which the conduction band electronic states are localised. Finally, attention is given to the heterogeneous conductor model which is frequently used to explain the electrical transport properties in conductive polymers

The results obtained from measurements of the conductivity and thermopower of PANi (in both the NMP and CSA forms) are presented and discussed in chapters three and four, along with details of the experimental apparatus and techniques employed. It is known that the electrical properties of PANi are affected by the method of sample

preparation. Control of the level of doping of PANi-CSA reveals the onset and progression of a metallic response in the temperature dependence of the electrical conductivity which is supported by the evidence from thermopower measurements.

PANi-NMP is found to be characteristic of a disordered conductor in which charge carriers are localised at some microscopic level. No metallic response is observed in the conductivity, although it is suggested by the thermopower behaviour observed along the axis of maximum conductivity, in stretch oriented samples.

In chapter five the role of order in conductive materials is highlighted again, with respect to the application of polymers in electronic devices. Spin cast films of a conjugated polymer 3[2(S2-methylbutoxy)ethyl]-polythiophene were incorporated within the active layer of a field effect transistor, allowing the mobility of charge carriers within the polymer to be studied. Treatment of the spin casting solution with a nonsolvent was found to increase the intramolecular order and thus the effective length of conjugation in the polymer chains. Spectroscopic analysis revealed that this order was preserved in thin films of the polymer spun from solvent-polymer-nonsolvent mixtures. A reduction in charge carrier mobility was observed within films spun from solutions treated with nonsolvent, compared to films spun from pure polymer-solvent mixtures. This is ascribed in part to increased interchain separation and also to the presence of grain boundaries between macroscopic aggregates.

Chapter 6 includes a summary of the findings and conclusions presented in previous sections and also contains some suggestions for the direction of future research.

CHAPTER 1

Introduction To Conductive Polymers

1.1 History

In the last twenty years there has been a great interest in the field of electroactive organic materials. In particular, the study of conjugated polymers has become an important branch of solid state physics. An early breakthrough was the discovery that treatment of polyacetylene with oxidative species, e.g. iodine, resulted in a transition to conductive behaviour, e.g. Berets and Smith [1]. An improvement, in the chemical synthesis of polyacetylene was made by Shirakawa in the early 1970's [2] and the material was later shown to undergo transition to high conductivity upon oxidative doping [3]. The result was that the electrical conductivity could be increased by up to 11 orders of magnitude to reveal almost metallic behaviour. Since this discovery, other conductive polymeric species have been synthesised and materials including polypyrrole, polythiophene, polyparaphenylene and polyanilines are now the subject of intensive studies.

Interest in the family of conductive polymers has arisen for two main reasons. Firstly, from a purely physical point of view, the majority of charge transport in a polymer is believed to be along the body or backbone of the polymer chain and of quasi - 1 - dimensional nature. However, carrier transfer between the chains must also have a part to play in the bulk properties of such a conductor. The exact mechanisms behind such electrical transport are not yet clearly understood.

Secondly, once synthesised, polymers are easier to process than inorganic conductors and semiconductors. They can be cast or spun from solution as thin films directly where they are required, without the need for high temperature processing. This has led the way to research into the use of the conductive polymers as the active material in devices such as thin film transistors [4,5] and light emitting diodes [6].

1.2 Polyacetylene

Polyacetylene has the simplest chemical form of the conjugated conductive polymers and has served as a starting point for most of the theoretical models developed for the wider family of materials.

The structure of trans-polyacetylene, see fig. 1.1, is shown pictorially as a conjugated arrangement of carbon atoms i.e. a chain of alternate single and double bonds, with one atom of hydrogen bonded to each carbon atom. A simple picture of the electronic structure within this system can be constructed if the arrangement of the chemical bonding is examined in more detail.

Each carbon atom possesses four valence electrons which are contained in so called bonding orbitals. Three of the electrons reside in sp^2 hybridised orbitals and form covalent or σ bonds with two adjacent carbon atoms and with one hydrogen atom. Such bonds are strong, i.e. a great deal of energy is required to excite the electrons in a σ orbital to a non bonding state and as a result these valence electrons remain localised. The fourth valence is contained in a p_z orbital which extends above and below the line of the polymer chain, perpendicular to the σ bonds. The p_z orbitals from adjacent carbon atoms overlap to form a π bonding orbital which extends above and below the entire length of the bond. The electrons contained in this orbital are not localised between particular atoms, as in the case of the σ bonding electrons, but are delocalised throughout the π orbital system. It is this delocalisation of electron states in the π system which gives conjugated polymers the possibility to exhibit electrically conductive behaviour.

Early theoretical models for polyacetylene predicted that its properties should tend from semiconducting to metallic as the chain length is increased. It was reasoned that each additional carbon atom would contribute a new state in both the π (ground state) and π^* (first excited state) molecular bands, as a result of the mixing of the new wave function with the system. This is the behaviour predicted by an application of the theory of the linear combination of atomic orbitals (LCAO) to a chain with

trans-polyacaetylene

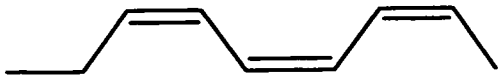

cis- polyacetylene

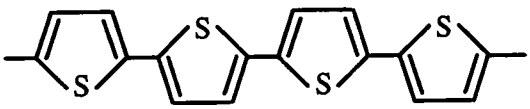

polythiophene

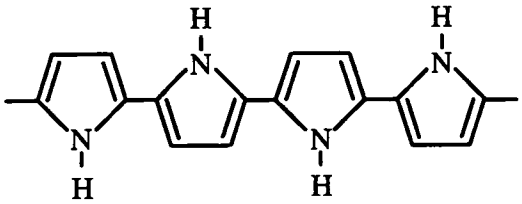

polypyrrole

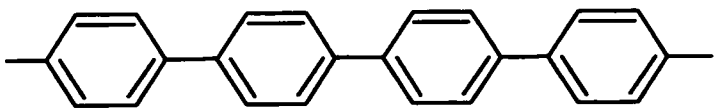

polyparaphenylene

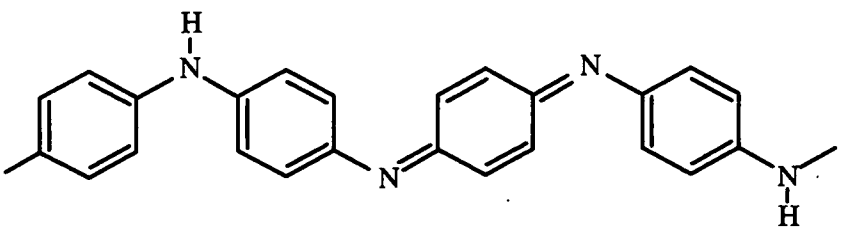

polyaniline, emeraldine base

Fig. 1.1 Chemical structures of some conductive polymers, ignoring C-H bonds.

all carbon-carbon bond lengths of equal size. The addition of these new states would then act to reduce the band gap of the π to π^* transition between the two degenerate energy levels. In the limit for this system, as the number of carbon atoms, n, tends to infinity the additional states would eventually fill the energy gap. Each carbon atom donates 1 electron per site and since from the Pauli exclusion principle, each site can be occupied by two electrons with opposite spins, the result would be a material with a half filled continuum band containing delocalised electrons, which should exhibit metallic characteristics.

However, polyacetylene is intrinsically semiconducting and can only be rendered conductive upon doping with electron withdrawing or electron donating species, even for long chain lengths [3]. Studies of the progression of the π to π^* bandgap energy as a function of the length of the conjugated chain in polyenes has revealed that it tends to a minimum energy around 1.4 eV for long chains, not to zero as first predicted by much earlier measurements on short chain conjugated species [7].

1.3 The Su, Schrieffer, Heeger Model

The shortcomings in the early model for polyacetylene, which a predicts metallic, rather than semiconductive band structure were tackled by Su, Schrieffer and Heeger [8]. In this approach (the SSH model) a Hamiltonian is constructed which consists of two parts, H_σ and H_π, to account for contributions to the total system energy from the σ and π bonding electrons respectively [9].

H_σ is written as:

$$H_\sigma = (K_0 / 2) \sum_n (u_{n+1} + u_n)^2 \qquad \text{eqn. 1.1}$$

Where u_n represents the displacement of the n^{th} atom from equilibrium and K_0 is the lattice force constant. This term describes the elastic potential energy of the lattice (chain) as a function of the relative displacement of adjacent carbon atoms. If we assume

that the carbon atoms are equally spaced, with bond length a, and a bond angle of 120° then the separation of atoms along the chain is $2a/\sqrt{3}$.

The second part of the Hamiltonian, H_{π}, contains the tight binding energy description for the π electrons:

$$H_{\pi} = -\sum_{n,s} t_{n,n+1}(c^{+}_{n,s}c_{n+1,s} + c^{+}_{n+1,s}c_{n,s}) \qquad \text{eqn. 1.2}$$

Where $c^{+}_{n,s}$ and $c_{n,s}$ are creation and annihilation operators for π electrons with spin s ($\pm$ 1/2) at carbon atom site, n. $t_{n,n+1}$ is the transfer integral and is a function of the carbon-carbon bond length. It is expanded linearly about the equilibrium C-C spacing to give:

$$t_{n,n+1} = t_0 - \alpha(u_{n+1} - u_n) \qquad \text{eqn. 1.3}$$

Where α is a coupling constant which links the process of electron transfer between carbon sites to displacements of those sites, in effect an electron - phonon coupling constant for π electrons, $t_{n,n+1}$ is then a representation of the π wave function overlap between adjacent carbon atoms. It becomes larger if the two atoms are moved closer together and smaller if the separation is increased.

For the case where all carbon-carbon bond lengths are chosen to be equal, i.e. u_n=0 for all n the model predicts a tight binding band with the dispersion relation:

$$E_k = -2t_0 \cos ka \qquad \text{eqn. 1.4}$$

This is then the continuous π band first predicted for polyacetylene. It has bandwidth of $4t_0$ and with each carbon atom contributing 1 electron it is half filled, thus constituting a 1-dimensional metallic system.

It is well known, however that polyacetylene displays an alternation in the bond length between the carbon atoms in the chain backbone, commensurate with the single bond - double bond picture in fig. 1.1. The distortion, or dimerisation of polyacetylene

into an alternating bond structure can be likened to the case of a 1-dimensional metal which has undergone a Peierls distortion [10,11].

Peierls showed that a 1-dimensional metal can achieve a lower system energy via distortion of the lattice. As a consequence of this distortion, a gap opens in the band structure at the Fermi level separating the occupied and empty states, see fig. 1.2. This state is more stable since the energy of the occupied states is reduced by the presence of the gap.

For polyacetylene, distortion of the chain as a result of dimerisation is equivalent to the system undergoing a Peierls distortion. The finite band gap then arises naturally as a consequence of this transition. The Hamiltonians used in the SSH model can be used to model the distorted system, with displacement of the carbon sites given by:

$$u_n = (-1)^n u_o \qquad \text{eqn. 1.5}$$

The result is a band structure with the dispersion relation:

$$E_k = (4t_0^2 \cos^2 ka + 4\alpha^2 u_0^2 \sin^2 ka)^{1/2} \qquad \text{eqn. 1.6}$$

This expression reveals a gap in the band structure for $\mathbf{k}=\pi/2\mathbf{a}$ which separates unoccupied and occupied states by an energy: $E_g = 8\alpha u_0$. The density of electronic states N(E) as a function of energy can be found using the tight binding model:

$$N(E) = \frac{N/\pi}{\left(4t^2 - (E - E_0)^2\right)^{1/2}} \qquad \text{eqn. 1.7}$$

In simple terms, the distorted system is more stable because the decrease in energy of the π electron system as a result of opening the bandgap at E_F is greater than the increase in potential energy driving the lattice distortion. Hence the system a whole can exist at a lower total energy by assuming a structure of alternating bonds. The energy gain per carbon atom as a function of the degree of distortion u, can be shown to follow the relation:

$$E(u) = 2k_0 u^2 - u^2 \ln(t_o / \alpha u_0) \qquad \text{eqn. 1.8}$$

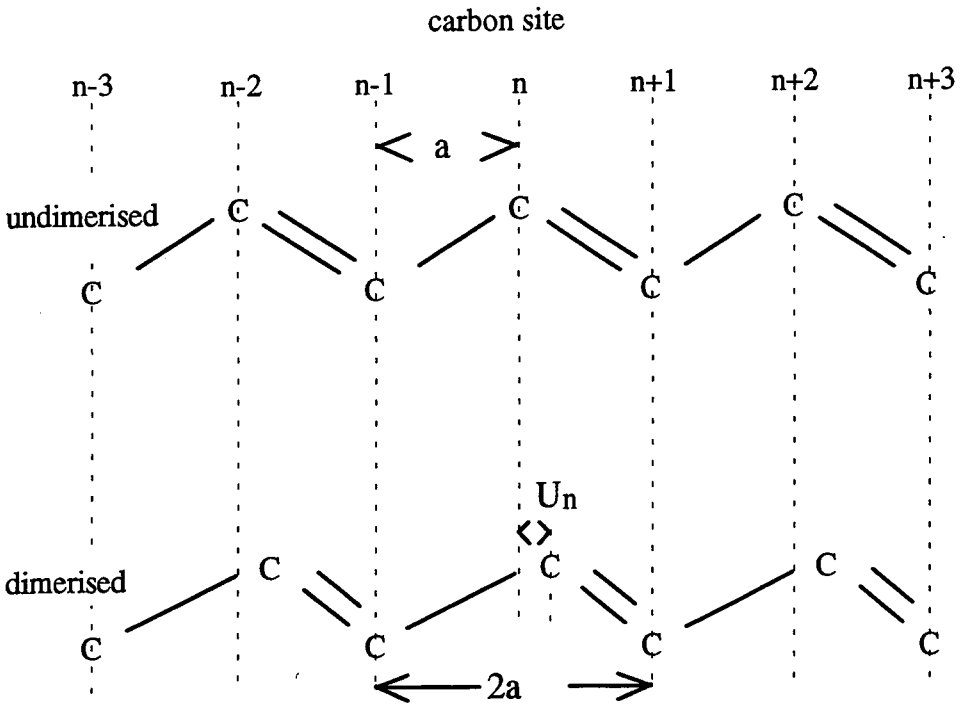

Fig. 1.2 The Peierls transition in polyactylene; dimerisation of the structure resulting from the unequal lengths of single and double bonds.

where the first term represents elastic potential energy increase due to distortion and the second the energy decrease in the π electron system. This expression has minima for $u = \pm u_0$.

The result is a model of polyacetylene with a filled π (valence) and empty π^* (conduction) bands separated by an energy gap E_g. This picture fits the experimental data, the existence of the bandgap is well known from optical studies and the very low intrinsic conductivity of polyacetylene is exactly what would be expected from a system with filled valence and empty conduction bands. High conductivity can thus only be achieved through altering the filling in these bands, by chemical doping to add or remove electrons to or from the polymer chain backbone. Improvements have been made in the synthesis of polyacetylene to increase chain length and purity such that examples capable of displaying conductivity of metallic magnitude upon doping are documented [12,13].

1.4 Bond Defects

Because it is the simplest of the conjugated polymers, polyacetylene has been widely used in the development of a great deal of the theory applied to conductive polymers in general. For example, all conjugated polymers are intrinsically semiconducting in that they exhibit some band gap which separates so called valence and conduction band electronic states. Also, like polyacetylene these materials only become conductive upon doping with an oxidative or reductive species to liberate some form of charge carrier which has a finite mobility on the polymer chain.

The important differences between polyacetylene and most of the more complex materials arise, unsurprisingly, from structural differences that, in turn, affect the way that charge carrying electronic states are accommodated into the π electron system. To develop a picture of how charge carriers exist within the conjugated system it is useful to look again at polyacetylene.

Consider the dimerised structure of polyacetylene, with alternating single and double backbone bonding. Clearly the distortion can occur in two resonance forms or

phases as illustrated in fig. 1.3(a) and 1.3(b) where the bond alternation runs in opposite senses. The energy gain for this dimerisation into phases A and B is equal since the forms are just equivalent to the two energy minima solutions ($u = \pm u_0$) given previously for equation 1.8. Hence these two phases are said to be degenerate. But, what would be the consequence if a chain was formed that contained both A and B forms?

This case is shown pictorially in fig. 1.3(c), where the change in the bond alternation pattern is at the centre of the chain. The separation of A and B phases forces a bond mismatch leaving one carbon atom unable to form a π bond with either of its neighbours. The defect thus has an associated spin, s $\pm 1/2$, as a result of the lone electron in the carbon $\mathbf{p}_z$ orbital, although no net charge is associated with the defect. A bond alternation defect of this type is called a soliton, partly as a result of its particle-like properties and because of its non dispersive nature i.e. a single defect of this type is trapped on the chain. The soliton is free to move in either direction on the chain and will convert successive regions of the polymer to either the A or B phase with no cost in energy (the two phases are degenerate)

The picture in fig. 1.3(c) which represents the soliton as a definite, localised entity separating the two dimerization phases is oversimplified, however, since it does not take into account the Heisenberg principle which links the uncertainty of position and momentum of a particle.

Rice [14] and Su, Schrieffer and Heeger [15] suggested a wave function for solitons, at site n in the chain, of the form:

$$\phi_n = u_0 \tanh\left(\frac{na}{\xi}\right) \qquad \text{eqn. 1.9}$$

Where a is the repeat unit length of the dimerised chain lattice and ξ is a variational parameter that represents the length scale over which the soliton extends. Numerical calculations to minimise energy with respect to ξ give an optimum of: $\xi \approx 7a$. Hence the soliton is really a region in which a gradual switch over of phases takes place, with a length of order 7a corresponding to an influence over some 14 carbon atoms.

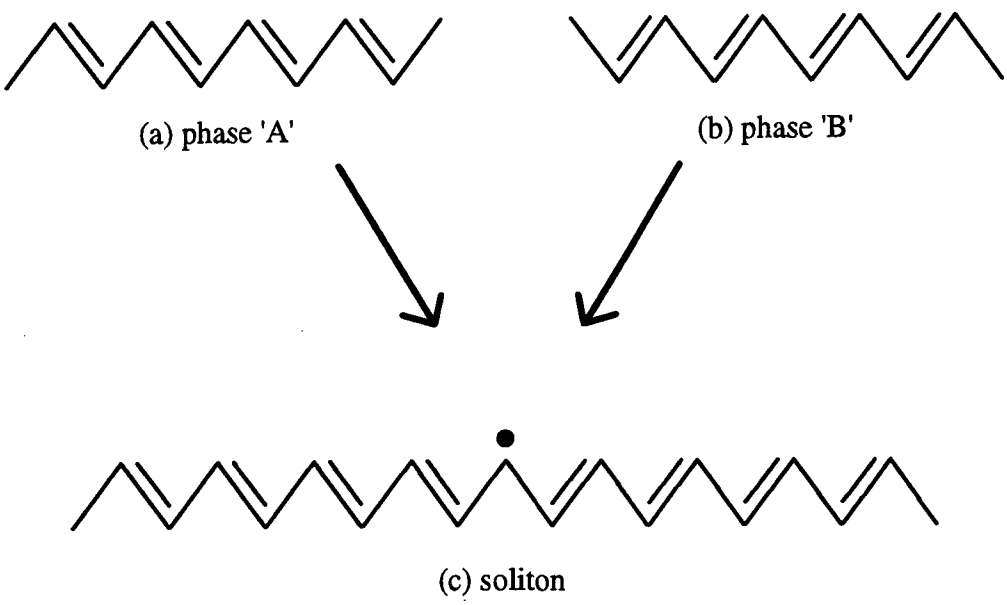

Fig. 1.3 Structural representation of a bond alternation defect (soliton) in polyacetylene, the dot represents an unpaired electron.

The distortion of the system around the soliton also results in a modification of the electronic structure. Creation of a soliton induces the creation of an electronic state halfway between the top of the valence (π) and bottom of the conduction (π^*) band. The lone electron associated with the bond mismatch is accommodated at this new energy level. The creation of the state at mid gap allows the lone electron to reside at an energy lower than a state in the conduction band. This mid gap state is, however, localised to the bond alternation lattice distortion, or soliton defect.

If this lone electron is removed or another added, by oxidation or reduction, it is clear that the soliton state can have three combinations of charge and spin as per fig. 1.4. These are:

1. Neutral soliton, S^0, as described above, which has zero charge and spin, S $\pm 1/2$ contributed by the lone electron in the mid gap state.

2. Negatively charged soliton S^- with two electrons occupying the mid gap state, hence possessing zero net spin.

3. Positively charged soliton S^+ with no electron at mid gap and thus no spin

The soliton then describes how charges may exist on the chain of polyacetylene after doping. Such charges are highly localised, being bound to the lattice distortion i.e. a situation analogous to strong electron-phonon coupling in conventional inorganic semiconductors.

In the process of doping (oxidative or reductive) of polyacetylene it can be shown that it is energetically favourable to create charged soliton states as opposed to removing or adding electrons from the conduction or valence bands respectively. It is this fact which outlines the major difference between organic and inorganic conductors.

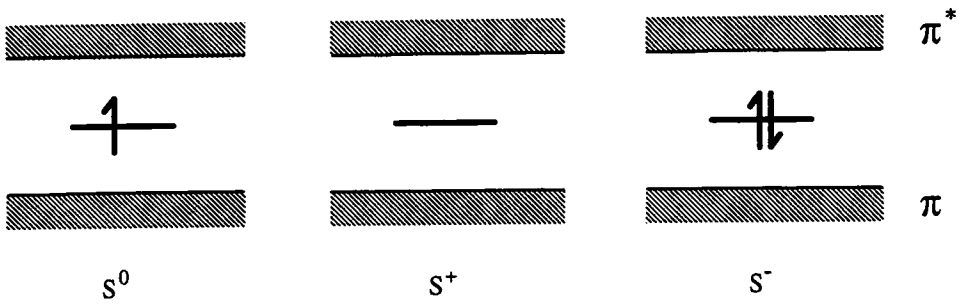

Fig. 1.4 Energy level diagrams for the three possible charge and spin combinations of the soliton state.

Of course, the presence of a few positive or negatively charged solitons cannot in itself give rise to electrically conductive, metallic behaviour since neither of the charged soliton species would give rise to a partially filled band structure with an appreciable density of states at the Fermi level. The solitons are also localised individual states. If the level of doping is increased, however, the density of charged solitons will reach a point where the mean distance between these defects is comparable with their length scale, ξ. This transition should occur when around 6% of the carbon sites are doped, if $\xi \approx 7a$. At this point the chain ceases to be a lattice of A and B phases separated by discrete charged soliton defects. Instead the lattice is considered to have a homogeneous displacement pattern in which interaction between soliton mid gap states gives rise to a band of delocalised states between the main conduction and valence bands, which extends along the chain backbone.

The soliton band is still only completely filled (negative soliton lattice) or empty (positive soliton lattice) and therefore metallic conductive behaviour, which is observed experimentally, would not be expected. To explain the observed conductive behaviour of doped polyacetylene requires a consideration of the effect of pinning of lattice defects by the charge of the electron donating or withdrawing species i.e. the dopant counterion. The description given here is only intended as a brief outline and the reader is referred to the paper of Rice and Mele [16] for a detailed explanation.

This model predicts a perturbation of the system as a results of defect pinning by charged species in proximity to the chain backbone of doped polyacetylene. This causes an extension of band tails into the valence-soliton and soliton-conduction band gaps. In this way it is possible to have a significant density of states at the Fermi level, so permitting metallic characteristics.

1.5 Polarons And Bipolarons

In polyacetylene then, charged solitons are formed as electrons are added to or removed from the polymer chain during doping. These entities are really a region of lattice distortion, with associated charge) 1, that separate two degenerate dimerisation phases of the chain system.

Consider a polymer with non-degenerate A and B phases e.g. Polyparaphenylene (PPP) as shown in fig. 1.5 (a)&(b). Here, the benzenoid (A) form is considered to be of lower energy than the quinoid (B) form. A single soliton defect cannot exist in this situation since it would separate two phases of unequal energy. Because a soliton is mobile it would be unstable to a shift in site position that would reduce the length of the higher energy quinoid form until the whole chain relaxed to the lower energy of the benzenoid structure.

Any bond alternation defect arising from the addition or removal of electrons to or from the polymer must therefore be configured in such a way that the chain returns to the same phase on either side of that defect. A defect of this type is termed a polaron and can be regarded as a bound pair of one charged and one neutral soliton. For PPP this is expected to take some form similar to that of fig. 1.5(b), in which a positively charged polaron has been formed as the result of removal of an electron from the chain [9].

The creation of a polaron, as for the soliton, causes a subtle change in the electronic band structure. In polyacetylene the formation of a polaron can be imagined when a neutral soliton approaches a charged soliton on the chain. At long separations i.e. greater than the soliton length scale, the two entities are discrete and the mid gap electronic states remain localised to the two specific sites. As the separation reduces to around one bond length, interaction of the two electronic states causes the mid gap state to split, leaving two new energy levels distributed symmetrically about the centre of the π–π^* band gap. The general form of the electronic structure characteristic of a positively charged polaron is shown in fig. 1.6(a). This singly charged defect has an associated spin ($\pm 1/2$) in contrast to the spinless nature of the charged soliton, S^+.

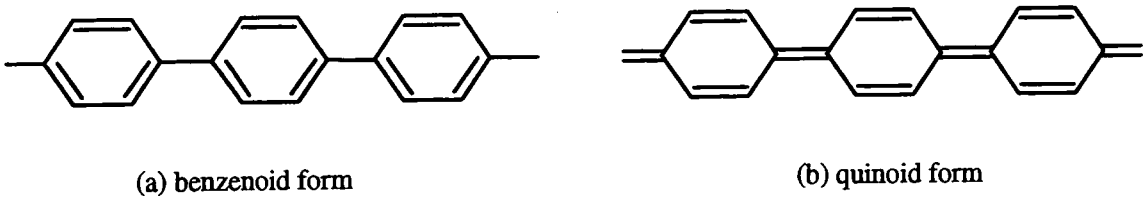

(a) benzenoid form

(b) quinoid form

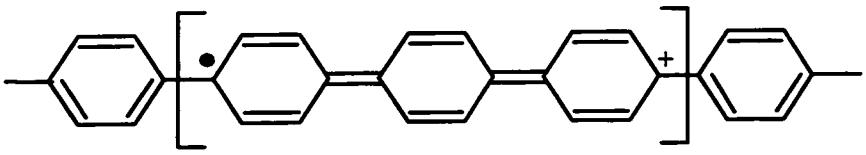

(c) polaron

Fig. 1.5 (a) and (b), the non degenerate conjugation phases of PPPand (c), charged polaron consisting of two bond defects.

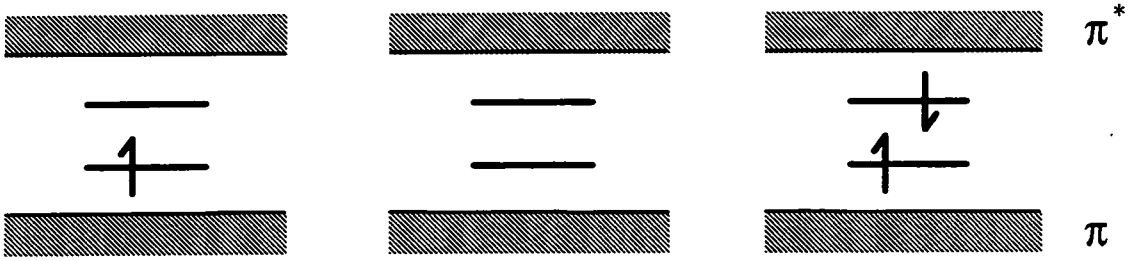

polaron, $\vec{B}^{+}$

bipolaron, $\vec{B}^{++}$

polaron-exiton

Fig. 1.6 Energy level diagram for three spin and charge configurations of the polaron.

This is contributed by a single unpaired electron which in simple terms, can be associated with the presence of the neutral soliton in the bound pair which forms the polaron [17]. Removal of the electron results in the formation of the doubly charged, spinless polaron or bipolaron, see fig 1.6(b).

Another way to view the polaron formation is to consider the possible energy schemes available for removal of an electron (ionisation) of, for example PPP. The Frank - Condon principle (which states that during an excitation, an electron is unable to change momentum) must apply during the ionisation process. Hence the electronic transitions are represented as vertical jumps in the energy diagram of fig. 1.7. In this diagram it can be seen that an effective lowering of the ionisation energy, E_{rel}, can be achieved if the structure is first distorted to the quinoid form. Hence the local distortion of the lattice provides a stable configuration for accommodation of a positive charge.

The formation of a bipolaron will take place if, when the unpaired electron is removed, further distortion of the lattice at the polaron site can produce an energy advantage greater than the reduction in electrostatic energy that would result from increasing the separation between the two positive charges. In polyacetylene bipolarons are expected to dissociate into two polarons as a consequence of the above energy consideration, whereas bipolarons are a favourable configuration in systems such as PPP and polypyrrole (PPy). Indeed, the very low Pauli paramagnetic susceptibility measured in both PPP and PPy at high doping concentrations would suggest the presence of spinless bipolarons and not polarons, which would contribute an appreciable concentration of unpaired spins.

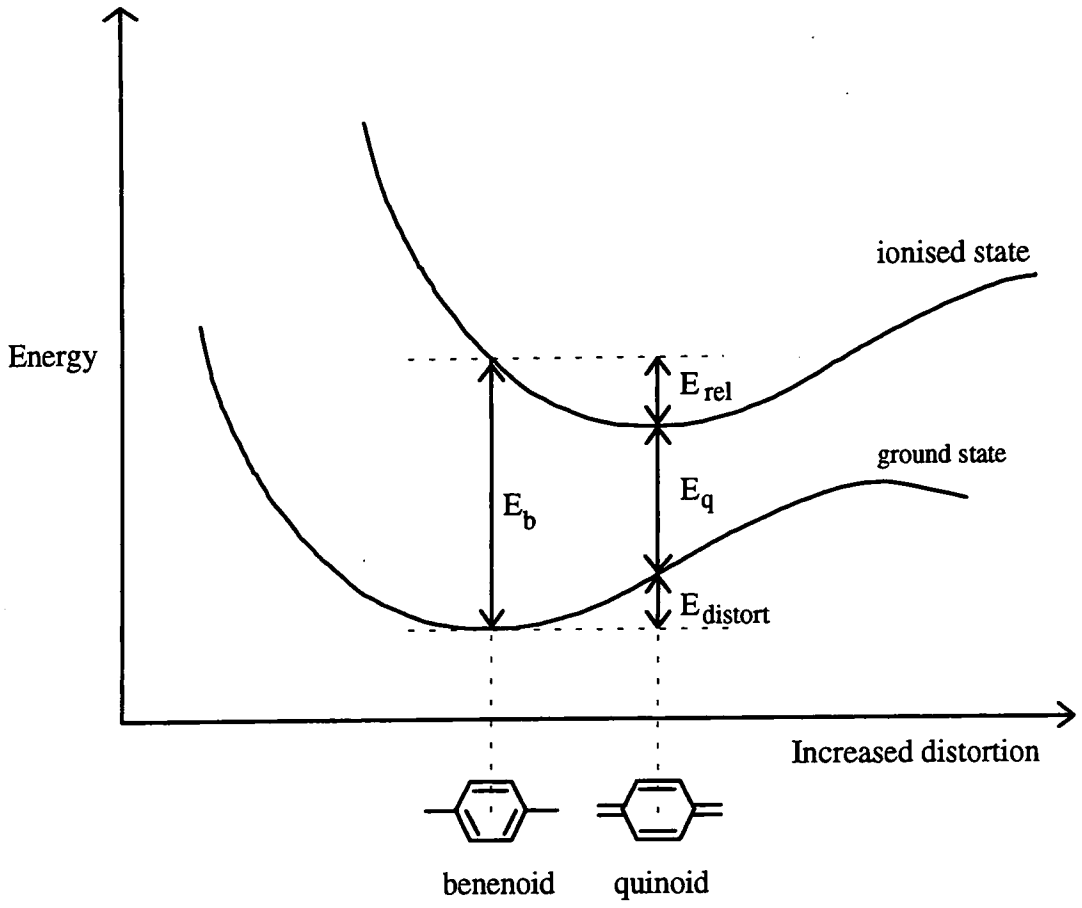

Fig. 1.7 Representation of the decrease in ionisation energy E_{rel} gained as a result of structural distortion in a non degenerate polymer e.g. PPP.

1.6 Polyaniline

Examples of polymers which contain heteroatoms are numerous and include materials such as polypyrrole (PPy), polythiophene (PT) and many other configurations incorporating elements of these structures. In these species atoms other than carbon are resident in the polymer chain. The sulphur and nitrogen atoms in PT and PPy are members of ring groups, hence the conjugation of carbon-carbon bonds is not broken in these structures.

The polyanilines are another family of heteroatomic polymers. Unlike the many thiophene and pyrrole variants, however, the nitrogen atoms in the polyaniline (PANi) structures occupy primary sites in the chain backbone. In these structures the heteroatom plays a key role in governing the properties of the system since there is no continuous carbon-carbon system. The name polyaniline applies in general to a group of three possible structures which were first synthesised in some form more than 100 years ago [18,19]. The three forms, shown in fig. 1.8, are regarded as different oxidation forms of a polymer [20], constructed from alternate benzene rings and nitrogen atoms. These, in increasing order of oxidation are:

1. Leucoemeraldine, fig. 1.8(a), the fully reduced form of the polymer which contains no quinoidimine units. This material is unstable to oxidation in air.

2. Emeraldine base, fig. 1.8(b), which has a mixture of benzenoid and quinoidimine groups. This form is stable in air and soluble in some polar solvents.

3. Pernigraniline, fig. 1.8(c), the fully oxidised form which is also conjugated to full extent. This structure is difficult to synthesise because of a susceptibility of the quinoid sites to hydrolysis.

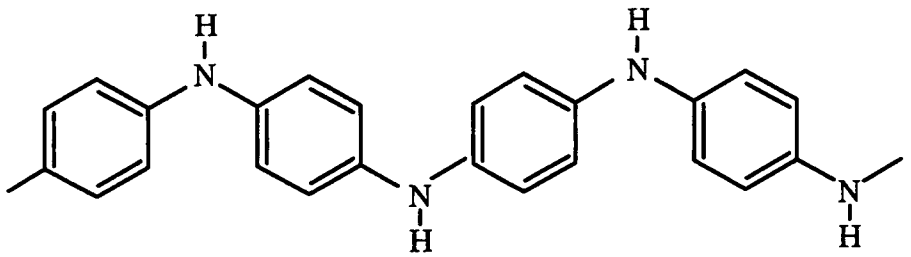

(a) leucoemeraldine base

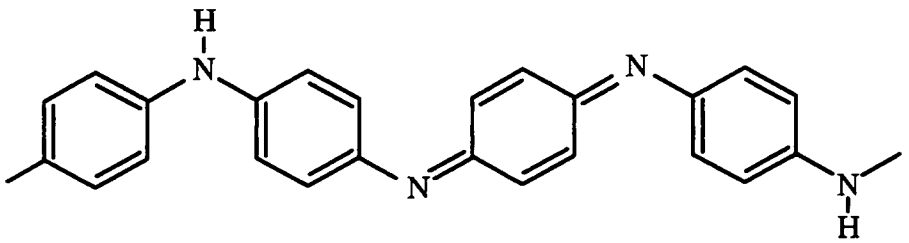

(b) emeraldine base

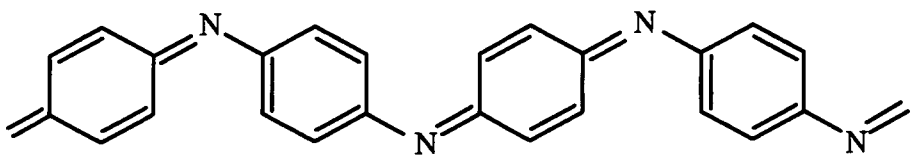

(c) pernigraniline base

Fig. 1.8 The polyaniline family

Although the intrinsic properties of the 3 oxidation states of PANi are those of electrical insulators, emeraldine base yields a salt form, PANi-ES upon treatment with acid of pH < 3. This protonation is accompanied by an increase in the electrical conductivity of the material by a factor in the region of 10^{11}. PANi-ES can be processed in the form of free standing films which have maximum conductivity in the range 200 to 400 Scm^{-1} as reported here (chapter 3) and elsewhere by other groups e.g.[21].

The degree of protonation can be controlled through variation of the pH of the acid, with lower pH values giving increased levels of protonation. It is widely accepted that the maximum doping level and hence the highest conductivity obtained occurs when half of the nitrogen sites on the chain are protonated. Treatment of PANi-ES with aqueous alkali causes de-protonation and the insulating emeraldine base form is recovered.

The transition to conductive behaviour observed upon acid doping is doubly intriguing. Firstly, the emeraldine base form of the polymer is not strictly conjugated i.e. alternation of single and double bonding does not extend along the full length of the polymer repeat unit, as it does in the pernigraniline structure. Secondly, the process of protonation does not alter the number of electrons on the chain c.f. oxidative doping of polyacetylene, polythiophene or polypyrrole. How then does PANi-ES fit in with the theories for the 'conventional' conjugated polymers discussed in previous sections?

To answer this question it is necessary to look at the effect on the system arising through protonation. In the doping process it is thought that protons attach themselves to the imine nitrogen atoms [20]. Therefore at full doping, both imine nitrogen atoms are protonated per repeat unit, in line with the theoretical maximum protonation (50% of the nitrogen atoms) mentioned above and the repeat unit might be expected to have the configuration shown in fig. 1.9(a). This is clearly a polymer chain with one bipolaron per repeat unit, contained in the quinoid structure. However, magnetic studies on well characterised PANi-ES [22] show that the material is strongly paramagnetic, in contradiction to the diamagnetic behaviour which would be expected of a lattice of spinless bipolarons.

The widely accepted view is that once the two imine sites have been protonated the bipolaron structure disproportionates into a polysemiquinone radical cation structure as per fig. 1.9(b) which has two separated polarons per repeat unit [23,24]. Alternative resonance forms of this structure are possible where the positive charges and spins reside on the other two nitrogen sites. With this configuration it is possible for significant delocalisation of charge and spin along the chain backbone.

Interaction of the polaron wave functions of neighbouring sites is predicted because polarons must have some spatial 'spread' similar to that described for soliton defects in section 1.4. Mixing of the polaron states then gives rise to a partially filled band of delocalised states [23]. This model of PANi-ES as a pseudo-one-dimensional lattice of interacting polaron states thus provides a possible explanation for the metallic properties which have been observed by experiment.

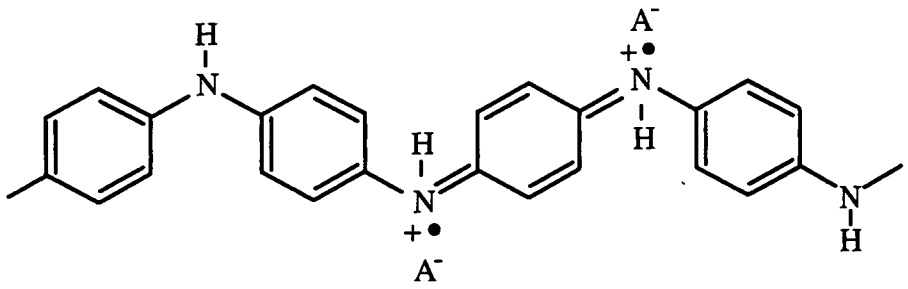

(a) bipolaronic structure in protonated emeraldine

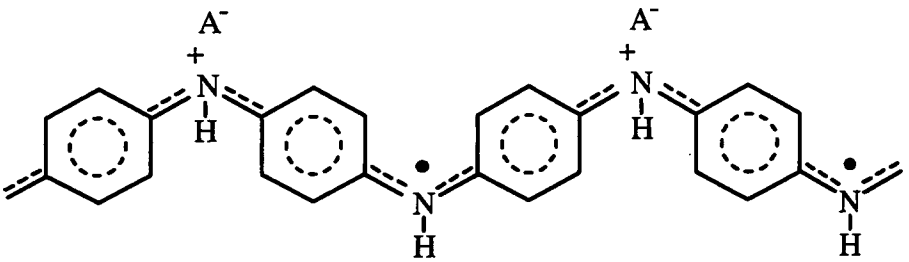

(b) polysemiquinone radical cation structure

(disproportionated bipolaron)

Fig. 1.9 Alternative arrangements for the structure of protonated emeraldine

1.7 Synthesis And Processing Of PANi

The experimental studies of the properties of PANi-ES presented later in this thesis were made using free standing films of the material. Synthesis and processing of the samples was performed 'in house' according to the following methods.

Emeraldine base polymer was synthesised chemically by oxidative coupling of aniline in acidic solution [25]. This process has been optimised by Dr P.N. Adams through careful choice of reaction temperature and oxidant to yield a material of high molecular weight, yet low concentration of impurities and chemical defects [26]. The high molecular weight of this material (typ > 100,000) as estimated by GPC analysis corresponds to polymer chains consisting of some 250 or more four ring repeat units. Emeraldine base is thus produced in the form of a blue-black powder which is moderately soluble in a limited number of organic solvents. Processing of this material into films of the highly conductive emeraldine salt is realised with either of two methods.

1. The NMP route: Emeraldine base is dissolved in N-methyl-2-pyrrolidinone(NMP) to a concentration of 5% by weight and homogenised to ensure complete dispersion of the polymer. The solution is centrifuged for 1 hour at 4000 rpm to force out any suspended particulates before it is poured onto the surface of glass slides at an approximate density of 0.05 gcm^{-2}. Evaporation of the solvent in a vacuum oven at approx. 60°C yields films with a dark coppery appearance of thickness ≈ 80 μm which can be peeled from the glass substrate. If desired the samples can at this stage be stretched to induce some uniaxial orientation of the polymer chains. This process involves the application of mechanical stress to the film under conditions of elevated temperature (typ 80 to 90°C). Finally protonation of the material to give the conductive form is performed by immersion of the film in aqueous methane sulphonic acid at a concentration of 15% by volume, for a period of 4 hours. After doping

the appearance of the films is changed to a glossy dark blue.This material is referred to as PANi-NMP

2. The CSA route: Quantities of emeraldine base and meta cresol are weighed such that a solution of 4% emeraldine base by weight will be produced. A small portion of the solvent is set aside before the polymer is dissolved, homogenised and centrifuged as per method 1. The polymer is then protonated in solution by addition of camphor sulphonic acid (CSA), dissolved in the unused meta cresol. The ratio of acid to polymer can be varied, thus the level of protonation and hence the charge carrier density in the polymer can be controlled. For example, ratio of 2 moles of polymer to 1 mole CSA would constitute 50% nitrogen site doping. This mixture is spread onto silicon wafers and dried in a vacuum oven to produce conductive films, approximately 50 μm thick. This material is referred to as PANi-CSA

A comparison of the films produced by these two methods reveals that there are advantages and disadvantages associated with each. The NMP route allows the production of very high quality films of even thickness which, are virtually free from pinholes. Alignment of the polymer chains within these samples is relatively easy through the stretching process developed by P.J.Laughlin which allows sample elongation exceeding 700% ($L/L_0 = 8$). This facilitates the study of electrical anisotropy arising from the partial orientation of the conductive chain backbones along a common axis.

However, the typical electrical conductivity obtained in NMP processed samples is significantly less than for comparable samples produced via the CSA route e.g. for unstretched films $\sigma_{NMP} \approx 40$ Scm^{-1} while $\sigma_{CSA} \approx 300$ Scm^{-1}. This difference is thought to be a result of more homogeneous dispersion of the dopant species when protonation takes place in solution (CSA route) as opposed to in the solid state (NMP

route). The NMP samples also show a strong relation between conductivity and moisture content. Removal of water absorbed by a film by placing it under vacuum is accompanied by a drop in conductivity to a around 20% of the original value measured under normal atmospheric conditions.

Samples produced via the CSA route, on the other hand, show a conductivity decrease of less than 5% after 24 hours under vacuum. It is, however, more difficult to produce large area films (>10 cm^2) of the CSA material with a quality comparable to that provided by that of the NMP route. In addition this material is not so readily stretch oriented (typical maximum extension $\approx$ 100%).

These two methods of producing conductive polyaniline films, provide two opportunities for the study of electrical transport mechanisms in a polymeric medium.

References

[1] D.J. Berets & D.J. Smith, *Trans. Faraday Soc.* **64** (1968) p. 823

[2] H.Shirakawa, T.Ito & S. Ikeda, *Polym. J.* **4** (1973) p. 460

[3] C.K. Chiang, C.Z. Fincher, Y.W. Park, A.J. Heeger, H. Shirakawa, E.J. Louis, S.C. Gau & A.G. MacDiarmid, *Phys. Rev. Lett.* **39** C (1977) p.1098

[4] J.H. Burroughes, C.A. Jones & R.H. Friend, *Nature* **335** (1988) p.137

[5] C. Horowitz, X. Peng, D. Fichou & F. Garnier, *J. Appl. Phys.* **67** (1990) p.528

[6] J.H. Burroughes, D.D.C. Bradley, A.R. Brown, R.N. Marks, R.H. Friend P.L. Burn & A.B. Holmes, *Nature* **347** (1990) p. 539

[7] H. Kuhn, *J. Chem. Phys.* **16** (1948) p. 840

[8] W.P. Su, J.R. Schrieffer & A.J. Heeger, *Phys. Rev. Lett.* **42** (1979) p. 1968

[9] R.H. Friend, from " Physics and Chemistry of Electrons and Ions in Condensed matter", D. Reidel Publishing Company (1984) p. 625

[10] R.E. Peierls, from "Quantum Theory of Solids", Oxford University Press (1955)

[11] "Introduction To Molecular Electronics" M.C. Petty, M.R. Bryce & D. Bloor, Edward Arnold (1995)

[12] Y.W. Park, C. Park, Y.S. Lee, C.O. Yoon, H. Shirakawa, Y. Suezaki & K. Akagi, *Solid State Comms.* **65** (1988) p. 147

[13] T. Schimmel, W. Riess, J. Gmiener, G. Denninger, M. Schwoerer, H. Narman & N. Theophilou, *Solid State Comms.* **65** (1988) p. 1311

[14] M.J. Rice & E.J. Mele, *Solid State Comms.* **35** (1980) p. 48

[15] W.P. Su, J.R. Schrieffer & A.J. Heeger, *Phys. Rev. B* **28** (1983) p. 1138

[16] E.J. Mele & M.J. Rice, *Phys. Rev. B* **25** (1981) p. 5397

[17] R.R. Chance & D.S. Boudreux, from "Handbook of Conducting Polymers" Vol. 2 Marcel Dekker, New York (1986) p. 825

[18] H. Letheby, *J. Chem. Soc.* **15** (1862) p. 161

[19] A.G. Green & A.E. Woodhead, *J. Chem. Soc. Trans.* **101** (1912) p.1117

[20] A.G. MacDiarmid & A.J. Epstein, *Faraday Discuss, Chem. Soc.* **88** (1989) p. 317

[21] R. Menon, C.O. Yoon, D. Moses, A.J. Heeger, & Y. Cao, *Phys. Rev. B* **48** (1993) p.17 689

[22] P.N. Adams, P.J. Laughlin, A.P. Monkman & N. Bernhoeft, *Solid State Comms.* **91** (1994) p. 875

[23] S. Stafstrom, J.L. Bredas, A.J. Epstein, H.S. Woo, D.B. Tanner, W.S. Huang & A.G. MacDiarmid, *Phys. Rev. Lett.* **59** (1987) p. 1464

[24] J.C. Chiang & A.G. MacDiarmid, *Synth. Met.* **13** (1986) p. 13

[25] A.P. Monkman & P.N. Adams, *Synth. Met.* **41-43** (1991) p. 891

[26] P.N. Adams, P.J. Laughlin, A.P. Monkman & A.M. Kenwright, *Polymer*, submitted for publication

CHAPTER 2

Conduction Mechanisms

2.1 Macroscopic Structure Of Polymers

In chapter 1 the mechanisms through which organic polymers such as polyacetylene and polyaniline are able to exhibit electrically conductive behaviour on the molecular scale have been described. At the macroscopic level, however, electrical conduction within a sample of material does not depend on transport along the polymer backbone alone. Other charge transport processes must also affect the progress of holes or electrons, for example transfer of carriers between polymer chains or across chemical defects in a chain. If the polymer has any crystal structure, grain boundaries may also be present within the material, and will make a contribution to the large scale electrical properties.

The electrical conductivity of bulk polymer samples can be modified if, via application of uniaxial stress, some alignment of the chain structures is introduced. Along the axis of alignment, conductivity can be increased markedly over that of an unoriented sample. Conversely, perpendicular to this axis, the conductivity is relatively unchanged.

This phenomenon provides evidence for the (quasi) one-dimensional nature of electrical carrier transport within individual chains. The electrical anisotropy induced in chain oriented samples indicates that the polymer backbone provides a path of least resistance for carriers, since the direction in which chains are aligned is also that for which the conductivity is a maximum. The conductivity observed in the direction perpendicular to alignment, for polyaniline (see chapter 3), is similar to that observed in unoriented samples. This is ascribed to the fact that the frequency of interchain transfer 'hops' required for carriers to traverse the sample along this axis is relatively similar to that in an unstretched sample of polymer. It is a widely held view that the interchain transfer process is a major limiting factor of conduction in polymer samples where there is little or no regular interchain order [1]. In fact, stretch orientation has been widely employed to enhance the conductivity of polymer samples in the search for the intrinsic

nature of the polymer chains. Polyacetylene prepared in this manner has been reported to exhibit conductivity >100,000 Scm^{-1} along the alignment axis [2]. This is an extremely high value for a polymeric conductor and is comparable with that of copper (≈ 650,000 Scm^{-1}).

The mechanisms involved in the transport of charge carrier species in any material can be investigated via measurement of properties such as conductivity and thermoelectric power. Most conductive polymers, including polyaniline, have electrical conductivity with a temperature dependence far removed from that of crystalline metals. Typically, there is an exponential dependence on temperature which fits the general form for variable range hopping (VRH) described in section 2.4.

In contrast to conductivity, thermoelectric power measurements on polyacetylene [3,4,5] and polyaniline [6,7] have repeatedly shown a linear dependence on temperature, which is strong evidence for the existence of metallic states in these materials. The dichotomy in measured electrical properties has given rise to a heterogeneous model as proposed by Kaiser [8,9,10]. The polymer is considered, on some microscopic scale, to be constructed from highly conductive metallic regions which are separated by thin, electrically insulating barriers. It is the presence of these barriers which then governs current flow in the bulk material. In this general model the insulating barriers could arise on the molecular scale, from the energy required for carriers to make the transfer to another polymer chain or the barrier to charge transfer between larger regions of the polymer in a granular system. In either case, the heterogeneous model provides one explanation for the absence of classical metallic behaviour in the conductivity properties of organic conductors. This model does, however, still allow for the character of the metallic regions to show up in non current carrying processes such as thermopower, see section 2.5.

In recent years, the chain length of polyaniline has been increased and the density of defects reduced by optimisation of the chemical synthesis described in sec. 1.7. In addition to this, development of the CSA solution state doping process has improved the conductivity to values of 300 Scm^{-1} or more in unoriented film samples. In addition, the

temperature dependence of conductivity has changed from the VRH form to that of a system very close to true metallic behaviour [11,12]. It is useful, therefore to consider the nature of these materials in more detail.

2.2 Disorder And Electron Localisation

For Polyaniline, the conductivity, displays characteristics which differ from classical metallic behaviour in two major respects. Firstly, the magnitude of conductivity reaches only to 300-400 Scm^{-1} in the best samples whereas typical metals are of the order 1000 times more conductive. Secondly the variation of conductivity with temperature typically shows a large positive coefficient i.e. conductivity increases strongly as a function of temperature and tends to zero in the limit of zero temperature. Most crystalline metals, Cu, Al, etc. display a small negative temperature-conductivity coefficient. However, according to Menon et.al. [11,12] some samples of polyaniline, in the form PANi-CSA, have recently been shown to exhibit slowly decreasing conductivity with increasing temperature over the range 180 to 300 K This metallic character was, however, frozen out at low temperatures and below a peak at 180 K, conductivity decreased as temperature was reduced.

A starting point for understanding the electronic properties of polyaniline (and other conductive polymers) is provided by theory developed for non crystalline inorganic semiconductors and metals and discussed in the book by Mott and Davis [13]. The structure of polyaniline, at the intermolecular level is strongly dependent upon the method of processing employed. PANi-NMP (in stretched or unstretched form) does not appear to posses any long range structural order. This would not be expected either, since the bulk polymer is likely to be a matrix of tangled chains of unequal lengths and dissimilar structural conformations. Hence there is little chance for regular crystalline structure to become established. However, x-ray studies upon PANi-CSA reveal that this material contains crystalline regions. This feature, combined with the (relatively) high magnitude and metallic response of its electrical conductivity, is commensurate with the

idea that charge transport in PANi-CSA is due in part to diffusion through metallic regions [11,12].

The absence of a regular lattice structure in a non crystalline material directly affects the nature of electronic wave functions therein. There is certainly little chance that they take the periodic or Bloch form imposed by a regular structure. Mott and Davis [13] suggest two possibilities for the scattering effect on electrons resulting from the presence of defects or impurities. The first is that the scattering is only weak so that the free electron approximation can be applied and the electron energy written as:

$$E(k) = \frac{\hbar^2 k^2}{2m} \qquad \text{eqn. 2.1}$$

Where k is the electron wavevector and m the effective mass. Since only two electrons (with opposing spins) can occupy the same energy level, the expression for density of states in a three dimensional solid can be written:

$$N(E) = \frac{(Em^3/2)^{1/2}}{\pi^2 \hbar^3} \qquad \text{eqn. 2.2}$$

Where $N(E)$ is the density of states at energy E per unit volume. This case is really only applicable to a lattice system containing defects or impurities at low density such that the mean free path is long i.e. $k\ell >> 1$.

In a non crystalline medium the disorder in the structure leads to both a reduction in mean free path and deviation from the simple density of states function of eqn 2.2. In this second case, first applied to amorphous metals and alloys, as the scattering becomes strong, i.e. $k\ell \approx 1$, there is a significant alteration of the density of states function from the free electron form and the concept of a Fermi surface becomes meaningless due to the large uncertainty in k. As the strength of scattering increased, the electron wave functions at some energies become localised, decreasing exponentially in amplitude with distance. Still stronger scattering results in a wider band of energies over which the electronic states become localised.

This phenomenon is known as Anderson localisation after Anderson who first proved that this effect occurs in the case of strong electronic scattering. The important feature of non crystalline systems revealed by this theory is that it is possible to have an electronic band structure with a finite continuous density of states function in which some, or all of the states are localised. Consider the case where the band states are filled to some Fermi energy, E_F, where the electronic states are localised. Anderson showed that it is possible to realise a condition where electrical conductivity vanishes as temperature approaches the absolute zero limit, even though the density of states N (E_F) is non zero. Materials in which this behaviour occurs are called Fermi glasses. For crystalline materials, insulating behaviour only occurs where $N(E_F) = 0$, a condition typically provided by the presence of an energy gap separating the filled and empty electronic states, e.g. in intrinsic semiconductors such as silicon.

In theoretical terms it is considered that the condition of Anderson localisation occurs when there is sufficient disorder in a given structure such that solutions to the Schrödinger wave equation are spatially localised. The model used by Anderson in order to picture the process of localisation begins with a regular array of potential wells, spaced at interval a. Application of the tight binding model to this system reveals that the allowed electronic states lie in a narrow energy band. This case is just equivalent to the creation of metallic impurity bands by donor/acceptor species in a semiconductor.

If the wave functions of adjacent wells have only small overlap and are assumed to have spherical symmetry, the energy levels for a simple cubic lattice take the form:

$$E = W_0 + W_k \qquad \text{eqn. 2.3}$$

Where W_0 is the energy for an electron in a single well and

$$W_k = -2I\left(\cos k_x a + \cos k_y a + \cos k_z a\right) \qquad \text{eqn. 2.4}$$

The factor I in eqn. 2.4 is the transfer integral which describes how strongly neighbouring states interact. It is considered to take the form, [13]:

$$I = I_0 \exp(-\alpha R) \qquad \text{eqn. 2.5}$$

where R is the distance from the well. So the wave function for an electron in a single well is modulated by the exponential factor in the transfer integral such that it decreases in amplitude with increasing distance with a length factor α shown to be:

$$\alpha = \frac{(2mW_0)^{1/2}}{\hbar} \qquad \text{eqn. 2.6}$$

where m is the electronic mass. The bandwidth of energies produced by the array of wells with lattice co-ordination number z, is given by the relation:

$$B = 2zI \qquad \text{eqn. 2.7}$$

Disorder can be introduced into this system in two ways such that the array of potential wells becomes aperiodic.

1. Random variation in the well potential.

2. Random spatial displacement of the well sites such that the long range order is destroyed.

For case 1 Anderson supposed that the well depths take values at random between theoretical limits at $\pm V_0$, which describe the spread of energies. The effect on electronic mean free path ℓ for small V_0 is described approximately [13], by the relation:

$$\frac{a}{\ell} = \frac{(V_0 / I)^2}{32\pi} \equiv \frac{V_0}{B} \approx 5z \qquad \text{eqn. 2.8}$$

where a is the lattice spacing and z is the co-ordination number.

What then is the critical condition which marks the onset of localisation? The Ioffe-Regel rule places a general lower limit on the mean free path of an electron such that the case $k\ell < 1$ is not allowed. Interpreted in another way, this means that ℓ cannot be shorter than the distance between scattering species. Therefore if this limiting condition $\ell \approx a$ is imposed, eqn. 2.8 gives:

$$\frac{V_0}{I} \approx \sqrt{32\pi} \qquad \text{eqn. 2.9}$$

This defines the condition for which the potential well energy disorder (characterised by V_0) becomes great enough to force the mean free path to its smallest theoretical limit.

Quantitatively, the onset of localisation is reached when V_0/B reaches some value, ≈ 2 according to Mott [13], such that wave functions of individual wells only suffer tiny perturbations from their neighbours. If the interaction is small enough, wave functions become localised and electrons are no longer free to diffuse. Hence the Fermi glass state is reached and conductivity tends to zero with decreasing temperature.

For a conductive polymer, spatial disorder is expected to have a strong bearing on the electrical behaviour of the material. An estimation of the localisation criterion in a system with such irregular order is again given by Mott and Davis [13] : For a material consisting of N atomic sites per unit volume the distance from one atom to its nearest neighbour is assigned the value r_1 where:

$$\frac{4}{3}\pi r_1 = \frac{1}{N} \qquad \text{eqn. 2.10}$$

The energy of an electron centred at either of the sites on any chosen pair of atoms is then defined, from the expression for the transfer integral (eqn. 2.5) as:

$$I_0 \exp(-\alpha r_1) \equiv V_0 \qquad \text{eqn, 2.11}$$

Because the distance r_1 is different for all pairs due to the spatial disorder, Mott uses the resulting spread in electron energy states to define an approximate V_0. This parameter thus provides an approximate representation for the range of site energies, in analogy with the case where disorder arises due to random variation in potential well energy. Similarly, a bandwidth B for the electronic states is defined from the average distance $r_2 = (N/2)^{-1/3}$ between site pairs. Using the transfer integral again, and by analogy to eqn. 2.7 this is:

$$B = 2zI_0 \exp(-\alpha r_2) \qquad \text{eqn. 2.12}$$

where z is the co-ordination number. From this approximation it is again possible, in theory, to define some criterion for the level of spatial disorder at which the ratio V_0/B approaches the range for which the electronic states become localised. For the case of a conductive polymer, where the electronic states are molecular, rather than the atomic

states assumed in the models of Anderson and Mott, it is difficult to apply the ideas discussed in this section except on a simple qualitative basis. However, the theory of disorder induced charge carrier localisation does provide one possible explanation for the low values of electrical conductivity displayed by polymeric materials, e.g. early polyaniline [6,7,11]

2.3 Conductivity In Disordered Media

Electrical transport in a disordered medium depends strongly on the nature of the electronic states at the Fermi level. The nature of these states, be they localised or diffuse, leaves its signature in the temperature dependence of the electrical conductivity of a material. In section 2.2 it is shown that as a conductive medium becomes progressively more disordered, localisation of electronic states occurs over a wider range of energy. For some typical amorphous materials it might be expected that electronic states up to some energy E_c are localised. E_c then defines the boundary that separates localised and non-localised states in a band. This boundary is termed a mobility edge.

The electrical properties of the system thus depend on the position of the Fermi level, E_F, in relation to E_c for which there are considered to be three important cases:

1. $E_F > E_c$

2. $E_F < E_c$

3. $E_F = E_c$

Condition 1 is the simplest configuration, since E_F lies in the region for which electronic states are delocalised. This is just the metallic case where the electrons which contribute to conduction (those with energy $\approx E_F$) are free to diffuse. In the second case, where the Fermi level is below E_c in the region of localised states, electron transport can

occur via two mechanisms: Thermally activated hopping (see section 2.4) and by excitation to the band of delocalised states above the mobility edge at E_c. The electrical conductivity in this latter case has an activation energy which depends upon $(E_F - E_c)$ and takes the general form [13]:

$$\sigma_{ex} = \sigma_{min} \exp[(E_F - E_c) / kT] \qquad \text{eqn. 2.13}$$

σ_{min} is the minimum metallic conductivity which occurs in the case $E_F = E_c$. It represents the smallest non-zero value that conductivity can have before the onset of localisation, whereupon conductivity vanishes in the zero temperature limit. The value of σ_{min} depends upon the factor V_0/B defined in section 2.2 and hence upon the ratio of ℓ, the carrier mean free path to a, the nominal spacing of electronic 'sites' and is described by Mott for the case of disordered alloys. An approximation for the minimum metallic conductivity is given [13] for the case where the criterion for Anderson localisation is satisfied, nominally $V_0/B \approx 2$. This is

$$\sigma_{min} \approx \frac{0.026e^2}{\hbar a} = \frac{610}{a} \text{ Scm}^{-1} \qquad \text{eqn. 2.14}$$

Menon et. al. [12] have found strong evidence from conductivity measurements that polyaniline, in the form PANi-CSA is characteristic of a material very close to the metal insulator transition boundary defined earlier by consideration of the relative positions of E_F and E_c. In this work a comparison is also drawn between the conductivity of the polymer ($\approx$300 Scm^{-1}) and typical estimates for the minimum metallic conductivity in disordered alloys, e.g.[13].

2.4 Variable Range Hopping

In section 2.3, two conductivity mechanisms are described for the case where E_F, the Fermi energy lies below the boundary energy separating localised and extended conductive states. These are excitation of electrons to the mobility edge at E_c for which the conductivity behaves according to the form of equation 2.13 and variable range hopping.

The excitation process is expected to make only fractional contribution to the total electrical transport unless the temperature is high, or the activation energy (E_F-E_c) is low. When E_F is situated well below E_c, the dominant mechanism of conduction arises via thermally activated hopping of electrons between localised electronic states. This gives rise to a conductivity of the form derived by Mott [13]:

$$\sigma = \sigma_0 \exp[-T_o / T]^{\frac{1}{d+1}} \qquad \text{eqn. 2.15}$$

for d = 1, 2 or 3 depending upon the number of dimensions for in which electron transport is allowed. In simple terms, this formula arises from a consideration of the fact that an electron at E_F will be most likely to make a hop to some state which requires the lowest activation energy. Mott considered that there is a greater number of suitable sites for larger hop distances. However, since the electrons are localised, the probability of making a hop reduces exponentially as a function of the distance between initial and final states.

The average distance of electron hops defines a localisation length, L_c upon which T_0, the characteristic temperature depends. For conduction in three dimensions, T_0 can be expressed as:

$$T_0 = \frac{16}{k_B N(E_F) L_c^3} \qquad \text{eqn. 2.16}$$

where K_B is the Boltzmann constant and $N(E_F)$ is the density of states at the Fermi level.

In the many studies of the conductive behaviour of heavily protonated PANi, the temperature dependence of the electrical conductivity fits a form of the variable range hopping model and appears to tend to zero in the limit of zero absolute temperature. Typically, in samples with lower ranges of conductivity (10-30 Scm^{-1}), as reported in [7] or [14], the behaviour is characteristic of a quasi-1-dimensional system i.e. d = 1 in equation 2.15. In more highly conductive samples e.g. [11,12] for which it has been claimed that the system is close to a insulator-metal boundary, the conductivity at low

temperatures (< 100 K) has a character suggestive of variable range hopping in three dimensions.

However, variable range hopping (VRH) is not the only means by which the macroscopic charge transport may deviate from a metallic nature in a system with disorder or defects. Other models which have been suggested to account for the non-metallic properties observed in conductive polymers include fluctuation induced tunnelling (FIT) and charging energy limited tunnelling (CLT).

The fluctuation induced tunnelling model of Sheng [15] provides a model for the electronic transport in a disordered or granular metallic system. In this case charge is not localised to states on the atomic level, as for VRH, rather the material is considered to comprise large regions with extended 'metallic' states separated by potential barriers. Tunnelling of electrons between these metallic grains or islands is considered to be the limiting factor for the conductivity of the bulk material. Sheng considered that the effective height of a given tunnel barrier could be reduced by fluctuation of the voltage across the tunnel 'junction' owing to the random thermal motion of charge (electrons) within the adjoining metallic regions. The result of this consideration is that the tunnelling current becomes temperature dependent. The form of conductivity which results from a network of metallic islands and barriers in a macroscopic system is calculated by Sheng [15] and described by the relation:

$$\sigma = \sigma_0 \exp[-T_1 / (T + T_0)] \qquad \text{eqn. 2.17}$$

where T_1 depends upon the average barrier height or grain spacing. T_0 represents the temperature for which the thermal fluctuations produce a significant contribution to the tunnelling current compared with the temperature independent elastic tunnelling.

Early polyacetylene results c.a. 1980 [16] were shown to have an electrical conductivity characteristic very close to that predicted by the FIT model. The metallic island and barrier structure required for true FIT conduction was thought to arise as a consequence of chemical bonding defects in the polymer chains or from inhomogeneous doping of the material.

Motion of electrons by tunnelling in a granular system is also subject to limitations due to electrostatic forces. If the metallic grains are small enough then the electrostatic energy required to move an electron from one grain to another will become significant compared to the thermal energy $\approx kT$ available to make the hop. In this case the conductivity of a material is expected to have the following form [17]:

$$\sigma = \sigma_0 \exp[-T_0 / T]^{1/2} \qquad \text{eqn. 2.18}$$

where T_0 depends upon the size and spacing of the metallic islands. It could be envisaged that such a process might affect the transfer of charge carriers between the metallic states of neighbouring chains in a conducive polymer.

The electrical transport within any disordered material is therefore subject to limitations arising from several possible phenomena. These effects can be described by models such as VRH between localised states on the atomic/molecular scale and tunnelling between extended metallic regions.

2.5 Thermopower

Measurement of the thermoelectric power (thermopower) of a conductive or semiconductive material provides another approach in addition to measurement of conductivity by which electrical transport mechanisms may be studied. Thermoelectric measurements are made with a zero current process, that is, no external electric field is applied to samples under test. This important factor permits the thermopower to show behaviour in a material which is not revealed in the data from electrical conductivity measurements. With particular reference to conductive polymers, such as polyacetylene and polyaniline, it is common for thermopower to reveal strongly metallic character whilst conductivity data best fits a hopping or tunnelling transport model.

The thermoelectric properties of metals were studied by Seebeck in the early nineteenth century. He discovered that the presence of a thermal gradient in a conductor gives rise to a small e.m.f., a phenomenon which is now known as the Seebeck effect. A quantitative definition for this property is as follows:

$$S(T) = \frac{\Delta E}{\Delta T} \qquad \text{eqn. 2.19}$$

$S(T)$ is the Seebeck coefficient, commonly referred to as the thermopower and has the units microvolts per Kelvin. It defines the e.m.f, ΔE generated across a small temperature gradient, $T \rightarrow T + \Delta T$ in a given material. The absolute thermopower is a function of temperature, so that the total e.m.f. resulting from a large temperature gradient, say from T_1 to T_2 is calculated by the integral:

$$E = \int_{T_1}^{T_2} S(T)dT \qquad \text{eqn. 2.20}$$

The property $S(T)$ depends on the exact electronic structure of the material in question, and is different for all metals and semiconductors. Indeed it is the difference in e.m.f. generated by two different metals under the same temperature boundary conditions that permits the construction of thermocouples for use in thermometry. The thermopower of a material therefore contains valuable information regarding the nature of electronic states involved in charge transport processes.

The simplest model of a metallic system is that of the diffusion thermopower, in which only the heat carried by electrons is considered [18]. The more complicated electron-phonon interaction is ignored at this stage. In simple terms the diffusion thermopower is the e.m.f. resulting from the movement of charge carriers in taking heat from the 'hot' to the 'cold' end of the sample. The thermal energy carried by an electron in a metal is the difference between its internal (total) energy and the Fermi energy such that:

$$h_i = E_i - E_F \qquad \text{eqn. 2.21}$$

The Peltier heat Π of a material is defined as the ratio of heat flow to charge flow, or the thermal energy carried per unit charge and can be expressed as:

$$\Pi = \frac{\sum_i h_i v_{i(x)}}{e\sum_i v_{i(x)}} \qquad \text{eqn. 2.22}$$

Where the total thermal and electrical current is the summation over individual electrons with thermal energy h_i and velocity component v_i along the x axis. The Peltier and Seebeck effects are related through the expression:

$$\Pi = TS \qquad \text{eqn. 2.23}$$

where T is the absolute temperature. Combining equations 2.21, 2.22 and 2.23 yields an expression for the thermopower:

$$S = \frac{1}{eT}\frac{\sum_i (E_i - E_F) v_{i(x)}}{\sum_i v_{i(x)}} \qquad \text{eqn. 2.24}$$

If the expression is changed from a summation over electron velocities to a summation over currents i.e. $j_i = ev_i$ and the electrons grouped according to energy, so that a current $j(E)d(E)$ is associated with all electrons in the energy range from E to E+dE it can be shown that [18]:

$$S = \frac{1}{eT}\frac{\int (E - E_F) j_x(E) dE}{\int j_x(E) dE} \qquad \text{eqn. 2.25}$$

The individual currents, j_x can be broken down in terms of $\sigma_x(E)$, the contribution to conductivity by electrons with a given energy, the electron distribution (Fermi) function, $f_0(E)$ and an electric field such that:

$$j_x = -\mathcal{E}_x \int \sigma_x(E) \frac{df_0}{dE} dE \qquad \text{eqn. 2.26}$$

substituting for j_x in equation 2.25 gives:

$$S = \frac{1}{eT} \frac{\int_0^\infty \sigma_x(E)(E - E_F) \frac{df_0}{dE} dE}{\int_0^\infty \sigma_x(E) \frac{df_0}{dE} dE} \qquad \text{eqn. 2.27}$$

This general expression contains the fundamental clues about the nature of the diffusion thermopower. In a metal df_0/dE, the differential of the Fermi-Dirac distribution function is only of a significant size over a range $\approx \pm kT$ about the Fermi energy. Hence, just as for conduction only the fraction of electrons with energies close to E_F make a contribution to the thermopower. Also, if $\sigma_x(E)$ is invariant with respect to energy then the integral in the numerator of equation 2.26 is zero and so in this case there would be no diffusion thermopower.

So, a non zero thermopower arises only where there is a difference in the thermal flux due to electrons above and below the Fermi level. The sign of this effect depends on the nature of the electron scattering. If the majority charge carriers are electrons and normal scattering applies i.e. higher energy electrons are scattered less, then $\sigma_x(E)$ increases with energy, so electrons transport heat and negative charge from the hot to the cold regions of a given sample. The thermopower is then of negative sign, since the resultant electric field is in the opposite direction to the thermal gradient. Positive thermopower is observed in semiconductors where holes are responsible for conduction e.g. the thermopower of p-type silicon. Therefore if only normal scattering of carriers is considered, the sign of the Seebeck coefficient should reflect the charge sign of species responsible for electrical transport.

To yield an expression for S specifically for metals it is possible to expand equation 2.27 with respect to temperature about E_F, since the expression is only significant for the small range of energies in the window $E_F \pm kT$. The temperature gradient is assumed to be one-dimensional along the x axis, so the suffices can be dropped. This yields the most familiar expression for the metallic diffusion thermopower [18]:

$$S(T) = -\frac{(\pi k)^2}{3|e|} T \left[\frac{\partial \ln \sigma(E)}{\partial E} \right]_{E=E_F} \qquad \text{eqn. 2.28}$$

where k is the Boltzmann constant and |e| is the magnitude of the electronic charge. The important feature of this expression is that the thermopower contribution resulting from thermal diffusion of charge carriers has a linear dependence upon absolute temperature. However, direct calculation of S(T) is impossible since $\sigma(E)$ cannot be evaluated.

The linear, negative thermopower predicted by the first order calculation of equation 2.28 is in fact widely disobeyed. For example the noble metals copper, silver and gold are all found to have positive thermopower. This phenomenon has been partly explained through a consideration that anomalous scattering of electrons may occur. In addition to this, a deviation from linear temperature dependence is observed in many metals (including the noble metals) at low temperatures, in the form of a peak at ≈50 K. This feature is known as the phonon drag peak. At low temperatures, the phonon-phonon interaction is weak and so a net phonon flux arises where a thermal gradient is present. It is thus possible for phonons to contribute a net momentum to electrons via the electron-phonon interaction. This effect gives rise to an additional thermopower from the so called phonon drag. The sign of this contribution depends upon the nature of the electron-phonon scattering, such that normal scattering causes a negative phonon drag e.m.f. whilst Umklapp or backscattering causes a positive term, with electrons scattered against the phonon flux.

At high temperatures, much greater than the Debye characteristic temperature of a material the phonon-phonon interaction is strong such that the phonons are in

equilibrium. In this case just as many phonons scatter an electron in one direction along the temperature gradient as in the opposite direction, so the net contribution to the total thermopower from phonon drag effects is practically zero.

An important feature observed in data obtained from highly doped conductive polymers such as polyacetylene [10] and, more recently, high quality polyaniline [12] is that the thermopower has an almost entirely linear dependence upon temperature. In fact the behaviour of the thermopower in these materials is closer to the form of pure diffusion thermopower as predicted in equation 2.28 than for most metallic elements. There appears to be little evidence for the occurrence of phonon drag effects except for isolated examples of polyacetylene, as suggested by Kaiser [9] in an analysis of the results of Park et. al. [4].

The positive sign of thermopower in oxidatively doped polyacetylene is concurrent with the theory that doping results in the formation of positively charged solitons i.e. electrical transport is by conduction of 'holes'. For polyaniline, the formation of polarons in the chain structure upon protonation might also be expected to fit this picture.

It can be shown [19] that the expression for diffusion thermopower can be written in an alternative form:

$$S = -\frac{\pi^2 k^2}{3|e|} T \left[\frac{1}{A}\frac{\partial A}{\partial E} + \frac{1}{\ell}\frac{\partial \ell}{\partial E} \right]_{E=E_F} \qquad \text{eqn. 2.29}$$

here S is expressed in terms of the Fermi surface area A and the carrier mean free path ℓ. This form is useful because it facilitates some qualitative explanations for some of the deviations from expected behaviour which occur in the thermopower of metals.

In the simple case, for a spherical Fermi surface, the area of the constant energy surface increases with increasing energy, hence $\partial A/\partial E$ is positive. If scattering is again assumed to be normal, then $\partial \ell / \partial E$ is positive also. This set of conditions yields the negative diffusion thermopower which is expected intuitively i.e. if electrons carry heat from hot to cool regions.

However for a system with a spherical Fermi surface in which positive holes are the dominant charge carrier the term $\partial A/\partial E$ is negative and so an overall positive thermopower can result where the magnitude of the term in A in equation 2.29 exceeds that of the term in E. In more complicated situations, distortion of the Fermi surface resulting in a non-spherical geometry and effects due to anomalous scattering affect the magnitude and sign of $\partial A/\partial E$ and $\partial \ell / \partial E$ respectively. Hence the thermopower of metallic systems depends on the electronic and physical structure of each individual material in such a way that there are few, if any general rules governing their thermoelectric properties, as revealed by experiment, e.g. the anomalous, positive thermopower displayed by the noble metals, Cu, Ag and Au [19].

Equation 2.29 also reveals that there is some dependence of thermopower on the mean free path length ℓ, of carriers in a conductive medium. This is of particular interest with reference to the properties of polymer samples for which electrical anisotropy introduced via strain induced chain alignment. The electrical conductivity of such samples is enhanced in one dimension, along the axis of chain alignment, which suggests that the mobility of charge carriers is higher when transport along chain backbones is predominant. Additional support for this theory is provided by the decrease in conductivity upon alignment for the conductivity perpendicular to the stretch axis. It is feasible to imagine that the mean free path length in aligned sample is anisotropic, with the largest value of ℓ in the direction parallel to the axis of chain orientation.

The supposed anisotropy in ℓ, in conjunction with the expression for thermopower given in equation 2.29 is one possible explanation for the anisotropy observed in the thermopower data obtained from stretch oriented polyaniline, as reported in both [14] and in this thesis, in chapter 4

When scattering of electrons becomes very strong, near the Ioffe-Regel limit in a disordered medium, what happens to the thermoelectric power, does it assume a different behaviour, just as the form of the conductivity changes? Previously, the effect of imposing disorder upon a conductive medium has been considered (sections 2.2 to 2.4). It has been shown that once disorder has reached the point where scattering

reduces the mean carrier path to the minimum defined by the Ioffe - Regel rule, further disorder forces electronic states over some range of energies to become localised. Increasing the disorder past this threshold widens the band of energies over which states are localised. Furthermore, when the Fermi level is situated in a region of localised states, the electrical conductivity ceases to show a metallic behaviour and becomes temperature activated, tending to zero at zero temperature. This is the Anderson transition, and the material is described as a Fermi glass.

According to Mott and Davis [13] if the mean free path is shortened such that $l \approx a$, where a is a measure of atomic spacing for an inorganic conductor, equation 2.28 can be written as:

$$S(T) = -\frac{2}{3}\frac{(\pi k)^2 T}{|e|}\frac{\partial \ln[N(E_F)]}{\partial E} \qquad \text{eqn. 2.30}$$

where $N(E_F)$ is the density of states at the Fermi level. This expression applies where scattering is not strong enough that electrons are localised. When the electronic states are localised and electron transport is by hopping it is necessary to calculate a new expression for thermopower by integration of equation 2.27 over the range of hopping energies. Mott suggests that this range is of the order:

$$W \approx k(T_0 T^3)^{1/4} \qquad \text{eqn. 2.31}$$

for which T_0 is defined in the expression for conductivity by variable range hopping (equation 2.15). So, for a system where the electronic states at the Fermi level are localised as a result of disorder, the thermopower due to charge carriers transporting heat in a thermal gradient is:

$$S(T) = -\frac{k^2}{2|e|}(T_0 T)^{1/2}\left[\frac{\partial \ln(N)}{\partial E}\right]_{E_F} \qquad \text{eqn. 2.32}$$

So, in an amorphous material, localisation of the electronic states and the transition to Fermi glass behaviour does lead to a change in the behaviour of thermopower: S is expected to vary according to the square root of absolute temperature.

Thermopower data commensurate with electron transport via variable range hopping (VRH) have been reported for samples of conductive polymers. In polyacetylene, where only a small fraction of chains were oxidised (light doping), thermopower has shown a temperature dependence very close to that predicted in equation 2.32, e.g. Park et. al. [3,4]. Polyaniline samples have also displayed character akin to VRH as gauged from thermopower data, e.g. Sakkopoulos et. al. [21]. Electrical transport via hopping might be expected in these cases, where doping is incomplete, or uneven, such that electronic states contributing to a conduction band are widely or unevenly spaced.

2.6 Heterogeneous Models

The data from measurement of electrical transport properties of conductive polymers frequently show a somewhat confusing behaviour. Whilst the electrical conductivity of a given material may have a temperature dependence most unlike that of a crystalline metal, its thermopower can display characteristics which fit the form for metallic diffusion thermopower almost perfectly.

The highly metallic nature of thermopower in these cases suggests that, unlike the inorganic semiconductors [18], the number of charge carriers is invariant with respect to temperature. Therefore the positive variation of the conductivity with temperature, always observed in the lower regions of the available experimental temperature range must arise from some other mechanism. One way in which this unusual behaviour has been tackled is through the heterogeneous model, introduced briefly in section 2.1. The general supposition upon which this model is based is that the material contains a microscopic network of distinct regions, each with individual conductivity values. In the simplest case the bulk medium would consist of two phases: highly conductive 'metallic' fibrils or islands and low conductivity or insulating barrier regions. The macroscopic electrical properties of the material depend on the quantity and electrical properties of both regions.

Kaiser [9] considered that the conductive and insulative regions are characterised by conductivities σ_1 and σ_2 respectively. In a given sample, the conductivity depends upon the combination of all path lengths and areas of the two phases such that:

$$\sigma = LA^{-1}\sum_{j}(L_{1j}A_{1j}^{-1}\sigma_1^{-1} + L_{2j}A_{2j}^{-1}\sigma_2^{-1})^{-1} \qquad \text{eqn. 2.33}$$

where L_{ij} is the length of the j^{th} path in material i and A_{ij} is the corresponding cross sectional area of the path. L and A are the respective length and cross sectional area of the bulk sample. If all paths through the sample have the same fractions of their total resistance arising from regions of each phase the conductivity can be written as:

$$\sigma^{-1} = f_1\sigma_1^{-1} + f_2\sigma_2^{-1} \qquad \text{eqn. 2.34}$$

where f_i are geometrical weighting factors that represent the contribution made by each phase to the total sample resistivity. For application to polymeric materials, Kaiser considered that the highly conductive regions are fibrils e.g. small bundles of chains. If all paths across the sample have the same resistance it is possible to write:

$$f_i = \frac{L_i A}{LpA_i} \qquad \text{eqn. 2.35}$$

here p is the number of fibrils which pass through the cross sectional area. In the case when $\sigma_1 >> \sigma_2$ the macroscopic conductivity can be written:

$$\sigma \approx \frac{(LpA_2)}{L_2}\sigma_2 \qquad \text{eqn. 2.36}$$

where L_2 is the effective length of insulating material in a sample of total length L.

The magnitude of the bulk conductivity in this case is governed by the length factor L_2, of insulating material, so if $L_2 << L$, σ can exceed σ_2. However, the nature of the conductivity (its temperature dependence) follows that of the insulating regions and reflects the electrical transport therein. The behaviour of the metallic regions is thus masked.

If a temperature gradient ΔT is applied to a heterogeneous sample, contributions to a thermoelectric voltage are expected from both phases of the material. The thermopower will be the sum of these two contributions i.e.:

$$S = \frac{\Delta T_1}{\Delta T} S_1 + \frac{\Delta T_2}{\Delta T} S_2 \qquad \text{eqn. 2.37}$$

where S_1 and S_2 are the absolute thermopower of the two material phases and $\Delta T_i / \Delta T$ is the fraction of the total temperature difference that exists across all regions of type i. It can easily be deduced that if the insulating barriers are thin i.e. $L_2 << L$ again, and they conduct heat well then since $\Delta T_1 >> \Delta T_2$ the macroscopic thermopower is essentially just that of the highly conductive regions, S_1.

With the use of a heterogeneous model applied to conductive polymers it is therefore possible to provide an explanation for the unusual mixture of electrical

transport properties which are commonly associated with highly conductive polymers. The heterogeneous 'structure' could arise in these materials as a result of inhomogeneous doping, such that undoped sites act as insulating barriers. Alternatively, on a larger scale it has been proposed that samples containing crystalline regions are separated by boundary regions of low conductivity. Much of the work by Kaiser [5,8,9,10] is concerned with the development and application of these theories to conductive polymers.

References

[1] A.J. Heeger, *Faraday Discuss. Chem. Soc.* **88** (1989) p.1

[2] T. Schimmel, W. Riess, J. Gmiener, G. Denninger, M. Schwoerer, H. Narman & N. Theophilou, *Solid State Comms.* **65** (1988) p. 1311

[3] Y.W. Park, A Denenstein, C.K. Chiang, A.J. Heeger & A.G. MacDiarmid, *Solid state comms.* **29** (1979) p. 247

[4] Y.W. Park, W.K. Han, C.K. Choi & H. Shirakawa, *Phys. Rev. B*, **30** (1984) p. 5487

[5] A.B. Kaiser, *Materials Science Forum*, **122** (1993) p. 13

[6] Y.W. Park, Y.S. Lee, C. Park, L.W. Shacklette & R.H. Boughman, *Solid State Comms.* **63** (1987) p.1063

[7] F. Zuo, M. Angelopoulos, A.G. MacDiarmid & A.J. Epstien, *Phys. Rev. B* **36** (1987) p. 3475

[8] A.B. Kaiser, from "Electronic Properties of Conjugated Polymers", Springer Verlag, Berlin 1989 p. 2

[9] A.B. Kaiser, *Phys. Rev. B* **40**, (1989) p. 2806

[10] A.B. Kaiser, *Synth. Met.* **45** (1991) p. 183

[11] M. Reghu, Y. Cao, D. Moses, & A.J. Heeger, *Phys Rev. B* **47** (1993) p. 1758

[12] R. Menon, C.O. Yoon, D. Moses, A.J. Heeger, & Y. Cao, *Phys. Rev. B* **48** (1993) p. 17 689

[13] N.F. Mott & E.A. Davis, from "Electronic Processes in Non Crystalline MMaterials" Clarendon Press, Oxford (1979)

[14] Z.H. Wang, C. Li, E.M. Scherr, A.G. MacDiarmid & A.J.Epstein, *Phys. Rev. Lett.* **66** (1991) p. 1745

[15] P. Sheng, *Phys. Rev. B* **21** (1980) p. 2180

[16] Y.W. Park, A.J. Heeger, M.A.Druy & A.G. MacDiarmid, *J. Chem. Phys.* **73** (1980) p. 946

[17] P. Sheng & J Klafter, *Phys. Rev. B* **27**, (1983) p. 2583

[18] J.S. Dugdale, from "The Electrical Properties of Metals and Alloys" Edward Arnold, London (1977)

[19] R. D. Barnard, from "Thermoelectricity in Metals and Alloys", Taylor & Francis, London (1972)

[20] S. Sakkopoulos, E. Vitoratos, E. Dalas, G. Pandis & D. Tsamouros, *J. Phys. Condensed Matter* **4** (1992) p. 2231

CHAPTER 3

Electrical Conductivity

3.1 Experimental Techniques

Aside from the scientific interest in conductive polymers it has long been recognised that they are a potential source of new electronic materials. For polyaniline, which offers the advantage of a relatively long term stability in air, applications such as electromagnetic shielding and electrically conductive coatings are envisaged.

It is therefore important that the electrical properties of the material are characterised and an attempt is made to understand its behaviour in physical terms. The electrical conductivity of a substance is perhaps the most fundamental measure of its 'electronic' nature. The magnitude of this property is a useful guide to the quality of the material and hence, its suitability for any for a particular application. Conductivity as a function of temperature can provide still more information about the mechanism(s) which govern charge transport in a material.

In order to measure the electrical conductivity of a material precisely, there are several factors which influence the choice of an appropriate technique. These include the range of magnitude of conductivity, whether or not samples display electrical anisotropy and lastly, upon their physical proportions. Two methods were used to obtain the electrical conductivity data, presented later in this chapter, on free standing conductive polyaniline films:

1. The Montgomery four point technique.

2. The four in line technique.

Although the mathematical treatments involved in processing the raw data generated by these methods are different, some fundamental aspects are common to both. In particular, both techniques require electrical contact to be made at four points

on the sample under test. This is to permit independent application of a probe current and measurement of voltage and thus avoid errors in measurement due to parasitic contact resistances.

For all measurements, voltage readings were made using a Keithley digital voltmeter (model 2000) which has a very high input impedance (>100 MΩ). This factor is important since the theoretical definitions of both techniques assume that no current flows through the voltmeter. A Keithley programmable constant current source (model 220) was used to establish a precise sample current.

3.1.1 The Montgomery Technique

This procedure for measuring conductivity was first described by Montgomery [1] who made a mathematical analysis of the electrical field distribution in a rectangular prism when a current is passed between adjacent vertices, based on the calculations of Logan et. al. [2]. For two reasons, this technique is of particular use in the conductivity analysis of stretch oriented polyaniline films. Firstly, it provides a method for simultaneous calculation of the two principle electrical conductivity components in an anisotropic sample. Secondly, special consideration is given in [1] to the case where the dimension of the prism is small, i.e. the technique is well suited to measurement of thin samples.

Consider a rectangular sample with dimensions l_1 and l_2 and of thickness t where $t << (l_1 l_2)^{1/2}$. If a contact is made at each corner, a measure of resistance, R_1 can be obtained if a current I is passed between corners 1 and 2 and the potential difference V between corners 3 and 4 is measured, see fig. 3.1. Similarly a value R_2 can be found if a 90° commutation of the voltage and current connections is performed. In the simplest case, for an isotropic sample the conductivity of the material is given by the relation [1].

$$\sigma = [H R_1 t]^{-1} \qquad \text{eqn. 3.1}$$

where H is a function of l_2/l_1 having a dependence described graphically and numerically in fig. 3.2. For a square sample i.e. $l_1=l_2$, then H = 4.531.

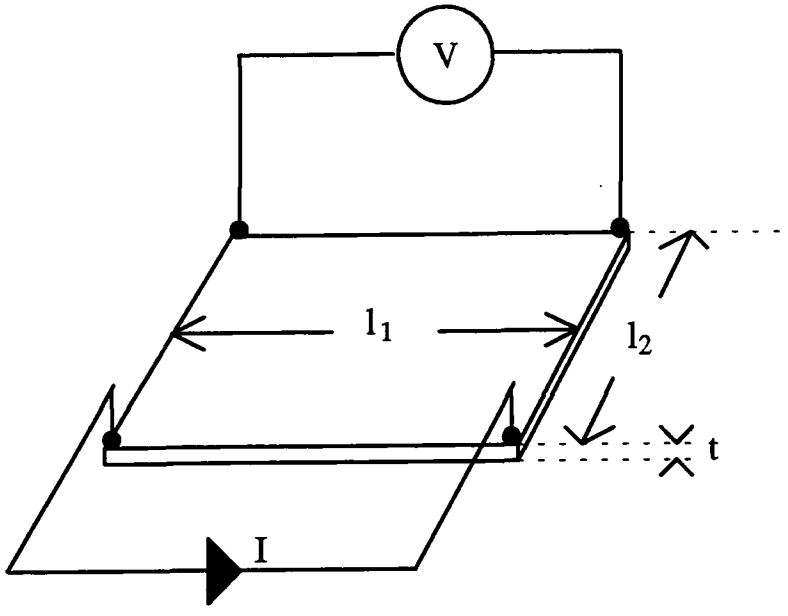

Fig. 3.1 The arrangement of electrical contacts to a sample during Montgomery type conductivity measurements.

If the sample is anisotropic and prepared so that the axis along which the conductivity is highest lies parallel to one side of the square, then analysis becomes more complicated. Two resistances R_1 and R_2 can again be obtained, for which $R_1 > R_2$ if the maximum conductivity σ_1 is in the direction of side l_1 in fig. 3.1. Along l_2 the conductivity has the value σ_2.

From the ratio R_2/R_1 an effective dimension ratio l_2' / l_1' must be defined. This quantity represents the dimensions which an isotropic sample (having the same average conductivity) must have to present the same ratio of resistances. The relation used to calculate l_2' / l_1' is shown graphically in fig. 3.3 along with a numerical solution. A new factor H must also be evaluated using the value obtained for l_2' / l_1' just as for the case of an isotropic sample in equation 3.1. Finally the two conductivity components parallel to the axes of the square sample can be calculated by substitution of the appropriate values into the equations:

$$\sigma_1 = \left[H\left(\frac{l_2'}{l_1'}\right) R_1 t \right] \qquad \text{eqn. 3.2}$$

$$\sigma_2 = \left[H\left(\frac{l_1'}{l_2'}\right) R_1 t \right] \qquad \text{eqn. 3.3}$$

Implementation of the Montgomery technique thus allows the electrical conductivity components of square, isotropic and anisotropic samples of polyaniline film to be calculated from two measurements of resistance and one of thickness (it can be shown that the sample dimensions need not be known explicitly).

Practical implementation of this method requires that electrical contact be made to each of the four corners of a square section of polyaniline film. This was achieved (for room temperature measurements) using a purpose built probe stage, with four

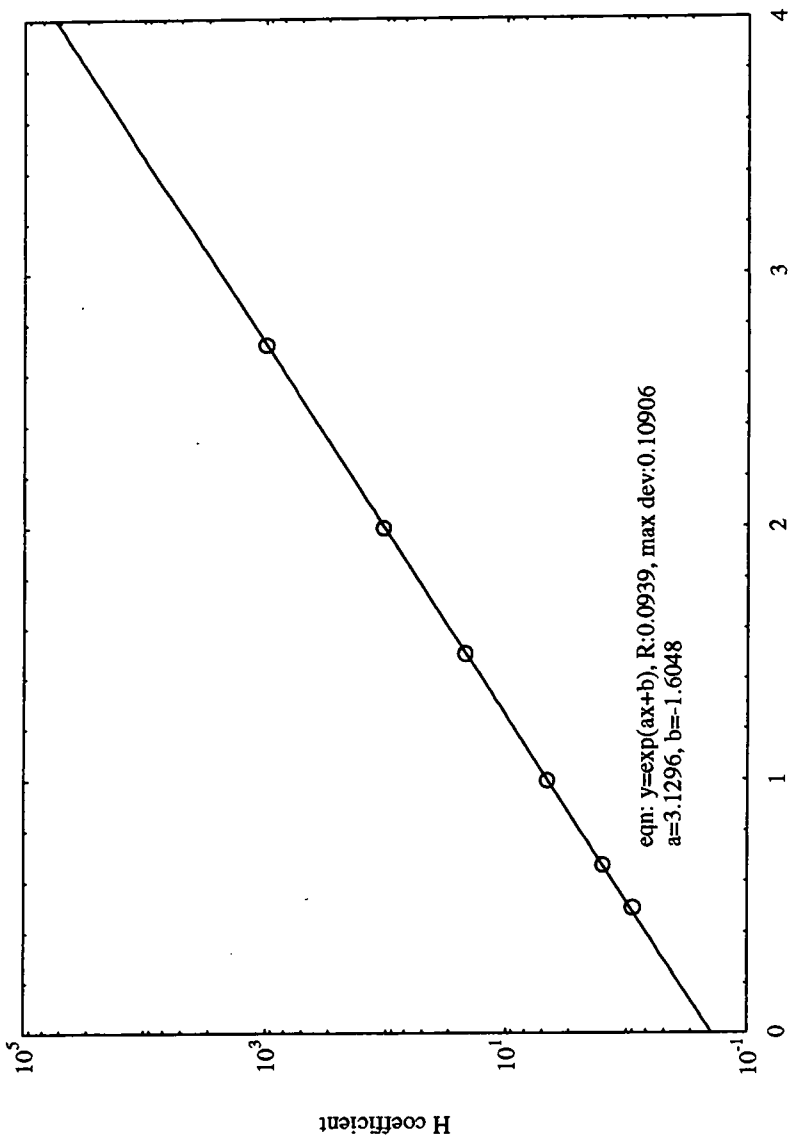

Fig. 3.2 Numerical model for calculation of the H coefficient in the Montgomery analysis to data from [1].

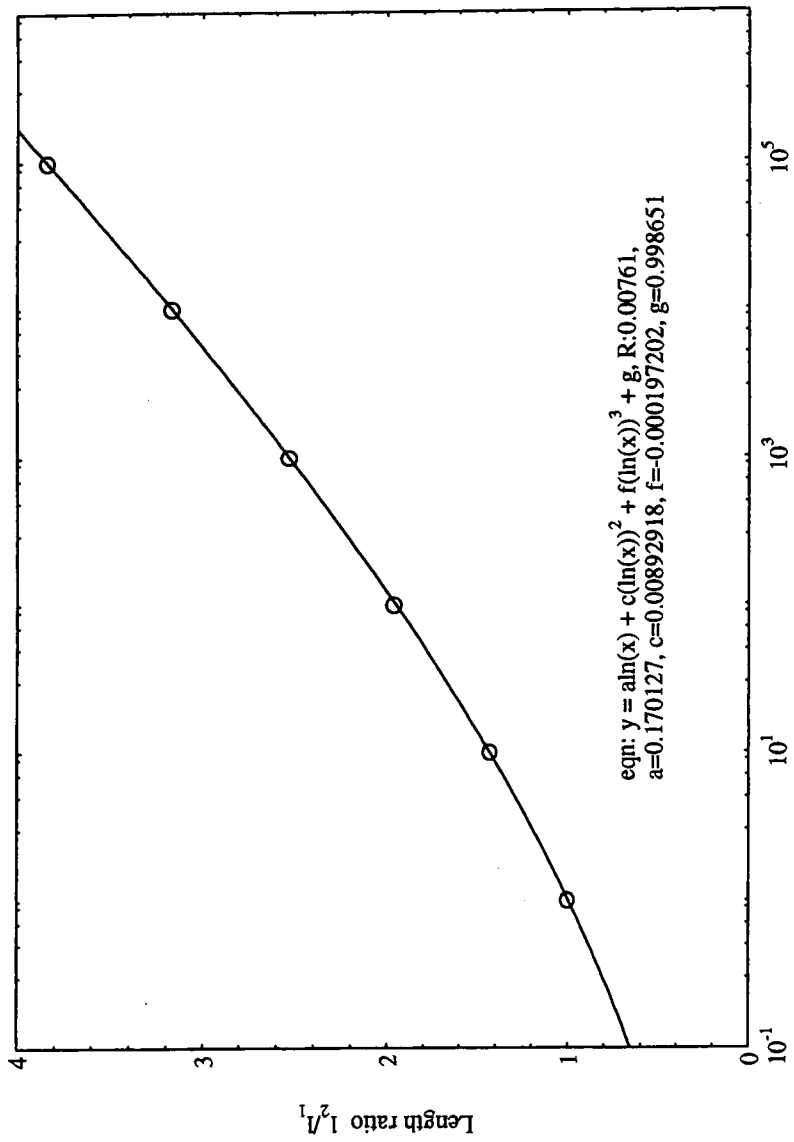

Fig. 3.3 Numerical model of the effective sample dimensions for the Montgomery analysis of samples with electrical anisotropy. The data points are taken from [1].

independently sprung gold probe tips arranged in a square configuration of dimensions 6 x 6 mm. These could be lowered gently onto a section of the film under test, cut to fit the probe arrangement. Errors were minimised by ensuring that the sample size exceeded the perimeter of the square defined by the probes by less than 0.5 mm. Gold is used for the point contacts for two main reasons. Firstly, it is an unreactive metal except in the most extreme conditions, therefore electrochemical degradation of the polymer does not occur at the probe junctions. Secondly it ensures that reliable, low resistance contacts can be established between the sample and measurement apparatus. This is important in order that noise in the voltage measurements is kept to a minimum to allow a high resolution in the final data.

Connections from the sample were fed to the current source and voltmeter via a four way switch unit. This arrangement permitted four successive 90° commutations of the voltage and current connections, without the need to disturb the probes in position on the film. In this way the risk of damage to the sample is minimised. It also allows values of both R_1 and R_2 to be obtained if the sample is inaccessible e.g. inside a cryostat.

Measurement of the conductivity of a sample of polyaniline film thus involved the following steps.

1. Cutting a square section of film to a close fit of the four point probe stage. For oriented (anisotropic) samples, the stretch axis must be parallel to one pair of edges of the square.

2. Measurement the thickness of the film, using a digital micrometer, checking to ensure uniformity of the sample.

3. Measurement of voltage/current ratios for each of the four probe commutations.

If the sample is unstretched (isotropic), all four resistance values will be equal. The conductivity can be calculated using equation 3.1, with $H = 4.531$. If the sample is from an anisotropic film, then the four resistance readings will comprise of two similar smaller and two similar larger values. The average of the smaller readings is calculated and taken as R_1. Similarly R_2 is the average of the two larger values. As described previously, the ratio R_2/R_1 is used to obtain an effective length ratio l_2' / l_1' which in turn is used to obtain an appropriate value for the factor H.

The two components of conductivity, along the axes of the square of the sample can then be calculated using equations 3.2 and 3.3. A computer program was written to perform this calculation, for which the functions connecting R_2/R_1, l_2' / l_1' and H were modelled numerically from data in the paper by Montgomery [1].

The accuracy of the technique was limited in this case to the accuracy of the sample thickness measurements obtained using the micrometer, which had a resolution of 1 μm The typical minimum sample thickness was of the order 15 to 20 μm. Therefore the maximum error introduced is approximately 6%.

Of greater importance is the precision with which changes in a sample conductivity can be measured. This is governed by the resolution which can be obtained in the reading of voltage. It was therefore desired that, in order to retain accuracy in the smallest readings, the system noise was kept well below 1 μV. This was ensured by the use of clean gold probes to contact the film surface. In this way voltage readings could be made to four significant figures.

The choice of probe current also affects the accuracy of readings, with higher currents resulting in increased voltage signals and therefore a greater signal to noise ratio. However, too high a current density at the probe/film junction can lead to a burning out of the film at the contact point. High currents can also lead to significant Joule heating of the film, with the result that readings are unsteady since the conductivity varies significantly with temperature. For measurements made at room temperature, a probe current of 1mA was found to provide a good compromise, giving ample resolution with no risk of damage to the sample, or erroneous effects due to film heating.

The Montgomery method does have some disadvantages. Firstly, samples must be cut exactly to fit the square outline of the probe. Subsequently, manipulation of the sample onto the probe stage so that contact is made to each corner of the sample is an awkward and time consuming process. The area of electrical contact made by each probe point is small and these must be cleaned regularly to ensure low junction resistances and hence minimise system noise. In addition to the above practical difficulties, a lengthy calculation procedure is required to obtain the conductivity values from the raw data. However, this method still provides the most convenient approach to the characterisation of electrically anisotropic materials.

3.1.2 The Four In Line Technique

This method is a simple alternative to the rather complex Montgomery technique described in the previous section. The theory is derived using Ohm's law and the physical definition of electrical conductivity with respect to sample dimensions and resistance.

Consider a thin, rectangular strip of uniformly conductive material of width W and thickness t with four parallel linear junctions extended across the width of the sample as illustrated in fig. 3.4. If a current I flows as shown, between the two outer contacts, then a potential difference V will be present between the inner pair, which are separated by a distance L. The resistance, R of this small section of the sample is simply V/I. If the dimensions W, T and L are known it can be shown that the sample conductivity can be calculated using the formula:

$$\sigma = \frac{L}{RWt} \qquad \text{eqn. 3.4}$$

So in this case the spacing between the voltage probes must be known explicitly, in addition to the other sample dimensions, unlike the Montgomery technique which requires determination of only one sample dimension - the thickness.

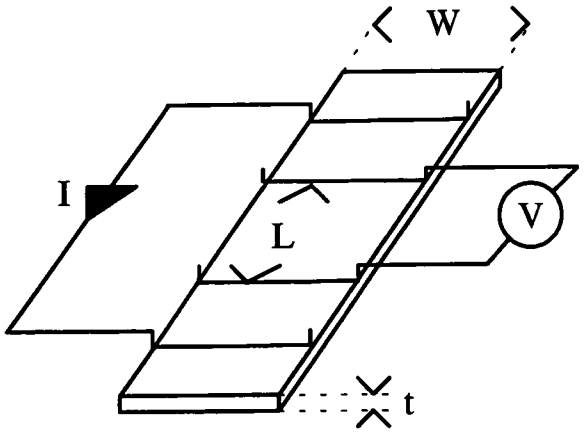

Fig. 3.4 The arrangement of sample and electrical contacts required for correct operation of the four in line method.

In order to measure the individual conductivity components of anisotropic materials, e.g. stretch oriented polyaniline, two separate strips must be prepared from the main sample such that probe current can be passed parallel to the elongation axis in one strip and perpendicular to this axis in the second.

To facilitate measurement of the conductivity of polyaniline films at room temperature a hand held probe unit was built. This consisted of four 0.25 mm diameter platinum wires stretched in parallel over an insulating perspex plate. The separation between the inner (voltage) and outer (current) contacts was 2 mm and 10 mm respectively. Platinum was used in order to provide a low resistance, chemically unreactive contact to the film surface to ensure reliable operation. This probe unit was easily positioned over a suitably prepared rectangle (typically. 5x15 mm) of the film under investigation and held under gentle hand pressure whilst current and voltage readings were taken. Lengthy manipulation of the sample/probe arrangement was not necessary to achieve reliable readings.

The increased surface area of the four in line junctions employed in this technique, compared to the point probes required by the Montgomery method provided excellent electrical contact to the film samples. This had two beneficial consequences, the first of which was that noise in the voltage measurement circuit was reduced, permitting high resolution in the final conductivity measurements. Secondly, as a result of the larger contact area, the current density for a 1 mA probe current at the outer contacts was much less than that at a point contact and hence the risk of damage to the sample is reduced.

The accuracy of the four in line technique is limited by the precision to which the sample dimensions can be measured. The sample thickness t, measured using a digital micrometer and the width W of the strip are considered to be the greatest possible sources of error. The maximum uncertainty in the final conductivity data is estimated at some 10%. However, when measuring the temperature dependence of the conductivity of a given sample it was possible to determine changes in the conductivity of less than 1% due to the high resolution of the voltage and current data. Since the larger errors

present in the size measurements were fixed once the sample is prepared, they need only be taken into account when comparing different samples. Therefore for individual samples it is feasible to present the much smaller changes observed as genuine functions of another parameter e.g. temperature.

3.1.3 Low Temperature Techniques

Whilst measurement of the electrical conductivity at room temperature provides some information on the nature of conductive polyaniline, from a physical viewpoint, the most important factor is the dependence of this property upon temperature. In chapter 2 it has been shown that nature of the electronic states near the Fermi level dictates the charge transport mechanisms and hence the behaviour of the conductivity. To gain a clearer picture of the physical nature of polyaniline it was therefore important to characterise electrical conductivity of various samples as a function of temperature. This process has been one of the major objectives during the author's research period.

To perform this task two special probe units were constructed so that either the Montgomery or four in line techniques could be performed within a Leybold closed cycle helium refrigeration cryostat. This unit, in conjunction with an Oxford Instruments ITC4 temperature controller provided the means to investigate sample properties in the temperature range from 10 to 300 K. Temperature control accuracy was better than 1 K over this range. The Montgomery probe consisted of four independently sprung gold point contacts arranged in a 4 mm x 4 mm square configuration which held the sample against a base plate. A thin layer of mica provided electrical insulation between this brass plate and the sample. The four in line probe had four parallel platinum wire contacts on an insulating former each 10 mm long, with the voltage sensing wires spaced 4 mm apart. The sample was held under light pressure by six fixing screws between the probe and an aluminium base plate, covered with an insulating mica sheet. Thin connecting wires were used to make internal electrical connections to the conductivity probe/sample holder units. The wires were carefully wrapped around the cryostat cold-

finger to minimise heat transmission to the sample and hence permit the lowest possible minimum temperature.

During early experiments it was found that at the low end of the temperature range, T<50 K, Joule heating of the sample by the current passed during resistance measurements led to a significant error in the results obtained. Fortunately, this effect could easily be identified by a drift in the voltage readings, after the constant current source was applied and the sample started to warm. To avoid this problem, which occurred with either measurement technique, the probe current was reduced at the lower temperatures from the typical 1 mA to levels as low as 10 μA so that steady readings were obtained. Since the sample resistance was generally much higher at low temperatures, the reduced probe current did not significantly reduce the resolution of the voltage readings. Consequently the electrical power dissipated momentarily during a particular reading could be kept well below 1 μW and errors due to sample heating effects are considered negligible.

Further problems were encountered with a longer term drift in the conductivity value of polyaniline samples at higher temperatures e.g. 300 K which has been associated with the removal of moisture from the films to the vacuum environment of the cryostat. Newly mounted samples were therefore allowed at least 10 hours to stabilise at 300 K under vacuum ($<10^{-3}$ Torr) before measurements were commenced.

The choice of measurement technique was governed by the nature of the sample. For stretch oriented, electrically anisotropic films the Montgomery probe was employed since it required only one sample preparation to permit simultaneous characterisation of the conductivity components in directions parallel and perpendicular to the axis of elongation. However the small area of the four sample contact points of the Montgomery probe sometimes led to contact failure at low temperatures. This could not be rectified 'in situ' as there was no way to adjust samples during operation of the cryostat. The only solution was to prepare a new sample for a fresh experiment.

The four in line technique was used for the measurement of conductivity of unstretched polyaniline samples. Although some problems with faulty contacts were

encountered at low temperatures, this difficulty was solved by a subtle modification to the probe - sample contact arrangement. Instead of four parallel wires held directly against the surface of the polyaniline as per room temperature measurements, samples were first prepared with four thin gold stripes on one surface in positions corresponding that of the probe wires. The gold was applied via a vacuum evaporation process and ensured excellent metallic contact to the film. In this configuration, the four in line method offered the highest resolution; changes of less than 1% in sample conductivity could be observed as a function of temperature.

3.2 Conductivity Of PANi-NMP

The first material available for study was polyaniline prepared via the NMP route (PANi-NMP) in the form of free standing films. Samples were supplied in two forms, unstretched films direct from the solution casting process and films elongated by 500% to induce a degree of uniaxial orientation of the polymer chains. Both types of sample were doped by immersion in aqueous methane sulphonic acid (MSA) with a concentration of 15% by volume, for a period of 4 hours.

3.2.1 Results

Spot measurements were made at room temperature (290 K) on each sample. These revealed some important general properties of the material. The conductivity of unoriented samples was found to be isotropic (within experimental error) and displayed a typical value of the order 30 - 40 Scm^{-1}. Films subjected to stretch elongation prior to doping displayed a significant electrical anisotropy, with the conductivity parallel to the axis of orientation greatly enhanced. In this case values of 250 Scm^{-1} were typical, with isolated samples having conductivity up to 300 Scm^{-1}. In contrast the conductivity perpendicular to the stretch axis was approximately 30 - 35 Scm^{-1}, apparently unchanged by the chain orientation process.

It is important to note that the conductivity values quoted above are much higher than comparable data obtained during measurements of the temperature dependence of the conductivity. A set of data typical of that obtained from many samples of PANi-NMP is presented in fig. 3.5. This anomaly arises from the strong dependence of the electrical properties of PANi-NMP upon the presence of moisture within the material as noted in previous studies e.g.[3]. In order to measure the temperature dependence of the conductivity, samples were contained under vacuum ($<10^{-3}$ Torr). The evaporation of absorbed water, under these conditions resulted in a dramatic reduction in the conductivity to approximately 20% of the value measured in ambient conditions, immediately after removal from the doping solution.

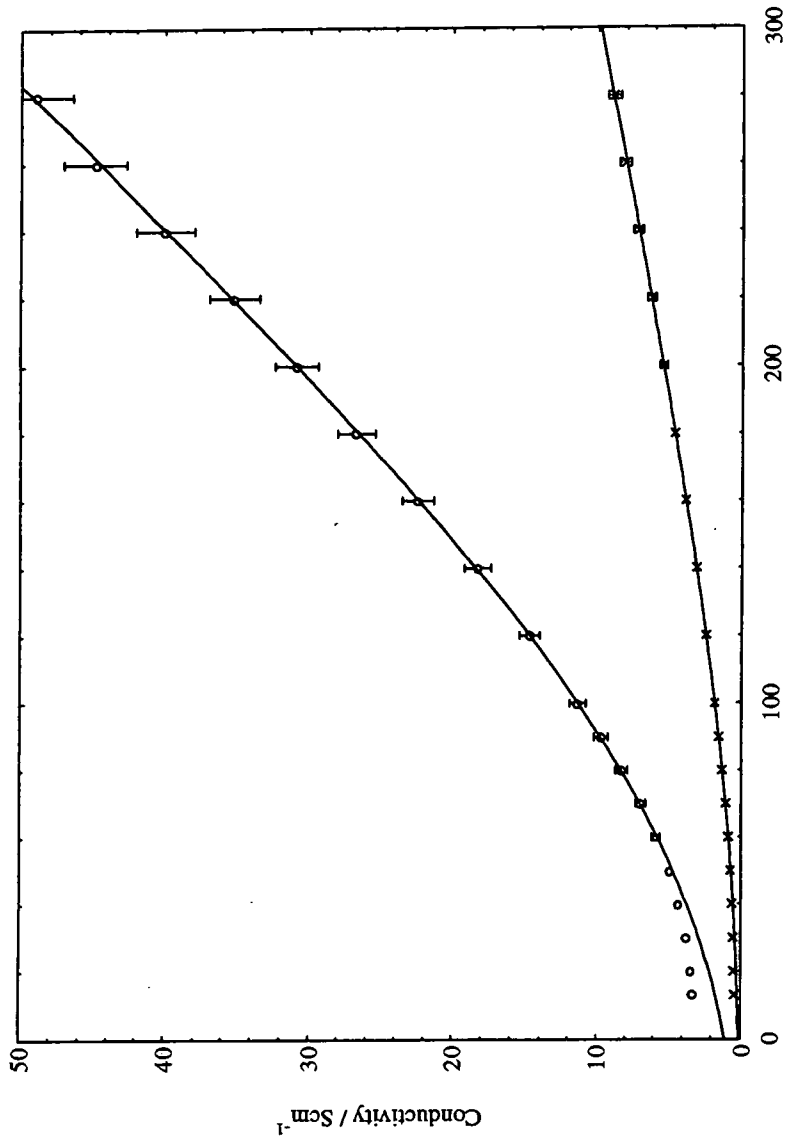

Fig. 3.5 Primary electrical conductivity components of 500 % stretch oriented PANi-NMP as a function of temperature. The lines are fits to the data using the FIT model.

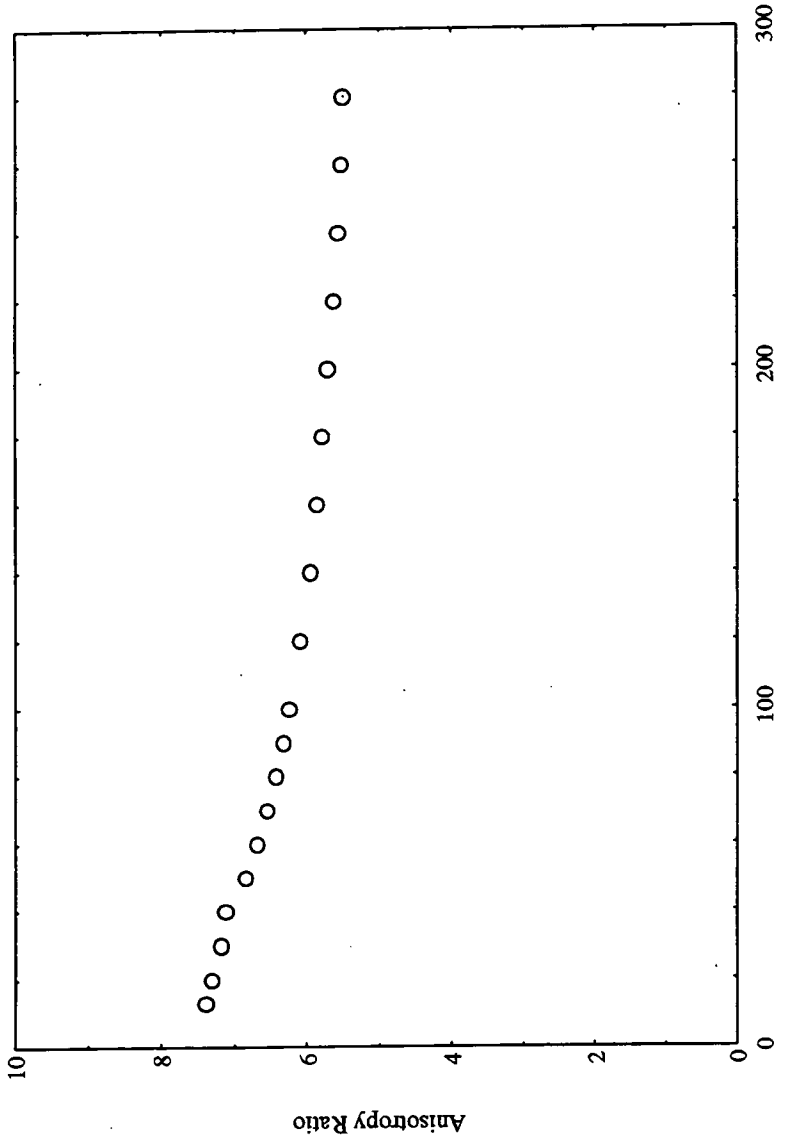

Fig 3.6 Electrical anisotropy factor of PANi-NMP Stretch oriented by 500% elongation.

Upon removal from the vacuum environment the conductivity was observed to return to approximately half the original value over the period of a few minutes, presumably as moisture from the atmosphere was absorbed. The absence of a full recovery is ascribed to a loss of MSA from the films. For this reason samples were allowed some 10 hours to reach a stable value of conductivity under vacuum, before measurements were commenced.

The graph in fig 3.5 shows the form of the temperature dependence of the electrical conductivity of stretch oriented PANi-NMP. The parallel component increases from 3.3 Scm^{-1} to 49 Scm^{-1} over the measured range (13 K to 300 K) whilst the perpendicular data extend from 0.4 Scm^{-1} to 8.9 Scm^{-1}. Both components have a similar temperature dependence, they increase monotonically with temperature. Additionally, the rate of increase, $d\sigma/dT$ increases as temperature becomes greater. The anisotropy ratio $\sigma_{Parallel}/\sigma_{Perpendicular}$ presented in fig. 3.6 has a weak dependence upon temperature, decreasing slowly from 7.3 to 5.5 over the range 13 K to 300 K.

3.2.2 Discussion

The results reveal that the conductivity of PANi-NMP decreases rapidly as temperature is reduced and therefore provide no evidence for metallic charge transport. Alignment of the polymer chains by stretch elongation prior to doping enhances the conductivity along the direction of orientation by a factor of six and induces a significant electrical anisotropy.

Many previous studies have been performed in which the electrical properties of PANi, doped by immersion of the solid state, base form of the polymer in aqueous acid. These include characterisation of unoriented samples [3,4,5] and stretched films [6,7]. Without exception, the temperature dependence of the conductivity reported in these cases is characteristic of charge transport by variable range hopping (VRH) of localised electrical carriers contained in either a quasi-1-dimensional, or a three dimensional system. However, the conductivity data presented in the preceding subsection of this

thesis do not fit the form of conduction by VRH and thus imply that the material investigated differs in some way from that available in previous studies. The strong dependence of conductivity upon temperature suggests that charge transport is limited by localisation on some unknown scale. However, since the VRH model cannot provide an explanation for the observed behaviour, some effect other than Anderson localisation due to disorder is thought to be responsible in this case. An equation of the form associated with fluctuation induced tunnelling (FIT), as described in section 2.4, has been used to compute the curve fits included with the data in fig. 3.5. In fact this model can only provide an acceptable fit for temperatures exceeding 50 K and it has not proved possible to explain the data at lower temperatures in terms of any of the contemporary models. The parameters used to produce the line fits to equation 2.17 are presented in the table below.

Orientation	σ_0 Scm^{-1}	T_0 K	T_1 K
Parallel	370 ±50	863 ±50	147 ±20
Perpendicular	75 ±5	890 ±50	140 ±20

Table 3.1. Curve fit parameters for the fluctuation induced tunnelling model of stretch oriented PANi-NMP.

The fact that the data presented in fig. 3.5 is best described by the FIT model implies that charge transport is dominated by a tunnelling process between metallic islands, rather than hopping between localised electronic states. In fact, thermopower

measurements on similar stretch oriented samples of PANi-NMP, presented in the following chapter, indicate that there are metallic states or regions within this material.

From table 3.1, it can be seen that there is little difference between the temperature parameters, T_0 and T_1 obtained for the parallel and perpendicular data by curve fitting to the FIT model. Only the intrinsic conductivity, σ_0 , is significantly different in these two cases, with the ratio σ_0(parallel)/σ_0(perpendicular) $\approx$5, which is similar to the real conductivity anisotropy ratio at 300 K ($\approx$ 6, see fig. 3.6). This would seem to suggest that any metallic regions are electrically anisotropic, presumably as a result of the stretch induced alignment of the polymer chains performed prior to the doping process. It is proposed that the doping of solid PANi-NMP by immersion in aqueous MSA results in inhomogeneous protonation of the material. If this is the case, poorly doped insulating or semiconductive regions might well be expected to separate well doped 'metallic' islands. In this case, in line with the heterogeneous model (see section 2.6), the insulating barriers prevent complete delocalisation of charge and it is the transport through these regions which dominates the nature of the conductivity of the bulk material. Thus true metallic behaviour is not observed and the electrical conductivity increases strongly with temperature as the energy available for charge carriers to tunnel between metallic regions increases.

The anisotropy in the conductivity of stretch aligned samples occurs because the direction along the polymer backbone is thought to provide the easiest path for charge carrier flow [8]. This is evident from the large enhancement effected by stretch alignment upon the electrical conductivity in one dimension, along the axis of elongation. Presumably, the alignment of polymer chains permits a greater proportion of charge transport by propagation along polymer backbones, so the frequency of scattering by incoherent interchain transfer processes is reduced in the parallel direction. Hence the anisotropy is considered to arise due to a stretch induced anisotropy in the carrier mean free path length. See also section 4.3.2, in the next chapter.

PANi-NMP is an amorphous material, as evidenced by neutron scattering studies [9] which provide no evidence for any crystal structure or large scale phase order

between the polymer chains. Therefore a relatively high probability of scattering is expected at interchain transfer events, even in 'metallic' regions of the material [10]. Therefore, even if there were no inhomogeneity in the dispersal of dopant within PANi-NMP, a conductivity of truly metallic magnitude cannot be expected even in highly aligned samples. This idea is supported by the low values of the intrinsic conductivity, σ_0, predicted by the fluctuation induced tunnelling model (see table 3.1) when compared to similar estimates for the intrinsic conductivity of polyacetylene [11] which exhibits a high degree of crystallinity.

3.3 Conductivity Of PANi-CSA

Polyaniline prepared in a conductive form via the CSA route (PANi-CSA) has very different electrical properties to those of PANi-NMP. Film samples of PANi-CSA doped to the theoretical maximum level (50% of nitrogen chain sites protonated) have electrical conductivity of the order 200 to 300 Scm^{-1} at room temperature before stretch alignment, this is almost tenfold greater than unstretched PANi-NMP. Moreover, stretch oriented films of PANi-CSA have exhibited conductivity values up to 800 Scm^{-1} at room temperature [12].

Unlike PANi-NMP, PANi-CSA is doped in solution prior to the film casting process, as described in section 1.7 of chapter 1. For two reasons therefore, this material provides an ideal opportunity to study the electrical properties of PANi as a function of the extent of protonation. Firstly, the camphor sulphonic acid (CSA) can be added to a quantity of undoped polymer in an accurately known molar ratio. Secondly, since the protonation is performed in solution it can be assumed that the dopant is diffused evenly throughout the samples.

3.3.1 Results

In order to probe the transition to conductive behaviour which PANi exhibits upon protonation, the temperature dependence of the electrical conductivity was investigated for unstretched PANi-CSA at different levels of doping. Films were prepared with CSA contents intended to yield 10, 20, 30, 40, 50 and 60% protonation levels, i.e. 10% = 1 in 10 nitrogen chain sites protonated. Conductivity was measured under vacuum (< 10^{-3} Torr) over the temperature range 10 K to 300 K via the four in line technique described in section 3.1.2. Samples were allowed 5-6 hours in the vacuum environment prior to the measurement process to ensure that moisture absorbed from the atmosphere was extracted. The conductivity of PANi-CSA upon removal of moisture is typically 80 to 85% of that measured in normal atmospheric conditions, a small reduction compared to that of PANi-NMP. Additionally, films recover their original

conductivity on standing in air for a few minutes, which suggests that no dopant is lost in high vacuum conditions.

The conductivity data for films at all doping levels are presented in fig. 3.7. It is clear that as the level of protonation is increased, the conductivity increases rapidly. At 10 K, the 60% sample is five orders of magnitude more conductive than the 10% sample. Also, the conductivity becomes a weaker function of temperature in the more heavily protonated films. The normalised conductivity, $\sigma(T)/\sigma(300\ K)$, for each data set is presented in fig. 3.8 and allows the trend in conductivity of each sample with temperature to be compared more easily. It reveals in detail, a transition in the conductive behaviour of PANi-CSA as the level of doping is varied.

At the two lowest levels of protonation (10% and 20%) the conductivity rises monotonically as temperature is increased. Additionally, the rate of increase of $\sigma(T)$ increases with temperature. When the protonation level is set to 30% and above the data reveal a very different behaviour. At low temperatures, conductivity increases as temperature rises, but $d\sigma(T)/dT$ decreases with increasing T. Moreover, each data set in the 30% to 60% doping range possesses a characteristic maximum in $\sigma(T)$ somewhere in the measured range. The temperature at which this peak occurs, T_p, has an inverse relation to the level of doping of the sample in question. In table 3.2, typical peak positions and their accompanying conductivity values are presented. For each case, at temperatures above that at which the peak occurs, the conductivity decreases slowly with increasing temperature, i.e. electrical conductivity has a negative temperature coefficient. In fig 3.9 the data from a 50% doped sample is presented on a linear scale to reveal in detail the temperature dependence of the conductivity of highly conductive PANi-CSA.

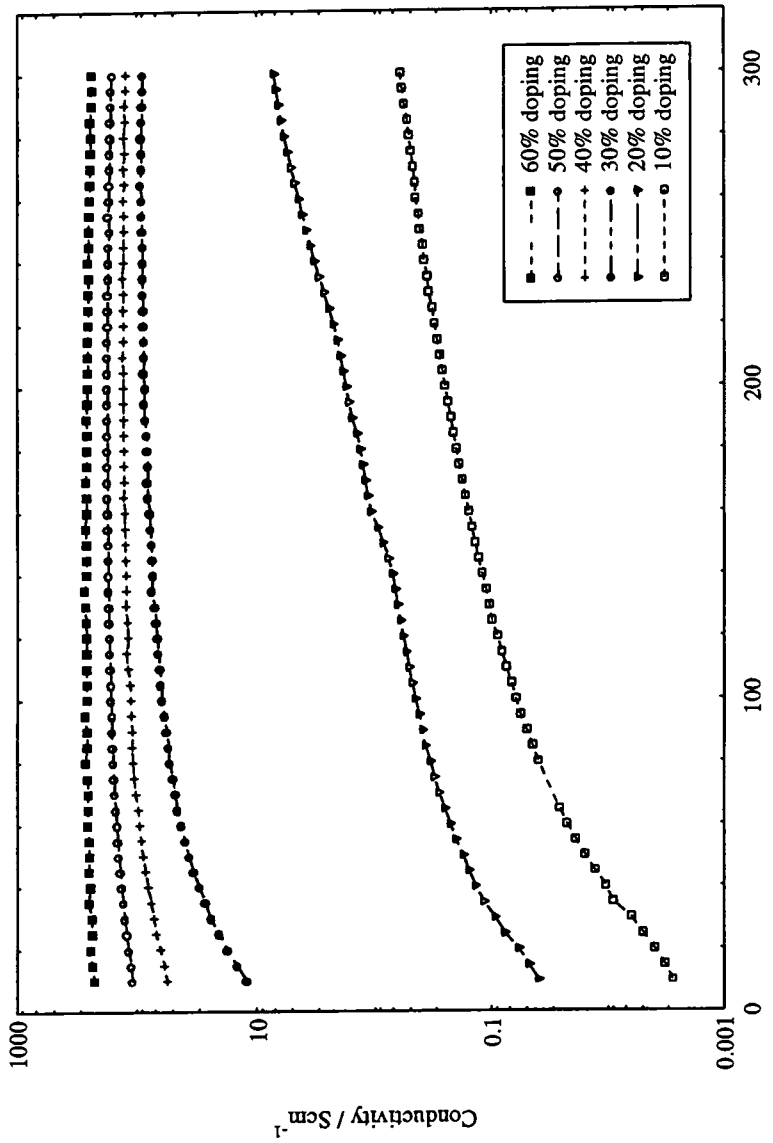

Fig. 3.7 Electrical conductivity versus temperature for PANi-CSA at doping levels between 10% and 60%.

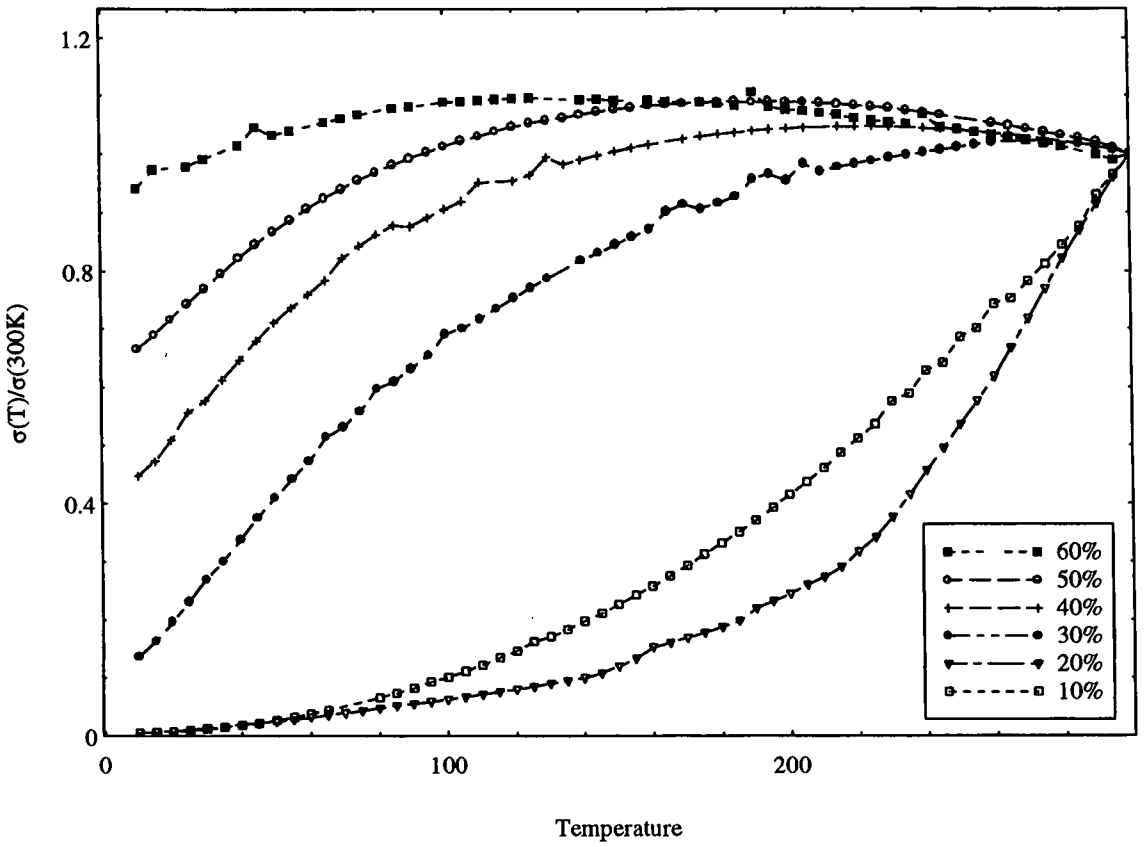

Fig 3.8 Normalised electrical conductivity data of PANi-CSA samples with doping levels between 10% and 60%.

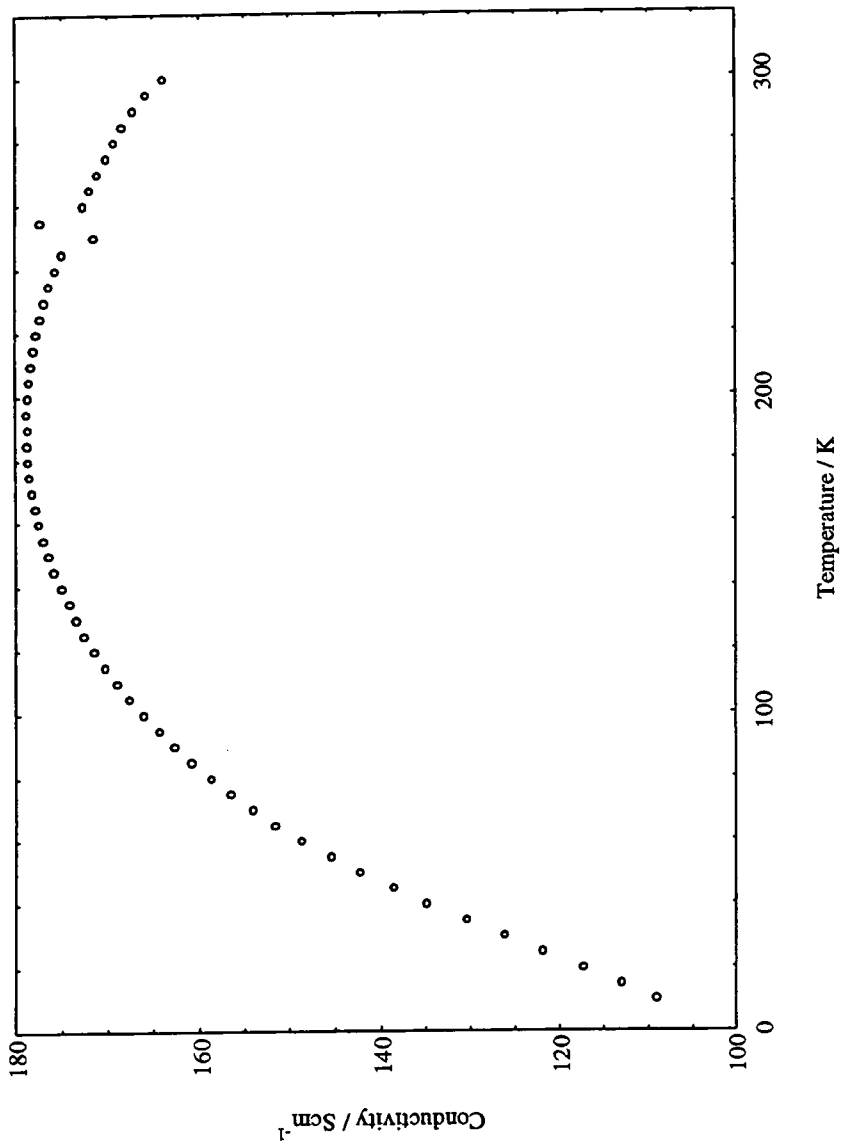

Fig. 3.9 Expanded view of the temperature dependence of the electrical conductivity of PANi-CSA prepared with 50% doping.

Protonation %	Peak conductivity Scm^{-1}	Peak temperature K	$\sigma(10)/\sigma(300)$
30	90	270	0.13
40	130	225	0.44
50	178	190	0.67
60	268	130	0.94

Table 3.2 Temperature values at which conductivity maxima occur in PANi-CSA.

It is widely accepted that the density of charge carriers within samples of conductive polyaniline is approximately equal to the density of protonated chain sites (see section 1.6). If it is assumed that all the CSA dopant added to the polymer causes protonation, even where the theoretical 50% level is exceeded, it is possible to estimate the charge carrier density in samples prepared at each of the six doping levels investigated. Furthermore, using the general expression for electrical conductivity:

$$\sigma = ne\mu \qquad \text{eqn. 3.5}$$

it is possible to make an estimate of the charge carrier mobility, μ, where n is the carrier density and e is the charge on an electron. Values of the charge carrier density and mobility, based upon the conductivity of each PANi-CSA sample at 300 K have been calculated and are included in table 3.3. In addition the mobility and conductivity data are also presented graphically, as a function of protonation level in fig. 3.10(a) and (b).Initially as the protonation level increases from 10%, the carrier mobility rises sharply, presumably as the separation between conductive states is diminished.

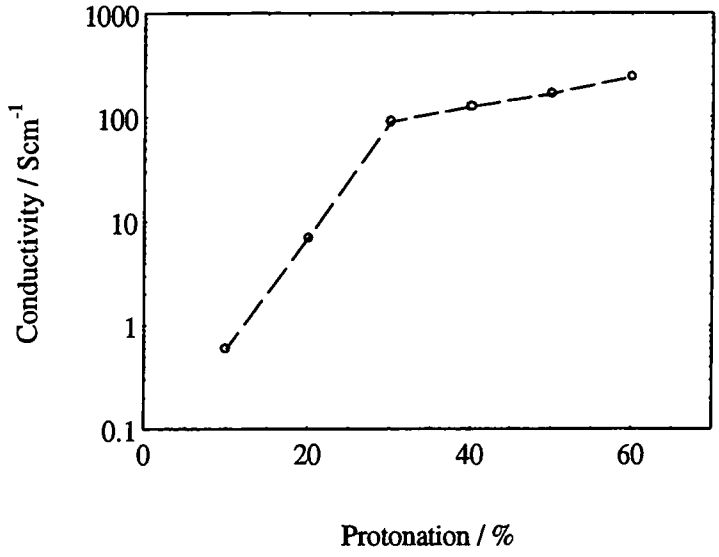

Fig 3.10(a) Conductivity of PANi-CSA at 300 K versus dopant concentration.

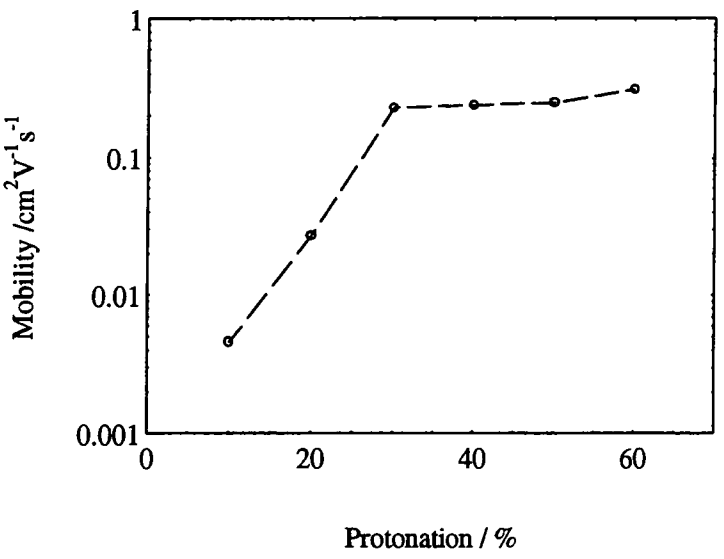

Fig 3.10(b) Mobility estimates for PANi-CSA prepared with different dopant concentrations.

Doping %	σ(300 K) Scm^{-1}	n(300 K) $x10^{21}\ cm^{-3}$	μ(300 K) $cm^2V^{-1}s^{-1}$
10	0.6	0.8	$4.6x10^{-3}$
20	7	1.6	$2.7x10^{-2}$
30	90	2.4	0.23
40	125	3.2	0.24
50	165	4.0	0.25
60	240	4.8	0.31

Table 3.3. Charge carrier density and mobility data from PANi-CSA at different doping levels.

Above the 30% level, however, a nearly constant mobility is observed, within the bounds of experimental error.

3.3.2 Discussion

The data presented in section 3.2.1 reveal a complex evolution in the conductive properties of PANi-CSA. From figs. 3.7 and 3.8 it would appear that there are two regimes of charge transport in this material, according to the level of protonation to which it is prepared. Samples prepared at 10% and 20% protonation, the two lowest doping levels, display an electrical conductivity which is a strong function of temperature, suggestive of a charge carriers dependent upon some form of thermal activation. The variable range hopping mechanism, in one or two dimensions, has been used to describe the charge transport observed in PANi from previous studies [3,4,7]. However, none of the data in fig. 3.7 is characteristic of transport by VRH. At temperatures above 100 K the 10% and 20% samples can be described by the

fluctuation induced tunnelling (FIT) model, described in chapter 2. At lower temperatures, a fit to this data, based upon the form of equation 2.17, deviates significantly from the measured values.

A very different trend is revealed by samples prepared with protonation levels in the range between 30% and 60%. At low temperature, the conductivity still displays an activated behaviour. As the level of protonation is increased from 30% the decrease in conductivity at the lowest temperatures is much reduced, as illustrated in table 3.2 by the values of $\sigma(10)/\sigma(300)$ in each case. The most intriguing feature of the samples in this doping range is that the conductivity exhibits a peak at some temperature, T_p, according to the doping level, see table 3.2. In each case, as temperature increases above the value at which the peak occurs, the conductivity decreases slowly in a manner characteristic of classical metallic behaviour. A similar trend has been reported in other recent studies of PANi-CSA, protonated to the theoretical 50% maximum implied by the polysemiquinone radical cationic structure discussed in section 1.6. In these cases a peak in conductivity is observed at approximately 180 K [13,14].

The results presented in this thesis reveal that attempts to protonate PANi-CSA in excess of the 50% level result in enhanced electrical properties. At 60% doping, the magnitude of the conductivity is increased significantly. From measurements of the temperature dependence of conductivity, the peak value of conductivity occurs at a temperature significantly lower than that 50% doped samples Also, the reduction in conductivity at temperatures below the peak is less pronounced. This evidence implies that doping above the 50% level is capable of driving the PANi-CSA system far closer to true metallic behaviour than observed in any of the previous studies. Two explanations are suggested which may account for this unexpected behaviour.

1. Samples prepared with 50% doping do not react completely with the CSA added to the polymer. An excess of acid is required to protonate all the imine sites on the polymer chain. Of course there will be some error, perhaps 5% on the the exact dopant level within a sample.

2. Protonation of more than 50% of the nitrogen sites generates more conduction band states and allows a higher charge carrier density within the material.

Some further investigation is required to determine the optimum doping level for PANi, and, if the actual protonation level does exceed 50%, the chemical structure is adopted by the system.

From the results obtained it is evident that PANi-CSA is an example of a conductor close to a metal-insulator (MI) transition. As the level of doping is increased from 10% to 60% the trends in conductivity imply that there is a transition in the nature of charge transport from hopping/tunnelling due to localisation of carriers on some scale, to partial 'metallic' diffusion transport. The exact mechanism by which this transition occurs is unclear but two explanations are suggested.

In the first picture, it is assumed that in the doping process, protonation occurs completely at random resulting in a homogeneous distribution over the available chain sites. At low concentrations, the conduction band states formed at protonated sites would be widely separated and the interaction between neighbouring sites limited. Consequently, charge carriers would be localised and thus conduction by thermally activated hopping, VRH, would be expected. In this case, as the doping level is increased the average separation between conduction band states would decrease. Since this would have the effect of increasing both the charge carrier density and the strength of interaction between carrier states, an increase in conductivity and carrier mobility would be expected. At the highest doping levels, the high spatial density of doped sites may result in the formation of a conduction band containing both localised and diffuse electronic states, separated at some energy by a mobility edge (see section 2.3). According to Larkin and Khmel'nitskii [15] in a system such as this, where the Fermi level resides in the region of localised states, but is close to the mobility edge, the conductivity at low temperatures follows a power law dependence upon temperature i.e.:

$$\sigma(T) \propto T^{1/\eta} \qquad \text{eqn. 3.6}$$

Where $1 < \eta < 3$. At high temperatures, where conduction by carriers thermally excited to the band of delocalised states, conduction could be limited by phonon scattering, giving rise to the negative temperature coefficient of conductivity observed by experiment.

This first theory provides a useful way to describe the behaviour of the highly conductive samples of PANi-CSA i.e. those with 30% doping and above. However, the prediction of VRH transport at low doping levels is not supported by the experimental evidence presented in the previous subsection. The second theory which might account for the evolution of the conductive properties of PANi-CSA is that the doping process is not homogeneous on all scales. Protonation may occur in such a way that favours repeated doping of polymer chains or conglomeration of doped chains rather than an unbiased distribution, such that metallic islands are present when the material is cast as a solid film.

As the level of doping is increased in this system, the number and or size of metallic islands would be expected to increase. Hence an increase in the conductivity would occur due to three factors: The increased 'metallic' content of the sample, a reduction in the tunnelling/hopping distance between metallic regions and the increased charge carrier density. At some threshold level of doping, significant overlap of metallic islands could permit a large fraction of charge transport via percolation. This would allow the charge transport within the metallic regions, rather than the tunnelling process, to become apparent in the properties of the bulk material.

Perhaps the most important feature of highly doped PANi-CSA is that the dc electrical conductivity is capable of displaying a negative temperature coefficient over a significant portion of the temperature range, e.g. above 130 K in the case of 60% doped samples. This provides direct evidence for charge transport mechanisms similar to those in crystalline metals. In this study, the onset and progression of this 'metallic' nature has been observed through measurements made on PANi samples with different doping

levels up to and above the theoretical maximum of 50%. The origin of this character is now discussed in more detail.

The stark change in the behaviour of the conductivity between 20% and 30% doping suggests that there is a threshold within this range that marks the boundary between two charge transport regimes. At 30% doping, PANi-CSA is just able to display a metallic signature above a peak in conductivity at 270 K even the conductivity (approximately 90 Scm^{-1}) is much lower than that of a typical metal. It is interesting to note that the transition to pseudo-metallic behaviour occurs where samples have a conductivity of similar magnitude to that of the minimum metallic conductivity criterion discussed in section 2.3. This describes a minimum value of conductivity which a disordered conductor can have, before diffuse conduction band electronic states become localised and metallic charge transport can no longer be supported, it is in the range 100 to 300 Scm^{-1}. As the doping level is raised above 30%, the metallic character becomes more evident; the peak conductivity occurs at a progressively lower temperature as the conductivity samples and thus the metallic behaviour is displayed over a larger range of temperature.

So far, the term 'metallic' has been used to describe some of the aspects of electrical conduction in the PANi-CSA system, but what does this really mean ? What factors affect the charge transport within this material and how do they interact ?

Theoretically for a typical crystalline metal (e.g. copper, which has no superconducting phase) the maximum value of the electrical conductivity occurs at absolute zero temperature. Conduction is via diffusion of valence electrons, which occupy a partially filled energy band, through the crystal lattice. Charge transport is limited by electron scattering by impurities, and atoms disturbed from their equilibrium lattice positions due to thermal vibrations, i.e. phonon scattering. At high temperatures it is the latter of these processes which dominates and in this case, the vibration of atoms in the crystal lattice can be treated classically. It can be shown that the mean time between scattering events is inversely proportional to temperature and thus the resistivity of the metal has an approximately linear dependence above liquid nitrogen temperature. The

observation of a similar behaviour in PANi-CSA implies that charge transport is less restricted by the effects of insulating barriers, or the static disorder in the polymer structure than is the case in PANi-NMP (this is evident from a comparison of the conductivity of these two materials). In fact, there is evidence that PANi-CSA can exhibit a significant level of crystallinity [5,14,15,16] and this has been verified in recent X-ray studies on the 50% doped samples used to obtain the data presented in this thesis.

In crystalline regions of the polymer a precise phase order exists between adjacent polymer chains and this is expected to allow coherent electrical carrier transport along and between individual chains, i.e. the system is a regular polaron lattice structure. Hence, carrier delocalisation can occur in more than one dimension, on a scale larger than the average interchain separation. Therefore, the mean free path is not limited by scattering at interchain transfer events, but by phonon scattering due to thermal motion of the crystal lattice, or by molecular vibrational modes. The properties of the crystalline regions could therefore account for the 'metallic' trends observed in the conductivity of PANi-CSA. It should be noted that oriented polyacetylene [11,17,18] has a highly crystalline structure and a conductivity which although of much higher magnitude, depends upon temperature in a manner similar to that observed in PANi-CSA. Coherent order on the molecular scale is therefore necessary if organic conductors are to realise high values of conductivity. For example unstretched PANi-CSA is seven times more conductive than unstretched PANi-NMP.

Macroscopic charge transport within highly doped PANi-CSA is, however, not characteristic of that within a metal and even in the case of the most highly conductive samples, the conductivity decreases with decreasing temperature. It would therefore appear that there are at least two charge transport mechanisms that contribute to the properties of the bulk material. These must include a temperature activated process which results in the drop in conductivity seen in all cases at low temperatures. Secondly at high temperatures the effects of a temperature dependent scattering process (phonon scattering) becomes apparent. This suggests that there is some transport by 'metallic' diffusion. The balance between these two mechanisms in any particular sample appears

to depend upon the level of doping. This is evident from three aspects of the data presented in subsection 3.3.1, as the level of doping is increased:

1. Conductivity and mobility increase.

2. The onset of temperature dependent scattering occurs at lower temperatures. This is characterised by the temperature at which the peak conductivity is reached

3. The drop in conductivity at low temperatures is reduced, i.e. the ratio $\sigma(10\ K)/\sigma(300\ K)$ is diminished.

It is feasible therefore to view PANi-CSA as a composite material and invoke the heterogeneous conductor model described in section 2.6. In this case, it is proposed that there are two charge transport mechanisms at large in the polymer. These are metallic diffusion within the crystalline regions and temperature activated transport in the disordered or poorly doped regions, or grain boundaries which surround the crystallites.

Using this assumption it is possible to model the electrical conductivity for samples doped in the range 30% to 60%. The simplest approach is to consider the way in which each region of the sample contributes to the total resistivity of the bulk material. For the 'metallic' regions, at temperatures above 10 K phonon scattering gives rise to an approximately linear increase in resistivity with temperature [19]. For the disordered regions, it is more difficult to justify the choice of any one mechanism. However, since the FIT model provides the best explanation of the conductivity data from PANi-NMP (see section 3.2.2) it has been chosen for this composite model. The resistivity of the heterogeneous material is simply the sum of the individual resistivities due to each mechanism:

$$\rho = AT + B\left[\exp\left(\frac{-T_0}{T_1 + T}\right)\right]^{-1} \qquad \text{eqn. 3.7}$$

where A and B are fitting parameters and T_0 and T_1 are the characteristic temperatures in the FIT model (see section 2.4). This expression has been used to generate curves that are a close fit to the conductivity data, see fig 3.11. The parameters for each curve are presented in the table 3.4

Sample % CSA	A ΩcmK^{-1}	B Ωcm	T_0 K	T_1 K
30	1.12×10^{-5}	4.49×10^{-3}	188	54
40	1.06×10^{-5}	2.93×10^{-3}	186	92
50	1.01×10^{-5}	1.48×10^{-3}	332	172
60	6.62×10^{-6}	9.31×10^{-4}	519	332

Table 3.4. Parameter values for the curve fits to the conductivity data from highly doped PANi-CSA.

Although it is impossible to prove that charge transport really is governed by the particular mechanisms chosen for this heterogeneous model, the combination of FIT with phonon scattering provided far superior fits to other models; e.g. an expression with a phonon scattering term and a temperature activated term modelled on VRH, or a power law re equation 3.6. To some extent, therefore, PANi-CSA appears to provide an example of a heterogeneous material in which there are crystalline, 'metallic' regions separated by disordered regions through which charge transport is via a tunnelling process.

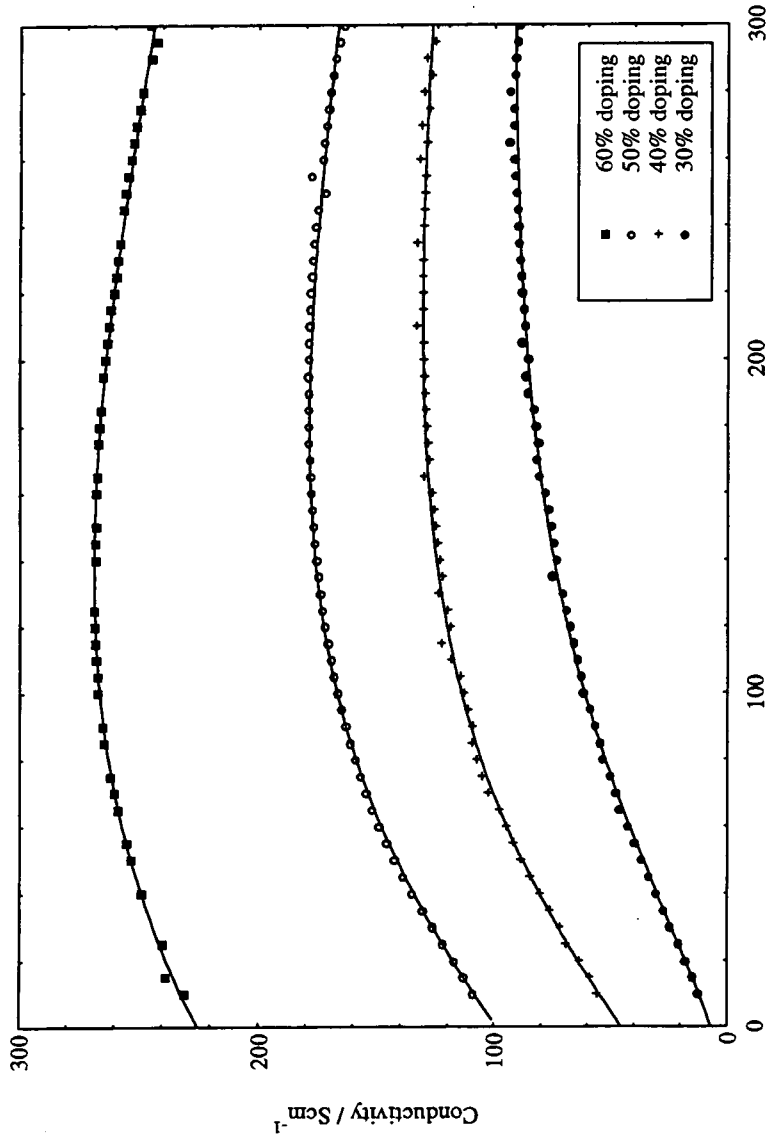

Fig. 3.11 Curve fits to the conductivity data from 'metallic' PANi-CSA, generated using a heterogeneous conductor model.

By variation of the level of protonation it is possible to alter the balance between these conduction mechanisms, presumably as the 'metallic' regions vary in number or size. The metallic character evident in PANi-CSA doped at 50% [13,14] can be enhanced by exceeding this theoretical level.

References

[1] H.C. Montgomery, *J. Appl. Phys.* **42** (1971) p. 2971

[2] B.F. Logan, S.O. Rice & R.F. Wick, *J. Appl. Phys.* **42** (1971) p. 2975

[3] Y.W. Park, Y.S. Lee, C. Park, L.W. Shacklette & R.H. Boughman, *Solid State Comms.* **63** (1987) p.1063

[4] F. Zuo, M. Angelopoulos, A.G. MacDiarmid & A.J. Epstien, *Phys. Rev. B* **36** (1987) p. 3475

[5] J. Joo, E.J. Oh, G. Min, A.G. MacDiarmid & A.J. Epstein, *Synth. Met.* **69** (1995) p. 251

[6] Z.H. Wang, C. Li, E.M. Scherr, A.G. MacDiarmid & A.J.Epstein, *Phys. Rev. Lett.* **66** (1991) p. 1745

[7] S.K. Jeong, J.S. Suh, E.J. Oh, Y.W. Park, C.Y. Kim & A.G. MacDiarmid, *Synth Met.* **69** (1995) p. 171

[8] A.P. Monkman & P.N. Adams, *Solid State Comms.* **78** (1991) p. 29

[9] A.J. Milton, *Ph.D. Thesis*, University of Durham 1993, A.J. Milton, N. Bernhoeft & A.P. Monkman, to be submitted

[10] A.J. Heeger, *Faraday Discuss. Chem Soc.* **88** (1989) p. 1

[11] Y.W. Park, A.J. Heeger, M.A.Druy & A.G. MacDiarmid, *J. Chem. Phys.* **73** (1980) p. 946

[12] L. Abell, S. Pomfret, E.R. Holland, P.N. Adams & A.P. Monkman, Society of Plastic Engineers, conference proceedings (1996) submitted for publication

[13] M. Reghu, Y. Cao, D. Moses, & A.J. Heeger, *Phys Rev. B* **47** (1993) p. 1758

[14] R. Menon, C.O. Yoon, D. Moses, A.J. Heeger, & Y. Cao, *Phys. Rev. B* **48** (1993) p. 17 689

[15] A.I. Larkin & D.E. Khmelnitskii, *Sov. Phys. JETP* **56** (1982) p. 647

[16] A.J. Epstein & A.G. MacDiarmid, *Synth. Met.* **69** (1995) p. 179

[17] Y.W. Park, C. Park, Y.S. Lee, C.O. Yoon, H. Shirakawa, Y. Suezaki & K. Akagi,*Solid State Comms.* **65** (1988) p. 147

[18] M. Ahmed, A.B. Kaiser, S. Roth & M.D. Migahed, *J. Phys. D : Appl Phys* **25** (1992) p. 79

[19] J.S. Dugdale, from "The Electrical Properties of Metals and Alloys" Edward Arnold, London (1977)

CHAPTER 4

Thermoelectric Power

4.1 Theory Of Measurement

In the measurement of electrical conductivity, the methods employed are said to be direct i.e. all the parameters used to calculate a final data point are just simple properties of the sample under test e.g. physical dimensions and electrical resistances. An entirely different approach is necessary where thermoelectric effects are concerned. Direct measurement of the thermoelectric e.m.f. generated by a material is impossible because there is always an additional component contributed by the thermal gradients in the connecting wires. Any method for measuring the absolute thermopower of a material must therefore involve a theoretical consideration of the thermoelectric properties of all components of the measurement circuit.

The technique used to obtain the thermopower data presented in this thesis required samples to be included as part of a thermoelectric network, as illustrated in fig. 4.1. The approach is similar to that detailed in [1]. This arrangement can be treated as two separate circuits with common nodes at the two junctions made to the sample. These circuits are the copper-sample-copper loop, with output e.m.f. V_1 and the constantan-sample-constantan loop which develops an output e.m.f. V_2. Making use of equation 2.20, the e.m.f. generated at the ends of the copper wires by the first circuit can be written as:

$$V_1 = \int_{T_{Ref}}^{T_1} S_{Cu}(T)dT + \int_{T_1}^{T_2} S_{PA}(T)dT + \int_{T_2}^{T_{Ref}} S_{Cu}(T)dT$$

eqn. 4.1

Where $S_{Cu}(T)$ and $S_{PA}(T)$ are the respective Seebeck coefficients (thermopowers) for copper and the sample material, at temperature T. T_{Ref} is a reference temperature at

which the outputs of both thermal circuits are anchored. If this value is constant equation 4.2 simplifies to:

$$V_1 = \int_{T_2}^{T_1} S_{Cu}(T)dT + \int_{T_1}^{T_2} S_{PA}(T)dT \qquad \text{eqn. 4.2}$$

Since the Seebeck coefficient is, in general, a slowly varying function of temperature, if $|T_1-T_2| < 1$ K the parameters $S_{Cu}(T)$ and $S_{PA}(T)$ can be treated as constants. With this assumption it is possible to re-write equation 4.2 in the form:

$$V_1 = [S_{PA}(T) - S_{Cu}(T)]\Delta T \qquad \text{eqn. 4.3}$$

where $\Delta T = T_2 - T_1$

A similar analysis of the constantan-sample-constantan circuit yields:

$$V_2 = [S_{PA}(T) - S_{CO}(T)]\Delta T \qquad \text{eqn. 4.4}$$

where $S_{CO}(T)$ is the Seebeck coefficient of constantan. Manipulation of equations 4.3 and 4.4 yields an expression for the Seebeck coefficient of the sample:

$$S_{PA}(T) = M[S_{Cu}(T) - S_{CO}(T)] + S_{Cu}(T) \qquad \text{eqn. 4.5}$$

where $M = V_1 / (V_2 - V_1)$ eqn. 4.6

Therefore by making measurements of V_1 and V_2 over a range of values of ΔT it is possible to evaluate the sample thermopower. Tables of $S_{Cu}(T)$ and $S_{CO}(T)$ were obtained from suitable sources [2,3]. The factor M is best obtained from the gradient of

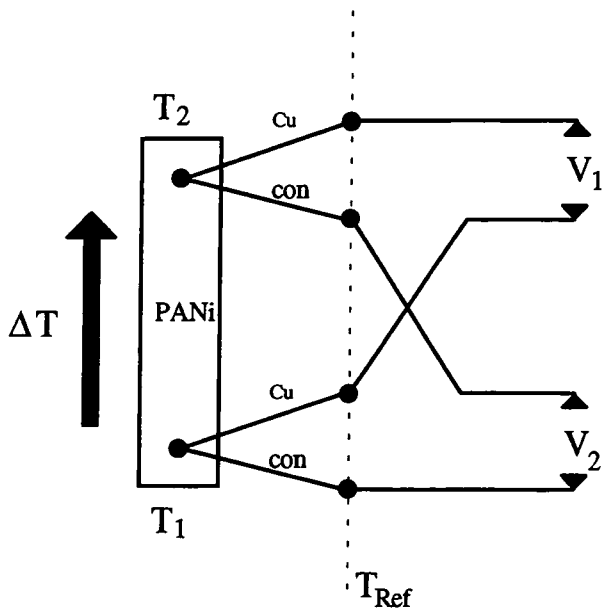

Fig. 4.1 Schematic diagram of the thermoelectric circuit employed for thermopower analysis.

V_1 versus $V_2 - V_1$, since in this way errors due to constant offsets in the signal voltages do not affect the accuracy of the technique.

An important feature of this method is that no knowledge of either ΔT or the temperatures T_1, T_2, or T_{Ref} are required explicitly. The calculation of the sample thermopower depends solely upon the relationship between the two voltage signals and the thermoelectric properties of the four wires connected directly to the sample. Only the average temperature of the sample is required so that the thermopower can be charted as a function of absolute temperature. The method is of sufficient accuracy given that the following conditions are met.

1. The maximum temperature difference ΔT extending across any sample must not exceed 1K, so that the approximations used to obtain equation 4.3 remain valid.

2. The reference junctions remain at equal, constant temperature during acquisition of all V_1, V_2 data set pairs used to calculate a particular thermopower point.

3. The instruments used to measure V_1 and V_2 have input impedances which far exceed that of the two sample circuits so that errors due to current flow are not significant.

The third condition is especially important because the thermopower measurement is assumed to be a zero current process. In addition to this, if the impedance of the voltage measuring instruments is too low, the two circuits cannot be considered independent and current flows around the circuit formed by the two copper-constantan junctions and the voltmeters themselves. In this case, spurious voltage readings occur which are independent of the presence of a sample.

4.2 Experimental Techniques

In order to facilitate measurement of the thermopower of conductive polyaniline films via the technique described in section 4.1, a suitable apparatus had to be designed and assembled. To ensure satisfactory operation, the following criteria were set.

1. To ensure accurate determination of the factor M (equation 4.6), a sufficient quantity of voltage data must be obtained. In addition, due to the small typical size of thermoelectric signals, voltage resolution should be better than 0.1 μV.

2. The temperature gradient applied to the sample must be variable, but not allowed to exceed a maximum of 1K. Also accurate control of the average sample (base) temperature is required.

3. Good electrical and thermal contact must be maintained between the sample and connecting wires at the two contact nodes shown in fig 4.1

The volume of raw data collection and extensive parameter control involved in such a system required the use of computer control to automate the measurement process. The architecture of the system developed to obtain the results presented in this thesis is shown in fig. 4.2.

Samples under test were contained in an Oxford Instruments MD4 cryostat, with temperature monitoring and control provided by an Oxford Instruments ITC4. Using liquid nitrogen as a refrigerant it was possible to investigate the thermopower of samples in the temperature range from 80 to 300 K. With a full charge of cryogen, the system was capable of running for at least 16 hours at any temperature. During operation, the sample chamber was evacuated, and a small quantity of dry helium gas

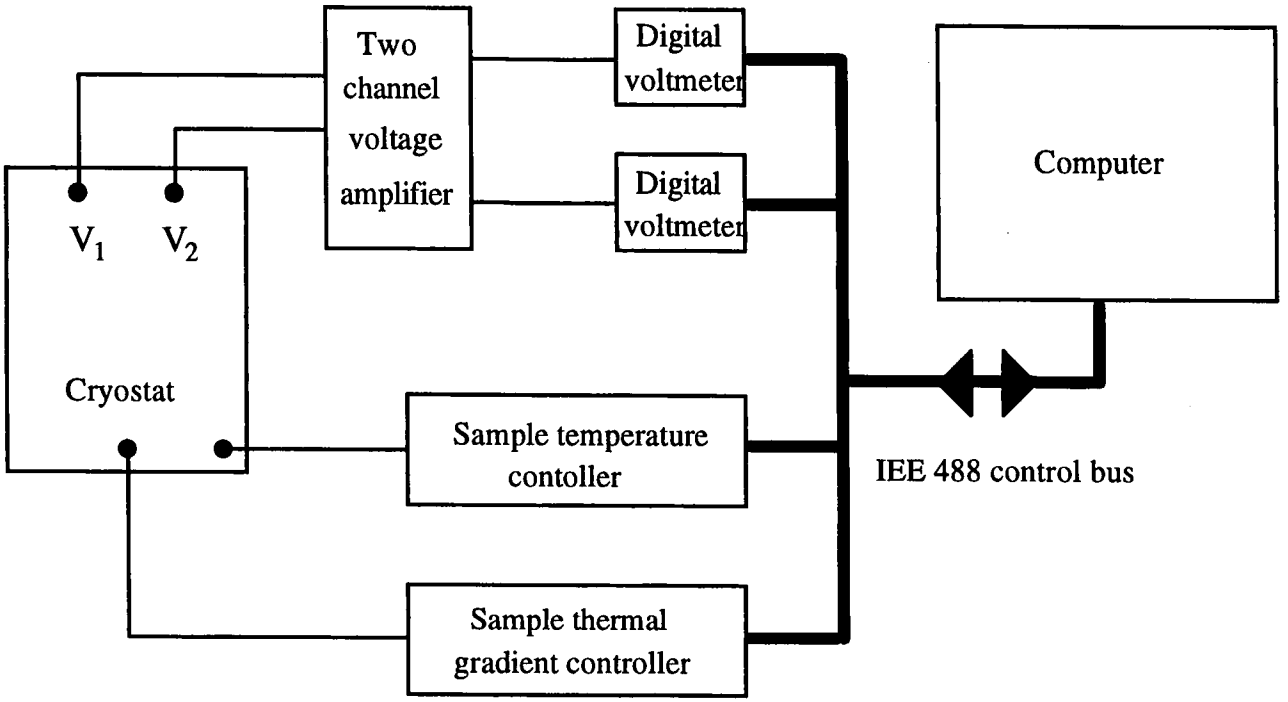

Fig. 4.2 Schematic diagram of the computer controlled thermopower measurement system

was admitted to provide a medium for heat transfer from the sample probe to the cryostat heat exchanger (typical pressure 10^1 Torr).

All instruments were connected to an IBM compatible 80286 PC via an IEEE 488 interface bus. This allowed automation of the voltage data acquisition sequence, sample temperature gradient control and control over the sample base temperature. Control software was written in Turbo Pascal to perform the required interfacing and data processing functions.

The greatest difficulty presented by the chosen technique was that of making accurate measurements of the two slowly varying dc signals, V_1 and V_2 as the thermal gradient applied to the sample is changed. It was initially thought that these could be measured by direct connection of the thermoelectric circuit to two precision digital voltmeters (Keithley DVM, model 195). These instruments provide adequate resolution (0.1 μV) and high input impedance (100 MΩ). However, thermal fluctuations and electrical interference induced in the leads connecting to the cryostat probe head led to spurious dc offset voltages and noise levels of a magnitude comparable to that of the expected signal.

It was therefore deemed necessary to amplify the voltage signals, with the physical link between the cryostat probe and the preamplifier made as short as possible in order to reduce problems due to thermal offsets and noise pickup.
In this way it was possible to increase the signal to noise ratio in the longer leads needed to carry signals to the voltmeters, in addition to this, the amplification increased the resolution of the measurements. The essential requirements of a dc coupled voltage amplifier for this task are:

1. High input impedance, $R_{in} > 100$ MΩ.

2. Low input offset voltage $V_{io} < 1$ μV, low offset drift and low noise.

3. High rejection of ac noise.

Several approaches were tried before the author designed the circuit, illustrated in schematic form in fig. 4.3. This circuit consists of two stages, the first of which is a non inverting amplifier with a voltage gain of 100. This was constructed using a self stabilising operational amplifier (op-amp) IC, the IC 7650, which offers an extremely low input offset voltage, high stability against thermal drift and a very high input impedance. The output of the first stage is fed into an ac noise rejection stage with overall gain 1/2, based around a standard low noise op-amp (TL 071). A low pass filter removes any noise generated by this circuit at frequencies above 10 Hz before the output is fed to a Keithley DVM.

Two such amplifiers were built, each with an independent, voltage regulated power supply so that the two voltage signals, V_1 and V_2 could amplified and measured separately. Careful design and construction of the circuits ensured that both amplifiers were of matched performance, independent and isolated from earth; no common connection between the two measurement circuits could be allowed, except where contact is made to the sample.

The accuracy of thermopower measurements obtained with this technique is dependent upon the quality of the electrical contacts in the circuit, particularly those at the sample surface. These must provide good thermal and electrical junctions to the sample at all times if the thermoelectric analysis of the system, presented in section 4.1 is to be accurate. In addition, good electrical contact must be maintained to ensure the minimum level of noise, given that typical signal levels are of the order of microvolts.

The sample holder/contact probe arrangement consisted of a flat copper plate, having a split along its centre to form a two bladed fork. This was mounted at the end of the cryostat cold finger, to a copper block containing a rhodium-iron temperature sensor and heating element which provided the means for measurement and control of the sample base temperature.

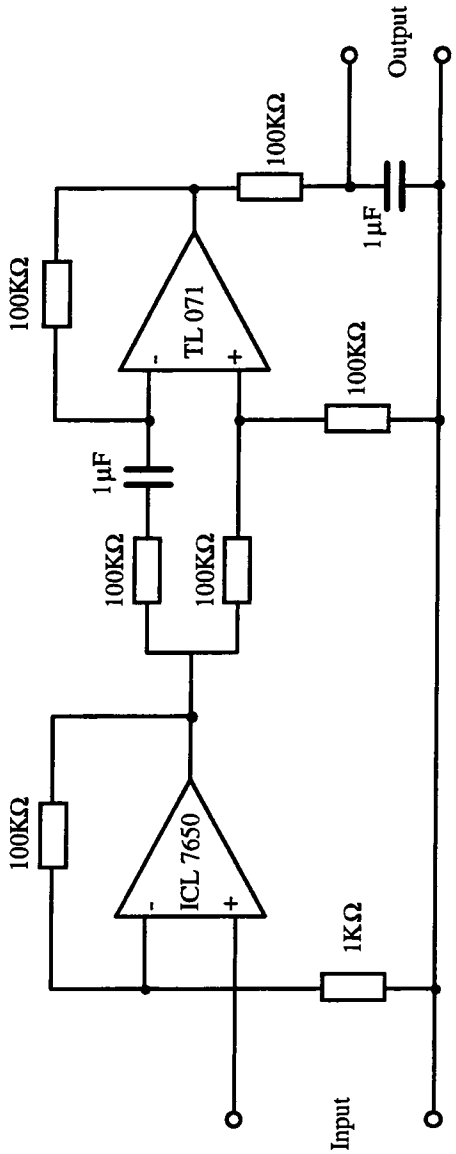

Fig. 4.3 Schematic diagram for the low noise dc preamplifier.

Electrical and thermal contacts to the sample were established by two copper-constantan thermocouple junctions, one to hold each end of a suitably prepared sample onto each blade of the probe so that it traversed the split. Samples were cut from a large film to typical dimensions of approximately 10 mm x 5 mm, though the exact size is not critical, nor is it required for the calculation of thermopower. The contacts were maintained by pressure from a PTFE plate bolted to the probe unit. A thin sheet of mica provided electrical insulation between the sample and the copper probe plate.

The two copper and two constantan wires were led approximately 10 cm up the cold finger to junctions which served as the constant temperature reference point (fig. 4.1). Four enamelled copper wires then transmitted the two signal voltages to a junction at the top of the cold finger from which they were transferred to the pre-amplifier via low noise screened cable. The cryostat body and cold finger chassis were earthed to ensure adequate screening of the unshielded wiring within the cryostat system. Also, routing of the signal cables along the cold finger was chosen carefully to provide maximum isolation against interference from the additional wiring required for operation of the cryostat.

An important note regarding the electrical junctions made to the surface of samples of polyaniline is that the polymer is susceptible to an electrochemical reaction with copper, resulting in a degradation of the film around the contact area. To prevent this, the two thermocouple contacts contained in the sample probe were bound with fine platinum wire. Reference measurements made on samples of aluminium and magnesium revealed that no discernible error was introduced as a result of this modification. For polyaniline samples, no degradation was observed. The platinum surfaces were polished with fine emery paper and cleaned with isopropanol to ensure good contact to each new sample.

Two purpose-built heating elements were attached, one to the underside of each blade of the probe. This allowed independent heating of the blades, thus enabling a thermal gradient to be established across the sample mounted between them.

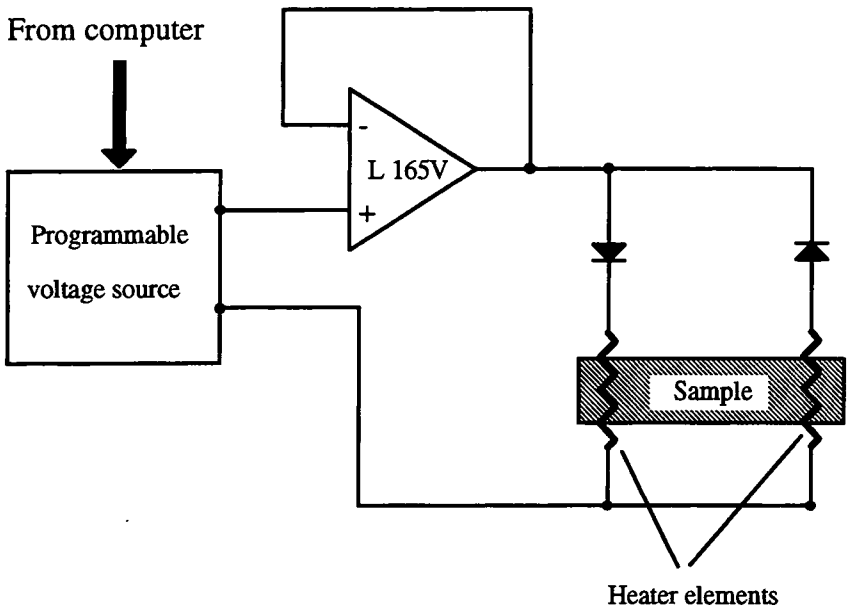

Fig. 4.4 Schematic diagram of the thermal gradient control system.

Stretch oriented samples could be prepared and mounted so that the thermal gradient extended either parallel or perpendicular to the axis of polymer chain alignment.

The power supplied to the two heating elements (and thus the size of the temperature gradient) was controlled by the computer software via A Hewlett Packard HP 59501 programmable bipolar dc voltage source. The output from this unit was fed through a current amplifier consisting of a power op-amp (L 165V) in a voltage follower configuration, to provide adequate power for the heating circuits. The two heating elements on the probe were connected to the supply as per the diagram in fig. 4.4. The diodes included in the circuit ensure that only one element receives power at a time, so that a thermal gradient can be applied to the sample. In this configuration one side of the sample is heated when the power supply output is positive with respect to ground, the other being heated when the output is negative.

This simple arrangement allows reversal of the direction of the direction of the temperature gradient to be achieved without the need for a computer controlled changeover switch. The software procedure written to control the output of the heater supply was programmed to perform a sweep such that the temperature gradient was varied up and down, first in one direction, then in the other, in a 'sawtooth' pattern over a period of approximately 6 minutes. The voltage source, stepped at 20 mV intervals to +/- 6 V, was programmed to avoid values in the range -1 V to +1 V, the diode forward voltage drop, in order to prevent a 'dead portion' during each sweep where no current could pass to either element. In this way, efficient control of the thermal gradient was achieved.

Acquisition of data was performed entirely by computer via the instruments connected to the IEEE 488 communication bus. Software was written to allow a fully automated scan of thermopower over some of temperatures (between 80 and 300 K) specified by the operator at the start of each experiment. Determination of the sample thermopower at one particular temperature interval involved the following steps:

1. Programming of the temperature controller with the appropriate base temperature and monitoring of the sample temperature until the set value is reached and under stable control.

2. Performing one cycle of the thermal gradient variation procedure whilst making simultaneous measurements of V_1 and V_2. To ensure sufficient accuracy, these values were sampled 400 times, each pair read at intervals of one second over the course of the gradient cycle.

3. The factor M used to calculate the sample thermopower in equation 4.5 is evaluated by linear regression, it is the gradient of V_1 with respect to $V_2 - V_1$. The sample thermopower proper is calculated using equation 4.5 and appropriate thermopower data for copper and constantan retrieved from an array in the program. This value is then saved to a previously specified file on disk.

This procedure was run four times at each chosen sample temperature in order that thermopower value could be calculated with greater certainty. Multiple measurements also ensured that an anomalous result from one particular scan could be ignored if necessary, without complete loss of data at that particular temperature. Occasionally the voltage data could be corrupted by noise 'spikes' carried on the mains electrical supply, which affected the highly sensitive amplifiers. For this, reason the apparatus was typically run overnight, out of normal working hours when the electrical supply was comparatively noise free. A typical scan of thermopower over the temperature range from 100 to 300 K would take approximately 14 hours, which could easily be completed under these favourable working conditions.

4.3 Thermopower Of Highly Doped PANi-NMP

As described in the previous chapter, stretching of PANi-NMP samples to induce alignment of the polymer chains enhanced the conductivity along the axis of elongation. As a result of this procedure, the samples were electrically anisotropic. To obtain more information about the effect of chain alignment upon charge transport properties, thermopower measurements were made on stretch oriented (elongated by 500%) and unstretched samples of highly doped material. The results from this study have also formed the basis of a recent publication [4].

4.3.1 Results

Thermoelectric power was measured over the temperature range 100 K to 300K. In the case of oriented samples, the thermopower components parallel and perpendicular to the axis of elongation were measured using separate sections from a common sample. A plot of typical results is shown in fig. 4.5.

The data obtained for the thermopower measured parallel to the elongation axis in stretched samples (parallel thermopower) have a marked linear dependence upon temperature. The data are positive throughout the available temperature range and rise from $\approx 2\ \mu VK^{-1}$ at 100 K to $\approx 6\ \mu VK^{-1}$ at 300K. They represent a typical result for the parallel thermopower component, which displayed excellent reproducibility between samples. Some similarity to data obtained from highly doped 'new' polyacetylene is evident [5,6,7,8].

Perpendicular to the stretch axis, thermopower displays a strikingly different behaviour. At the low end of the temperature range, thermopower is negative ($\approx -0.7\ \mu VK^{-1}$) and decreases in magnitude with increasing temperature. A crossover to positive values occurs at 220 K and as temperature is increased, the thermopower rises, reaching $+0.6\ \mu VK^{-1}$ at 300 K.

The thermopower of unstretched PANi-NMP is similar in form to the perpendicular thermopower component of oriented samples. However, no change of sign

is observed and values are all negative, but with a positive slope (-1.5 μVK^{-1} at 100 K to 0.5 μVK^{-1} at 300 K).

The anisotropic nature of the thermopower of stretch oriented PANi-NMP bears some resemblance to the data presented by Wang et. al. [9], although there are some subtle differences. Firstly, the parallel data presented in this thesis have a temperature dependence closer to linear behaviour than any comparable data in [9]. Secondly, a comparison of the perpendicular data sets from fig. 4.5, and [9] reveals a different behaviour of this quantity. In the case of [9], the perpendicular data at lower temperatures (100 to 200 K) has a U shaped temperature dependence. Additionally, at higher temperatures (200 300 K) the positive gradient of the perpendicular thermopower increases, tending toward a slope similar to that of the parallel data, much steeper than for the data presented in fig. 4.5.

4.3.2 Discussion

The observation of a strong anisotropy in the thermopower of stretch oriented PANi-NMP suggests that the microscopic electrical properties of this material are strongly dependent upon the order at a microscopic level. This should not be surprising, given that the typical electrical conductivity anisotropy is of order 10 for samples elongated by 500%.

The linear dependence of the parallel component of thermopower fits the form of equation 2.29 closely. This behaviour indicates, to first order, that carrier transport along the direction of alignment of the polymer chains contains a large contribution due to metallic diffusion [10]. It is possible that, for thermal transport at least, the alignment of polymer chains within a film allows the character of 'metallic' transport to dominate along the axis of orientation.

This view is supported by the enhanced electrical conductivity which is observed in the direction parallel to the stretch axis of oriented films. The temperature dependence

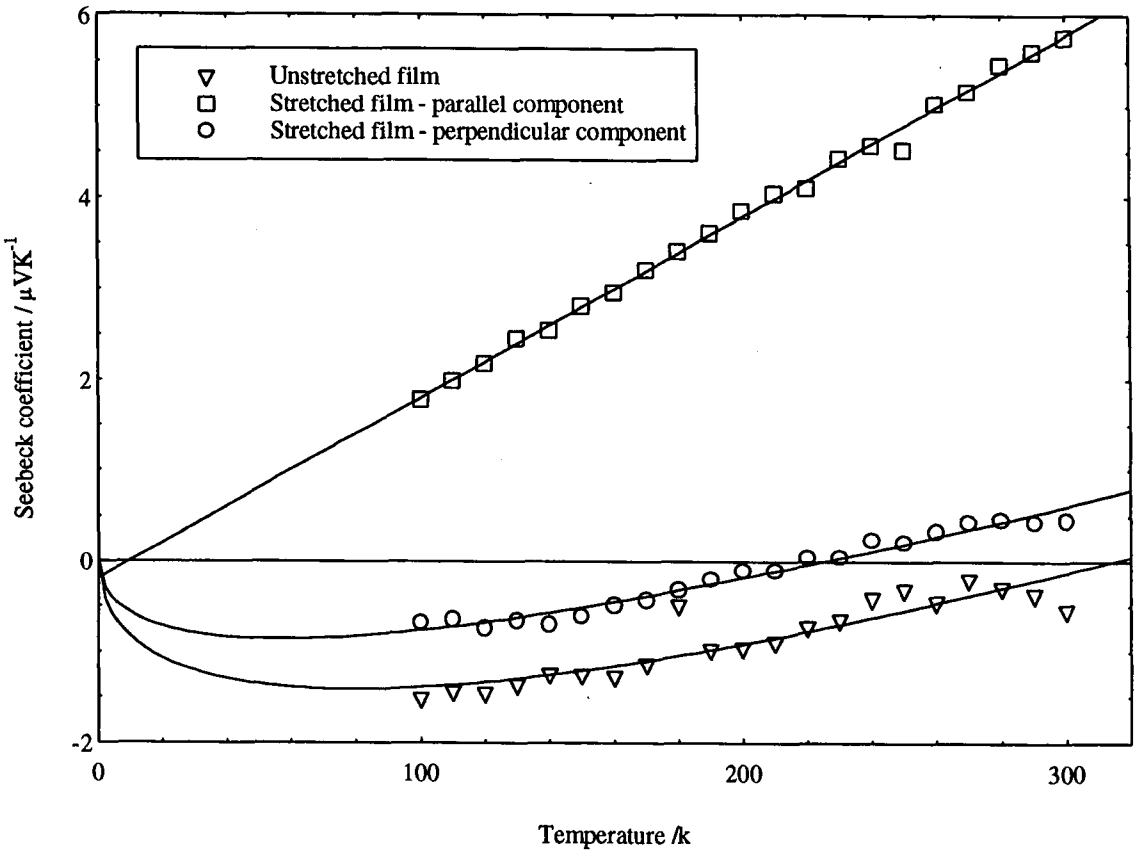

Fig. 4.5 Thermopower of Highly doped PANi-NMP versus temperature from samples subjected to 500% stretch alignment, and unoriented samples.

of the electrical conductivity parallel and perpendicular to the axis of alignment are remarkably similar, as revealed in fig 3.5.1. These data sets reveal a trend which is not typical of metallic conduction, nor does the conductivity appear to tend to zero at zero temperature and is therefore not commensurate with the model for variable range hopping (VRH). This is in contrast with the conductivity data presented by Wang et. al. which suggest transport via 3-D VRH in their material [9].

However, the temperature independence of Pauli magnetic susceptibility in PANi-NMP, prepared to the same specifications as that used to obtain the results presented for thermopower in this thesis, provides more evidence for the existence of 'metallic' electronic states [11]. The evidence for metallic character which these results provide implies that the charge carrier density is relatively invariant with temperature. In turn this suggests that the temperature dependent variation of the electrical conductivity cannot be explained by considering the polymer to be a conventional semiconductor e.g. silicon. Instead, the electrical properties of polymeric conductors are widely considered to be a function of structure or order within the material via the effect which this factor has upon the communication of charge along and between polymer chains [10,12]. The low magnitude of the parallel thermopower presented in this thesis, compared with that for polyacetylene e.g.[8] and in some cases for PANi, [13,14] can be attributed to a density of states function with little variation (with respect to energy) near the Fermi level.

In contrast to the parallel data, the thermopower observed perpendicular to the axis of orientation (perpendicular thermopower) and that of unstretched samples is difficult to interpret. In the simplest terms, however, the results suggest the influence of a different charge transport mechanism in these two cases i.e. not metallic diffusion. A comparison of these two sets of data provides some indication that there is a similar balance of transport mechanisms at work, despite the difference in order of the two samples. How might this arise?

Consider, at the molecular level, an unstretched film of PANi-NMP. It is envisaged that the tangled matrix of chains leaves very little opportunity for charge to travel significant distances along individual polymer chains. As a result of this, the

interchain transport mechanism will dominate the bulk properties of the material. In a stretch oriented film, there is partial alignment of the polymer chains along the axis of elongation. For electrical transport of charge in the direction perpendicular to this axis it is logical to assume that interchain transport has a larger influence over the bulk properties than the intrinsic properties of the polymer chains, just as expected in the unstretched samples.

In the theoretical limit of a perfectly aligned sample i.e. all polymer chains lie along one axis it might be expected that in the direction perpendicular to the alignment, the charge transport would display the characteristics of VRH or tunnelling mechanisms due to quasi-one-dimensional charge localisation. However, in the case of the samples studied in this thesis, perfect alignment of the chains cannot be achieved. This is apparent from the low value of electrical conductivity anisotropy of chain aligned PANi-NMP, when compared to examples of other polymers subjected to stretch orientation e.g. polyacetylene [15]. For this reason, it is possible that the thermopower of unstretched films and the perpendicular component measured in stretched samples both contain contributions due to 'metallic' diffusion and interchain transfer processes.

A simple model has been constructed in an attempt to describe the behaviour of the thermopower of PANi-NMP samples. This is based upon the heterogeneous model for electrical transport proposed by Kaiser, which is described in chapter 2. Application of this model to thermoelectric properties reveals that the thermopower of a material can be considered as the sum of components generated by each particular transport mechanism, as per equation 2.37.

In the case of the parallel thermopower data, a linear interpolation, included in fig 4.5, results in an excellent fit to the measured values. This supports the argument that transport parallel to the chain alignment axis is predominantly governed by metallic diffusion of the form described in section 2.5. To describe the thermopower data obtained perpendicular to chain alignment and also for unstretched films of PANi-NMP, a composite model has been constructed. The general expression used to produce the line fits presented in fig 4.5 for these two cases is shown below:

$$S = AT - BT^{1/2} \qquad \text{eqn. 4.7}$$

Where A and B are fitting parameters and T is the absolute temperature. The term proportional to temperature is included to model a 'metallic' contribution to thermopower, which could arise if some fraction of charge transport is via intrachain diffusion, or if there is strong interaction of the electronic states between some polymer chains. The term in $T^{1/2}$ is included to account for interchain hopping between states or chains which are localised as a result of disorder in the polymer structure. This is based upon the temperature dependence of thermopower which arises where charge transport is via VRH, re equation 2.32. Both the 'unstretched' and 'perpendicular' data sets in fig 4.5 have an acceptable correlation to the line fits based upon equation 4.7. However, data is required at temperatures below 100 K to test the validity of this model.

In the previous chapter, the idea that orientation of the polymer chains induces an anisotropy in the carrier mean free path, was introduced. It is now proposed that this factor might offer a partial explanation for the anisotropy observed in the thermopower of stretch oriented PANi-NMP, in addition to the more obvious consequences for the conductivity. As described in section 2.5, diffusion thermopower can be expressed in a general form (equation 2.29) to reveal a dependence upon the mean free path ℓ, and the energy dependence of the area of the Fermi surface. The reader is referred to section 2.5 for a full description of the parameters in this expression. For convenience, the equation is written again below:

$$S = -\frac{\pi^2 k^2}{3|e|} T \left[\frac{1}{A}\frac{\partial A}{\partial E} + \frac{1}{\ell}\frac{\partial \ell}{\partial E} \right]_{E=E_F} \qquad \text{eqn. 4.8}$$

In the case of stretch oriented PANi-NMP the carrier mean free path perpendicular to the axis of chain alignment is expected to be significantly shorter than the mean free path in the parallel direction. This factor might be expected to have some bearing upon the size of the component arising from diffusion transport which contributes to the thermopower in directions parallel and perpendicular to the alignment axis. If as described in section 2.5, the first term (within the square brackets) in the above

equation is negative, and the second term positive then for large ℓ the expression will yield 'large' positive thermopower. For short ℓ, the second term, which is inversely proportional to ℓ would have a greater magnitude, so the overall magnitude of the diffusion thermopower would be reduced.

The precise effect which an anisotropic mean free path could exert upon thermopower depends upon the relative sizes of the two terms contained in square brackets in the above equation. Unfortunately, there is no way to make a quantitative analysis of the factors contained in this expression. However, the contrast in the size of the positive gradient of thermopower versus temperature between the parallel and perpendicular data suggests that there is a much larger diffusion thermopower in the parallel case. This lends some qualitative support to the theory that mean free path variations are partly responsible for the anisotropy observed in the thermopower of stretch oriented films of PANi-NMP.

The negative values of thermopower observed at low temperatures (<200 K) in the perpendicular data from stretched samples and over the whole experimental range for unstretched films are more difficult to explain. The heterogeneous model used to generate line fits to these results includes a negative term which models a contribution from VRH or tunnelling.

Another possibility is that effects due to electron-phonon (E-P) interactions make a contribution to thermopower in addition to diffusion. This effect, termed phonon drag, is evident in the thermopower vs. temperature curves of many metals, e.g. copper, as a peak or 'shoulder' in the region below the Debye temperature of the material. The sign of such contributions (where conduction is by electrons) are negative for 'normal' E-P interactions, i.e. electrons given additional momentum along the direction of a thermal gradient by collisions with phonons. If the E-P interaction is via Umklapp or backscattering processes, the phonon drag thermopower is positive. However, there is little evidence for phonon drag effects from any thermopower studies on conductive polymers, except perhaps for highly conductive polyacetylene [8,10].

It is really necessary to test the explanations proposed for some features of the thermopower of the PANi-NMP samples presented in this section by investigation at much lower temperatures. The minimum temperature of 100 K, imposed by the limitations of the experimental apparatus placed a significant restriction on the detail revealed by thermopower results, in comparison to the conductivity data presented in chapter 3.

4.4 Thermopower Of PANi-NMP vs. Doping

The thermopower measurements made on stretched films of highly conductive PANi-NMP presented in the previous section, revealed that electronic transport in parallel to the polymer chain alignment has some character akin to that of metals. To probe this behaviour in more detail, the thermopower of similar samples was investigated as a function of the level of sample doping.

4.4.1 Results

Films of emeraldine base, stretch oriented by 500% elongation were doped by immersion in an aqueous solution of methane sulphonic acid (MSA) for four hours. To obtain samples with different levels of protonation, four acid solutions were prepared at concentrations (by volume) of 0.2%, 1%, 5%, and 15%. The room temperature conductivity of each sample, parallel to the axis of stretch orientation was measured on its removal from the doping solution. Typical values for each case are presented in the table below:

Doping Solution		Conductivity
% MSA	pH	Scm^{-1}
0.2	1.8	0.05
1	1.0	50
5	0.3	300
15	-0.2	300

Table 4.1 Doping preparations of PANi-NMP.

The data reveal a sharp transition to a conductive state for doping solutions with pH < 2. This is in general agreement with the results presented by Park et. al. in a study of unoriented PANi, although the highest conductivity values presented here are

approximately ten times that of comparable samples in [13]. This difference is thought to arise from a number of factors. Firstly, the samples used in [13] were unoriented and secondly, their conductivity was measured under vacuum, so the removal of water will have had an adverse effect on the values obtained.

Investigation of the of the films doped in different concentrations of MSA solution was restricted to determination of the thermopower developed parallel to the axis of polymer chain alignment. This is the component which provides most evidence for diffusion thermopower, which in turn indicates the presence of metallic states or regions within the polymer [10]. A set of typical results is shown in fig. 4.6. Unfortunately, samples prepared at the lowest doping level (0.2% MSA) presented a very high resistance in the thermopower measurement circuit. Consequently this introduced a large degree of noise into the system, particularly at low temperatures where the sample conductivity decreased still further. It is for this reason that data is only presented over a limited temperature range (200 to 300 K) in this case. The results show a clear trend towards larger values of thermopower as the level of doping was decreased. The linear dependence of thermopower upon temperature, seen in the most heavily doped sample (15% MSA) was retained in the samples doped in 5% and 1% MSA, though the gradient of the lines increases as the protonation level is reduced.

4.4.2 Discussion

The results obtained suggest that the metallic character of stretch oriented PANi-NMP observed parallel to the chain alignment in highly conductive samples is evident even at low levels of protonation, despite the marked reduction in room temperature conductivity. This is inferred by the linear dependence upon temperature of the thermopower of samples prepared from 1%, 5% and 15% doping solutions, which matches the form of diffusion thermopower (equation 2.28). Whilst the data from samples prepared in 0.2% doping solutions are included for comparison, the limited

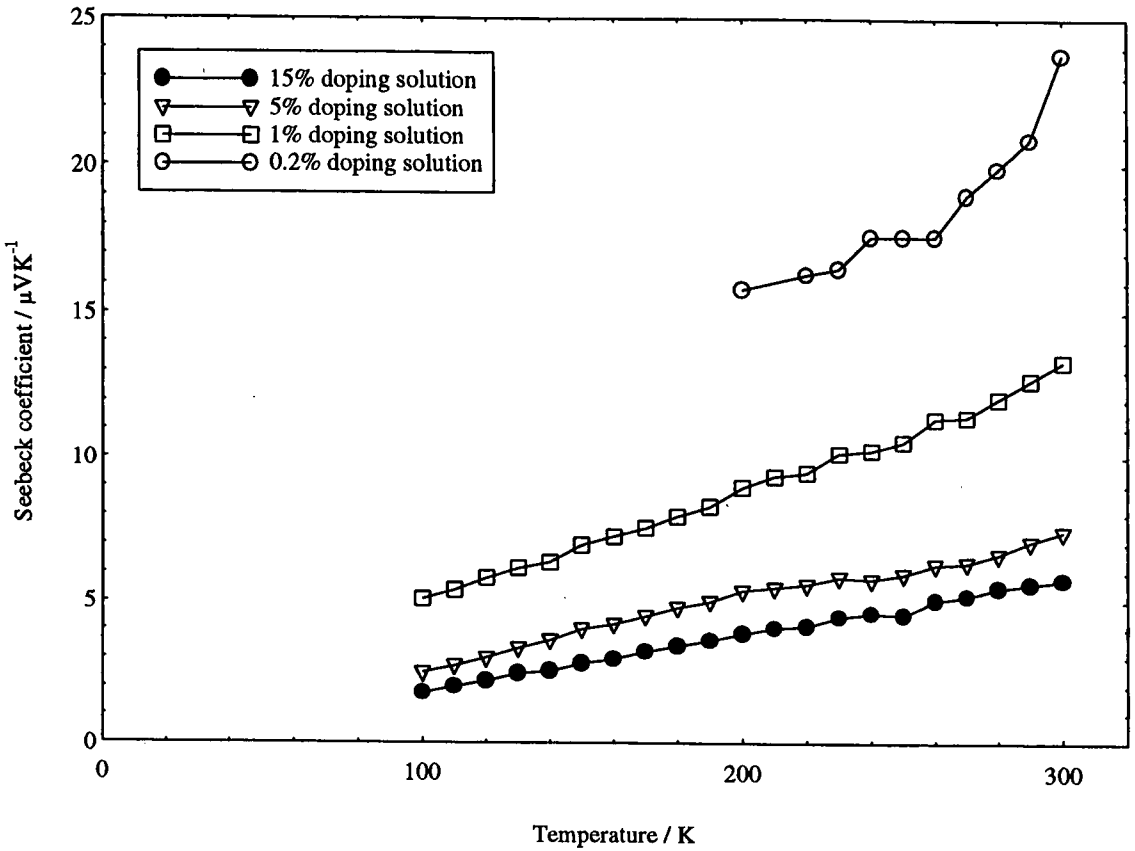

Fig. 4.6 Thermopwer (parallel to axis of orientation) of 500% stretched PANi-NMP samples doped in aqueous MSA solutions of concentations in the range 0.2% to 15%.

range of this set means that it cannot be used to determine the presence of any particular charge transport mechanism.

As described in chapter 2, diffusion thermopower arises in a conductor where there is an imbalance in the heat transported by charge carriers at different energies when the material is subjected to a thermal gradient. The most significant contribution is from the charge carriers within a thermal energy window, of width ≈kT about the Fermi energy. Hence the size of thermopower is chiefly determined by the rate of change (with respect to energy) of the density of states function at the Fermi level. The expression for diffusion thermopower (equation 2.28) can be written as a function of n(E), the density of states per carrier, per unit energy at the Fermi level [16]:

$$S = -\frac{\pi^2 K^2 T}{3|e|} n(E_F) \qquad \text{eqn. 4.9}$$

This simplified expression is reached using the assumption that carrier scattering is independent of energy, i.e. μ(E), the carrier mobility is invariant with respect to energy. Park et. al. [6] have made use of this formula to estimate n(E) in samples of highly conductive polyacetylene, from dS/dT, the gradient of thermopower vs. temperature. A similar analysis of the results for the most highly conductive of the PANi-NMP samples, e.g. the parallel data from fig. 4.5, suggests a value for n(E) of ≈1.5 states/eV/carrier. Application of this model to the data of fig. 4.6 would lead to the conclusion that the density of states per carrier (at E_F) increases as the level of doping is reduced, since dS/dT becomes larger in this case. However, the density of radical cation states in the material is directly related to the extent of protonation and it is these states which are thought to be responsible for the conductive nature of the polymer (see section 1.6). As the number of protonated sites is reduced, the average separation of states which contribute to a 'conduction band' would be expected to increase. Hence the extent of interaction between states must also depend upon the level of doping and this in turn will affect the density of states function. It might therefore be expected that the density of states is smaller at reduced doping levels. According to equation 4.8, a decrease in the

magnitude of thermopower would then be predicted as the level of protonation is reduced, contrary to the observed behaviour.

Therefore, it does not seem possible to explain the change in thermopower characteristics (as a function of doping) purely in terms of variation in the density of states parameter in equation 4.8. Additionally, the validity of this model to PANi-NMP is uncertain since it cannot be assumed that carrier scattering is energy independent.

If the linear form of the thermopower data observed for the samples doped in 1%, 5% and 15% solutions of MSA is a result of a dominant diffusion thermopower, the general expression of equation 2.29 is perhaps the best standpoint from which to interpret the nature of these results. As described previously, at levels of doping less than the theoretical maximum (50% of nitrogen sites protonated on each polymer chain) it is expected that interaction between 'conduction' states becomes weaker as their average spacing is increased. In addition, decreasing the level of protonation reduces the charge carrier density. The effect of both these factors is reflected in the large decrease in conductivity as the doping level is decreased. In these samples, it is therefore suggested that there are two effects which may influence the behaviour of the diffusion thermopower. Firstly, the density of states function will depend upon the protonation level, because the strength of interactions between doped states on and between PANi chains will vary according to their separation in the material. Secondly, the mean free carrier path will be reduced if the interaction between electronic states is weakened by increased separation.

No evidence for localised charge carrier states is apparent in the thermopower of the stretch oriented samples (measured parallel to the alignment axis). Transition to hopping transport, characterised by a square root dependence of thermopower upon temperature (equation 2.32), might be expected to occur at low levels of doping if the separation of protonated sites is large enough to prevent significant overlap of the electronic states which contribute to a conduction band. Although the much reduced conductivity and greater magnitude of the thermopower of samples doped in 0.2% MSA suggest that there could be significant differences in comparison to the more heavily

doped samples, the limited range of data precludes any attempt at a quantitative explanation.

Therefore in the case of PANi-NMP it is suggested that there are two effects which result from a variation of the level of protonation, that influence the behaviour of diffusion thermopower. Firstly, the mean free carrier path will be reduced if the interaction between neighbouring electronic states is weakened by reduction of the density of protonation. Secondly, the density of states function is expected to vary because the strength of interaction between electronic states contributing to the conduction band will also depend upon the average separation of doped sites. The quantitative effect which these factors exert upon the thermopower of this material is impossible to predict with any accuracy since the thermopower of metals is not fully understood.

4.5 Thermopower Of PANi-CSA

The electrical conductivity studies detailed in chapter 3 revealed a significant difference between polyaniline films prepared via the NMP and CSA routes. Unstretched PANi-NMP displays a relatively low conductivity (≈30 Scm^{-1} at 300 K) that has a dependence upon temperature characteristic of charge transport via tunnelling. In contrast, unstretched PANi-CSA (250 Scm^{-1} at 300 K) is far more characteristic of a partially metallic system. The thermopower of unstretched PANi-CSA was measured, with the aim of a further investigation into the metallic nature of the electronic properties of this material.

4.5.1 Results

Unoriented PANi-CSA films were prepared according to the process detailed in chapter 1, with dopant concentrations of 30% 40% and 50%, The thermopower of these samples was measured as a function of temperature over the range 100 K to 300 K. A set of typical results from samples of each doping level is presented in fig. 4.7. Except for a larger magnitude, the data reveal a trend similar to that observed in the thermopower component of stretch oriented PANi-NMP parallel to the axis of elongation (see fig. 4.5); the thermopower of PANi-CSA is positive and displays a linear dependence upon temperature. A small reduction in the gradient, dS/dT, is apparent as the level of doping is increased. This behaviour is similar to that observed for stretch oriented films of PANi-NMP in which the level of protonation was controlled by variation of the doping solution pH (see section 4.4).

4.5.2 Discussion

The thermopower data obtained from PANi-CSA is broadly similar to that described in other reports [17,18] for material prepared by similar methods. By comparison with theory (see chapter 2) the linear dependence of the data upon temperature implies that the thermopower is dominated by 'metallic' diffusion transport. This correlates with the data from electrical conductivity studies made on similar

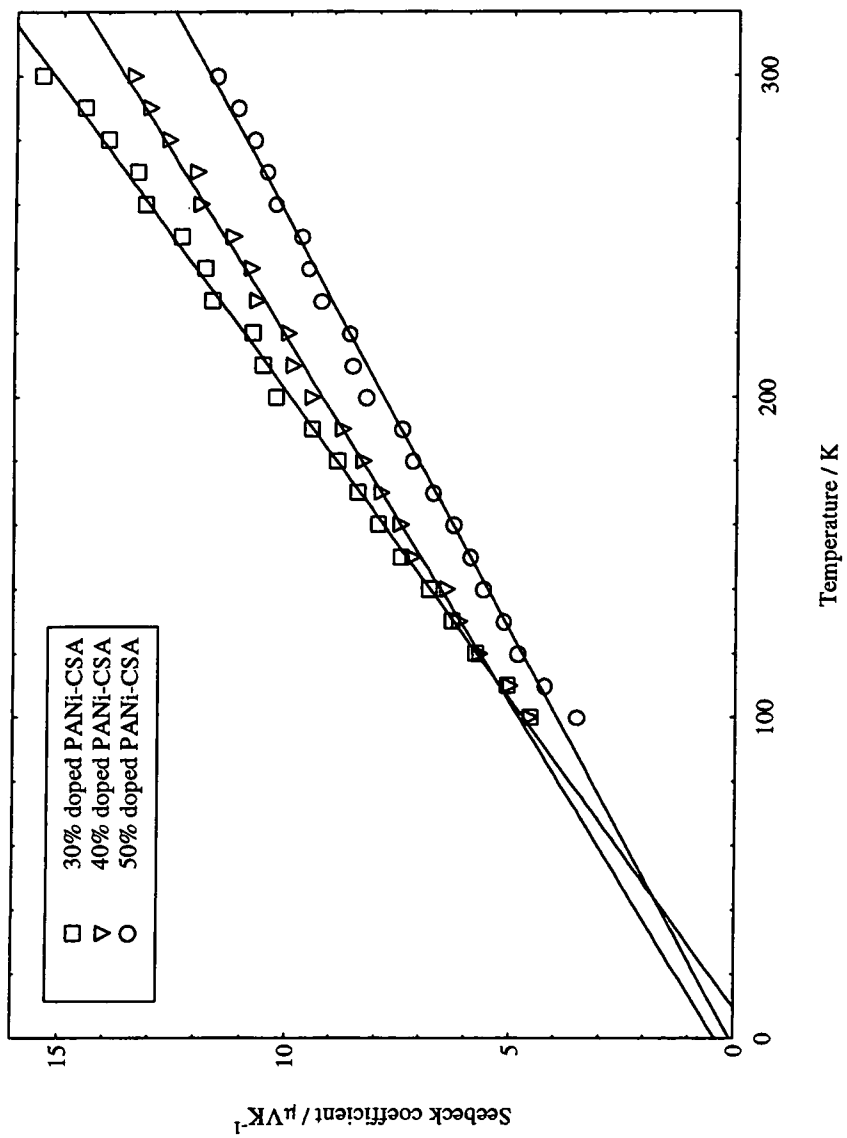

Fig. 4.7 Thermopower of PANi-CSA versus temperature, from samples prepared with dopant concentration in the range 30% to 50%, the lines are included as a guide.

samples, presented in chapter 3, which revealed a negative temperature coefficient of conductivity in the high temperature regime near 300 K. This is a typical feature of the behaviour of crystalline metals. Thus, the information provided by conductivity and thermopower studies provide strong evidence for the presence of metallic charge transport within PANi-CSA. The bulk properties of this material suggest that it is not purely metallic, but very close to a metal-insulator transition.

The variation of dS/dT with respect to sample doping concentration, is somewhat more difficult to understand than the origin of their linear form. The general expression for diffusion thermopower (equation 2.29) would seem to provide a suitable starting point from which to consider this behaviour. However, it is envisaged that variation of the dopant concentration within PANi-CSA will result in a complex alteration of the system parameters. For example, in a similar fashion to that described in section 4.4, at different doping levels there must be a different charge carrier concentration and a different average separation between polaronic states. Variation in the density of states function and/or the position of the Fermi level within the electronic band structure and thus the value of dA/dE at E_F is therefore expected. In addition, the mean free carrier path, ℓ, is thought to depend upon the level of protonation of the polymer, because the metallic character evident in the conductivity of PANi-CSA becomes more pronounced as doping is increased.

It is impossible therefore to quantify the influence exerted upon the thermoelectric properties of the polymer, by variation of the concentration of CSA. It is unusual that, unlike the differences in conductivity values, the thermopower readings from 30%, 40% and 50% PANi-CSA films are remarkably similar. This suggests that metallic regions of a very similar nature are present within all three sample types.

A heterogeneous model was used in chapter 3 to describe the conduction within the PANi-CSA system at compositions at and above 30% doping. This combined phonon scattering of charge carriers in crystalline regions of polymer in series with a tunnelling mechanism, thought to govern conduction in disordered boundary regions. The balance between these two mechanisms appears to depend upon the concentration of

dopant contained within a given sample; samples gain more metallic character as the doping level is increased.

The Kaiser model of heterogeneous conductors (described in chapter 2) states that metallic regions contained within a heterogeneous system can provide a dominant contribution to thermopower if other regions are small and conduct heat well. It is clear from the results presented in fig. 4.7, that a similar situation presides in PANi-CSA; the excellent fit to each data set by linear regression suggests that thermopower is almost entirely due to charge carrier diffusion within metallic regions for temperatures in the range 100 K to 300 K. Additional contributions to the thermopower of PANi-CSA may be generated within non-metallic regions, but are not evident in any data obtained from PANi-CSA samples. Measurement of thermopower in the temperature range below 100 K is required to confirm this suspicion and also might reveal a deviation from metallic behaviour, as displayed in the conductivity of similar PANi-CSA samples at low temperatures. Investigation over a wider range of sample doping levels, e.g. 10% to 60%, could provide additional information about the transition observed in the electronic properties of this material upon protonation.

The contrast in electrical behaviour between PANi-NMP and PANi-CSA revealed by electrical conductivity studies is again evident, in the thermopower data collected from these two materials. Unstretched PANi-CSA has a positive thermopower with a linear dependence upon temperature, typical of charge transport via metallic diffusion. Highly doped unstretched PANi-NMP on the other hand, has a negative thermopower with a complex form that is difficult to ascribe to any particular charge transport mechanism. Upon stretch orientation, the thermopower of PANi-NMP (parallel to the axis of elongation) undergoes a transition to a linear form comparable with that of PANi-CSA, see figs. 4.5 and 4.7. Unlike PANi-CSA however, the electrical conductivity of stretch oriented PANi-NMP displays none of the features associated with metallic charge transport.

Clearly the thermoelectric properties of unstretched polyaniline films prepared by the NMP and CSA methods, reflect differences in charge transport mechanisms

suggested by the electrical conductivity data from each material. This provides more evidence that the structural arrangement of polymer chains at the molecular scale has a great influence upon the electrical nature of the bulk solid. The non-metallic thermopower and the temperature activated behaviour of conductivity observed in unoriented PANi-NMP suggest charge carrier transport is limited by a disordered structure. This conclusion is in good agreement with the results of neutron scattering studies made upon stretched and unstretched samples [19] which indicate that this form of polyaniline is amorphous. Alignment of the polymer chains within PANi-NMP, by a process of stretch elongation enhances the magnitude of the conductivity and yields a metal like response in the thermopower, in one dimension. The lack of regular intermolecular order is thought to prevent coherent interchain charge transfer even in stretch aligned PANi-NMP, with the result that no metallic character is observed in the electrical conductivity.

The partially metallic properties observed in the thermopower and conductivity of PANi-CSA are ascribed to the presence of crystalline regions in the polymer, indicated by recent (as yet unpublished) X-ray diffraction studies upon film samples. Therefore it is envisaged that a significant proportion of charge transport in this material is by metallic diffusion of carriers in a regular lattice of polaronic states. At low temperatures, the effect of non-metallic regions becomes evident from a change over in the sign of $d\sigma/dT$ to positive values. Since this feature occurs at lower temperatures in more highly doped samples, it is taken to imply that the influence of the crystalline 'metallic' regions increases as a function of the protonation level (this is described in detail in chapter 3, section 3.3).

References

[1] A.P. Monkman, F. Hampson & A.J. Milton, from "Electronic Properties of Polymers", *Springer Series in Solid State Sciences* **107**, Springer Berlin (1992) p. 255

[2] R.D. Barnard, from "Thermoelectricity in Metals and alloys", Taylor & Francis, (1972) London

[3] British Standard 4937: Part 5 (1974)

[4] E.R. Holland & A.P. Monkman, *Synth. Met.* **74** (1995) p. 75

[5] Y.W. Park, A.J. Heeger, M.A. Druy & A.G. MacDiarmid, *J. Chem. Phys.* **73** (1980) p. 946

[6] Y.W. Park, A Denenstein, C.K. Chiang, A.J. Heeger & A.G. MacDiarmid, *Solid state comms.* **29** (1979) p. 247

[7] Y.W. Park, W.K. Han, C.K. Choi & H. Shirakawa, *Phys. Rev. B*, **30** (1984) p. 5487

[8] R. Zukok, A.B. Kaiser, W. Pukacki & S. Roth, *J. Chem. Phys.* **95** (1991) p. 1270

[9] Z.H. Wang, C. Li, E.M. Scherr, A.G. MacDiarmid & A.J.Epstein, *Phys. Rev. Lett.* **66** (1991) p. 1745

[10] A.B. Kaiser, *Synth. Met.* **45** (1991) p. 183

[11] P.N. Adams, P.J. Laughlin, A.P. Monkman & N. Bernhoeft, *Solid State Comms.* **91** (1994) p. 875

[12] F. Zuo, M. Angelopoulos, A.G. MacDiarmid & A.J. Epstien, *Phys. Rev. B* **36** (1987) p. 3475

[13] Y.W. Park, Y.S. Lee, C. Park, L.W. Shacklette & R.H. Boughman, *Solid State Comms.* **63** (1987) p.1063

[14] S. Sakkopoulos, E. Vitoratos, E. Dalas, G. Pandis & D. Tsamouros, *J. Phys. Condensed Matter* **4** (1992) p. 2231

[15] Y.W. Park, C. Park, Y.S. Lee, C.O. Yoon, H. Shirakawa, Y. Suezaki & K. Akagi, *Solid State Comms.* **65** (1988) p. 147

[16] J.M. Ziman, from "Properties of the Theory of Solids", Cambridge University Press, 2nd edition (1972) p. 235

[17] R. Menon, C.O. Yoon, D. Moses, A.J. Heeger, & Y. Cao, *Phys. Rev. B* **48** (1993) p. 17 689

[18] S.K. Jeong, J.S. Suh, E.J. Oh, Y.W. Park, C.Y. Kim & A.G. MacDiarmid, *Synth Met.* **69** (1995) p. 171

[19] A.J. Milton, *Ph.D. Thesis*, University of Durham 1993, A.J. Milton, N. Bernhoeft & A.P. Monkman, to be submitted

CHAPTER 5

Polymeric Field Effect Devices

5.1 Introduction

Recently there has been a substantial interest in the use of conjugated polymers as the active semiconductor in field effect transistor (FET) devices [1,2]. From a technological viewpoint, these materials offer a considerable advantage over conventional inorganic semiconductors with respect to the ease of processing. Spin coating, for example, can be employed to deposit high quality thin films of polymer. From a purely scientific viewpoint, the characteristics of a polymer based FET can provide useful information about the electrical properties of the material, such as the charge carrier sign, and mobility [2]. The effect of order and disorder in the polymer film upon its charge transport properties can therefore be studied through the utilisation of such devices.

It is generally accepted that for a conjugated polymeric material, the degree of straight intrachain conjugation has an important effect upon its conductive properties. This is mainly through increased conjugation leading to an increase in the mobility of carriers along the polymer backbone, because there are fewer defects in the conjugated structure able to act as scattering centres. In the work described in this chapter, the role of polymer chain order, with respect to carrier mobility, was investigated. This was achieved by measuring the field effect mobility in thin films of the regioregular, chiral, 3[2(S2-methylbutoxy)ethyl]-polythiophene, (PMBET) [3] prepared from solutions containing different amounts of a nonsolvent. The results from FET device analysis were combined with optical absorption measurements upon similar film samples. The findings of this investigation form the basis of a publication [4].

5.2 Theory Of Field Effect Devices

The operation of a thin film FET relies upon the metal-insulator-semiconductor (MIS) system and its behaviour with respect to electrical biasing. There are two possible

configurations of an MIS structure, depending on whether it is formed with n-type or p-type semiconductor. The latter case is appropriate to describe the operation of the polymer FET.

In order to understand the action of an FET it is useful to consider the energy band structure of an ideal MIS diode under different regimes of voltage bias [5]. These conditions are represented pictorially in fig. 5.1. E_i is the theoretical Fermi level for the intrinsic (undoped) semiconductor, and lies midway between the edges of the valence and conduction bands. In this explanation it is assumed that the insulator is perfect, i.e. no charge can pass from the metal to the semiconductor, hence the Fermi level in the semiconductor remains unchanged when the system is biased. The voltage bias, V is that of the potential applied to the metal, with respect to the semiconductor.

The simplest case, $V = 0$, i.e. zero bias, is termed the flat band condition, see fig. 5.1(a). The Fermi levels in the metal and semiconductor are equal and the charge carrier density in the semiconductor at the interface to the insulator is the same as in the bulk material. In the case of a MIS structure formed with a p-type semiconductor, there are three further regimes induced by electrical biasing:

The first is the depletion regime, with $V > 0$, see fig. 5.1(b). The applied potential difference has the effect of raising the Fermi level in the metal, with respect to the semiconductor. This causes a distortion of the energy band structure from the flat band condition, due to the variation in electrostatic potential energy across the structure. As the majority carrier (hole) concentration P is dependent upon the difference between the intrinsic and true Fermi levels:

$$P = n_i \exp\left(\frac{E_i - E_F}{kT}\right) \qquad \text{eqn. 5.1}$$

where n_i is the intrinsic electron concentration. Near the insulator-semiconductor interface, where band bending occurs, the carrier concentration is reduced and a depletion layer is formed.

If the positive bias applied to the metal is increased to very large values, $V >> 0$,

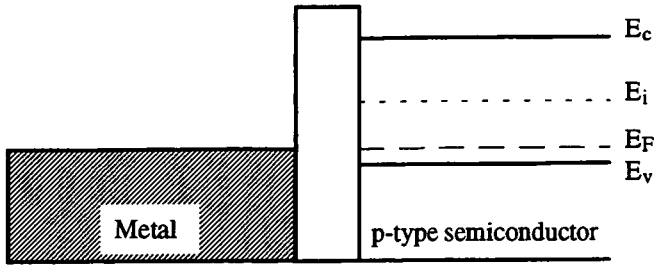

(a) V = 0, The flat band condition.

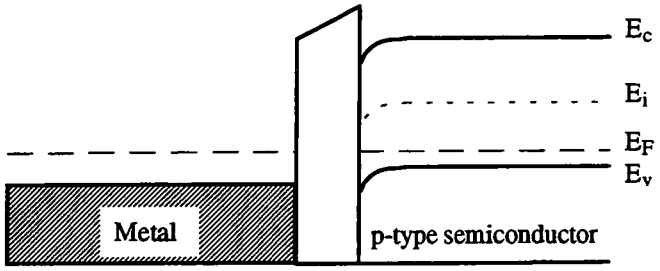

(b) V > 0, The depletion regime.

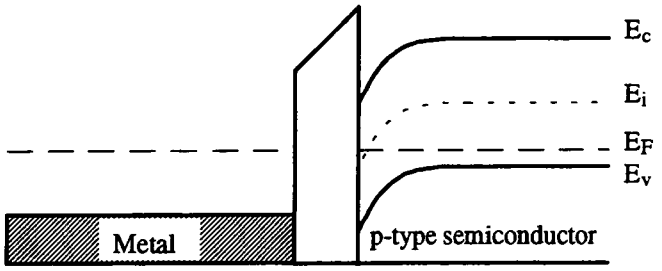

(c) V ≅ 0, The inversion regime.

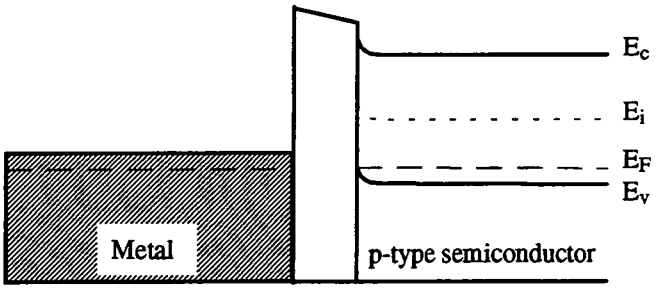

(d) V < 0, The accumulation regime.

Fig. 5.1 Energy band diagrams for an ideal MIS structure under electrical bias.

the energy band distortion induced in the semiconductor reaches the point where the intrinsic Fermi level is depressed such that $E_i < E_F$, as illustrated in fig. 5.1(c). The electron concentration N, described by equation 5.2 thus exceeds the hole concentration in a layer of semiconductor near the interface.

$$N = n_i \exp\left(\frac{E_F - E_i}{kT}\right) \qquad \text{eqn. 5.2}$$

This is termed an inversion layer, since the majority carriers in this region are electrons, not holes -a small portion of the p-type material has been forced into n-type behaviour.

A different situation exists in the accumulation case, where $V > 0$. As illustrated in fig. 5.1(d) the Fermi level of the metal is raised with respect to that of the semiconductor, causing a distortion of the semiconductor which increases the value of $E_i - E_F$ near the semiconductor-insulator boundary. By comparison with equation 5.1 it can be seen that the application of positive bias results in an increase in the hole concentration in a thin layer at the surface of the semiconductor. This is termed an accumulation layer.

In each of the above cases, the changes induced in the semiconductor extend only a very short distance from the interface with the insulator, the bulk of the semiconductor remains unaffected by the biasing conditions. The operation of a field effect device depends upon the change in charge carrier density, and hence the conductivity that can be induced in this surface layer in a MIS sandwich. The so called MISFET employs a structure similar to that illustrated in fig. 5.2. Basically, this is a MIS diode, to which source and drain electrodes have been added, such that the semiconductor is contained in a channel region of length L and width W. The metal contact underneath the channel region is termed the gate electrode. The influence of an electrical bias applied to the gate alters the electrical conductivity of the surface layer of the semiconductor. In the MISFET, this is exploited to provide a means of control over the flow of current between the source and drain contacts [5].

It is common to consider transistor operation with the source electrode at earth potential (common source mode). With a p-type semiconductor contained in the channel

region, positive electrical bias applied to the gate electrode causes carrier depletion in the semiconductor, near its interface with the insulator as per fig. 5.1(b). Hence the resistance of the channel is increased. On the other hand, negative gate bias results in the formation of an accumulation layer at the semiconductor-insulator interface so the charge carrier concentration within the channel is enriched, and the channel resistance is decreased.

The electrical behaviour of a MISFET depends upon the sign and magnitude of the electrical bias applied to the source, drain and gate electrodes and the physical dimensions of the device. In the common source configuration ($V_S = 0$), the source-drain current I_{DS}, which passes through the channel region is considered for negative gate and drain voltages (V_G and $V_D < 0$). This is known as accumulation or enhancement mode because raising the magnitude of V_G increases the device current. It can be shown that [5]:

$$I_{DS} = \frac{\mu W C_i}{L}\left[(V_G - V_o)V_D - \frac{V_D^2}{2}\right] + I_\Omega \qquad \text{eqn. 5.3}$$

where μ is the charge carrier mobility, W is the channel width, L is the channel length and C_i is the gate capacitance per unit channel area. The parameter V_o is an offset voltage which accounts for the effects of surface charge states trapped at the semiconductor-insulator interface. The first term in this expression describes the gate-voltage-modulation of the source-drain current, caused by the formation of an accumulation layer in the negative gate bias regime. The term I_Ω is included to account for current flow in the bulk semiconductor, i.e. the region unaffected by gate biasing, and can be described, to first order by the expression:

$$I_\Omega = \frac{\sigma W t}{L} V_D \qquad \text{eqn. 5.4}$$

where σ is the electrical conductivity of the channel material and t is the total thickness of the layer. It will be seen that this term contributes a significant proportion of the total source-drain current in PMBET devices because the 'static' conductivity of the channel

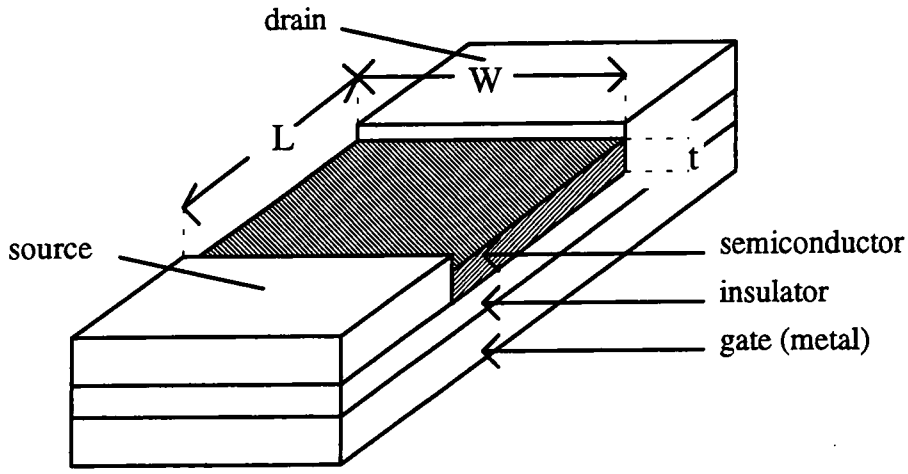

Fig. 5.2 Architecture of the thin film field effect transistor.

material is comparable to any enhancement of the conductivity induced by gate terminal biasing.

The main factor of interest in the study of MISFET devices that employ a conjugated polymer in the channel is the mobility of charge carriers within the polymer. A high value of μ is essential if these materials are to yield devices with a performance comparable to that provided by inorganic semiconductors, e.g. porous silicon, which has electron mobility $\mu \approx 10^2$ $cm^2V^{-1}s^{-1}$. The carrier mobility within the channel can be calculated from measurements of the characteristics the FET. The method developed for obtaining the field effect mobility are now described: When the device is operating in the linear regime [5], with $|V_G| > |V_D|$, it can be shown that I_{DS} has a linear dependence upon V_G. Differentiating equation 5.3 with respect to V_G gives:

$$\frac{dI_{DS}}{dV_G} = \frac{\mu W C_i}{L} V_D \qquad \text{eqn. 5.5}$$

Therefore a plot of I_{DS} vs. V_G for a device with constant V_D results in a straight line with gradient M, from which the carrier mobility can be calculated:

$$\mu = \frac{ML}{WC_iV_D} \qquad \text{eqn. 5.6}$$

The electrical conductivity of the channel material can also be estimated using equation 5.4, if V_G is set to zero and it is assumed that there is no contribution to I_{DS} from the first term in equation 5.4.

5.3 Experimental Techniques

A typical example of the structure used to fabricate polymeric MISFETs is illustrated in fig. 5.3 The devices were built on a conductive (n^+ doped) silicon wafer substrate that acted as the metal control gate in the MIS system. 2000 Angstroms of silicon dioxide (insulating layer) was grown on the top of the top of the wafer and upon this, interdigitated gold electrodes were deposited to form source and drain terminals. The channel width, W and length, L were available with all permutations of W: 3 mm to

20 mm and L: 2 μm to 20 μm. The conjugated polymer semiconductor, PMBET, has the chemical structure illustrated in fig. 5.4. It was dissolved in tetrahydrofuran (THF) to a concentration of 0.5% by weight and deposited in a thin film upon the surface of the device substrate from solution, by spin coating at 1000 rpm.

Typical electrical biasing conditions employed during the measurement of carrier mobility and electrical conductivity from FET devices were: V_D set to a fixed value between -1 and -5 V (with respect to V_S at 0 V) whilst V_G was scanned from -20 to -10 V and I_{DS} measured. The mobility was calculated using equation 5.5. Scans were made with V_D set to several different values to enable repeated measurements of μ. The conductivity of the polymer was calculated using the I_{DS} vs. V_D characteristics with V_G = 0 V and equation 5.4. All electrical measurements were made using a Hewlett-Packard 4140B pA meter/DC voltage source, controlled via computer to facilitate automation of the data acquisition process.

To obtain PMBET with various degrees of chain order a technique used in the field of polydiacetylenes (PDA) was exploited; that of adding quantities of nonsolvent to solutions of PDA in good solvent [6]. In the case of PDAs such as 9BCMU [7] this would be chloroform (good solvent) and hexane (bad solvent). In the case of PMBET the solvent used is THF and the nonsolvent added to it is methanol. In the study described in this thesis, a typical set of solutions was studied. All sample solutions were made by first dissolving 0.02 g of PMBET in 4 ml of THF. After all the polymer had dissolved, different quantities of methanol were added to the solutions at the ratios (by volume) given in table 5.1.

In solution a solvatochromic effect was observed. Progressive methanol addition caused the originally orange solution to become dark orange red and then dark red. When the ratio of methanol to THF exceeded 4:10 a red precipitate was formed, indicating that the polymer had been forced out of solution. From each of the five solutions detailed in table 5.1, thin films of PMBET were spin coated under identical conditions, onto glass slides and FET structures, so that their optical and electrical properties could be investigated.

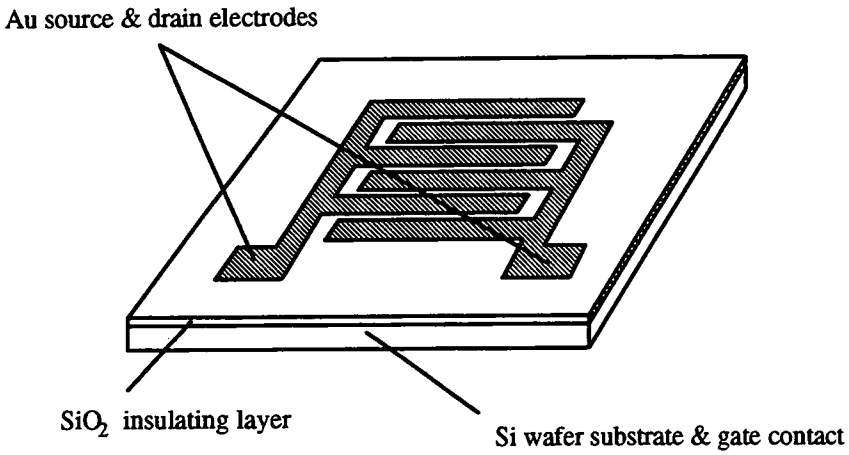

Fig. 5.3 Polymer MISFET device structure

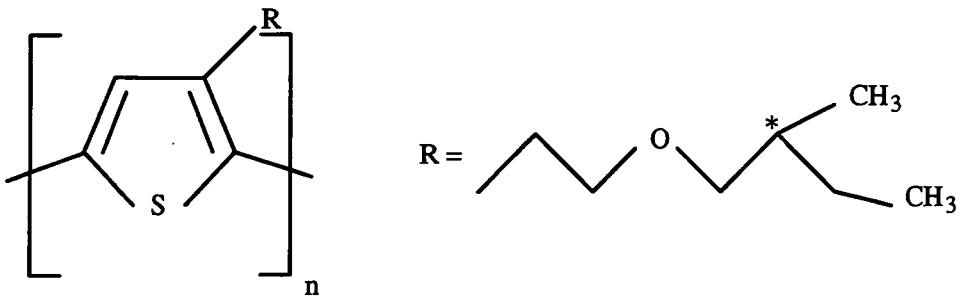

Fig. 5.4 Repeat unit structure of 3[2(S2-methylbutoxy)ethyl]-polythiophene (PMBET), * denotes a chiral centre.

Sample	Ratio of THF : CH_3OH	Solution colour
1	100% THF	yellow-orange
2	10:1	dark orange
3	10:2	red
4	10:3	dark red
5	10:4	dark red

Table 5.1 Details of the solutions used to prepare spin cast films of PMBET.

5.4 Results

5.4.1 UV-vis Spectroscopy

The solvatochromic effects observed in the initial spinning solutions are preserved in the optical absorption properties of the spin cast polymer films. However, the red shifts, induced by the presence of nonsolvent in solution, are enhanced in the solid state. The absorption spectrum of a PMBET film spun from pure THF solution (sample 1) shows a main peak at 546 nm, with a shoulder at around 600 nm (fig. 5.5). PMBET films spun from solutions with increasing methanol content show this main peak to shift to longer wavelengths, 552 nm for sample 2 and 564 nm for sample 3. The peak absorbance decreases in intensity. A new peak emerges from the shoulder at 600 nm in sample 1, and also shifts towards longer wavelengths as the methanol content of the spinning solution is increased. For sample 3 the new peak is seen at 610 nm while for films spun from solutions 4 and 5 it occurs at 628 nm. It was noted that the films spun from methanol treated solutions caused a significant scattering of light. The degree of scattering was increased for films spun from solutions of greater methanol content, as suggested by an increase in their absorption in the UV range, circa 300 nm.

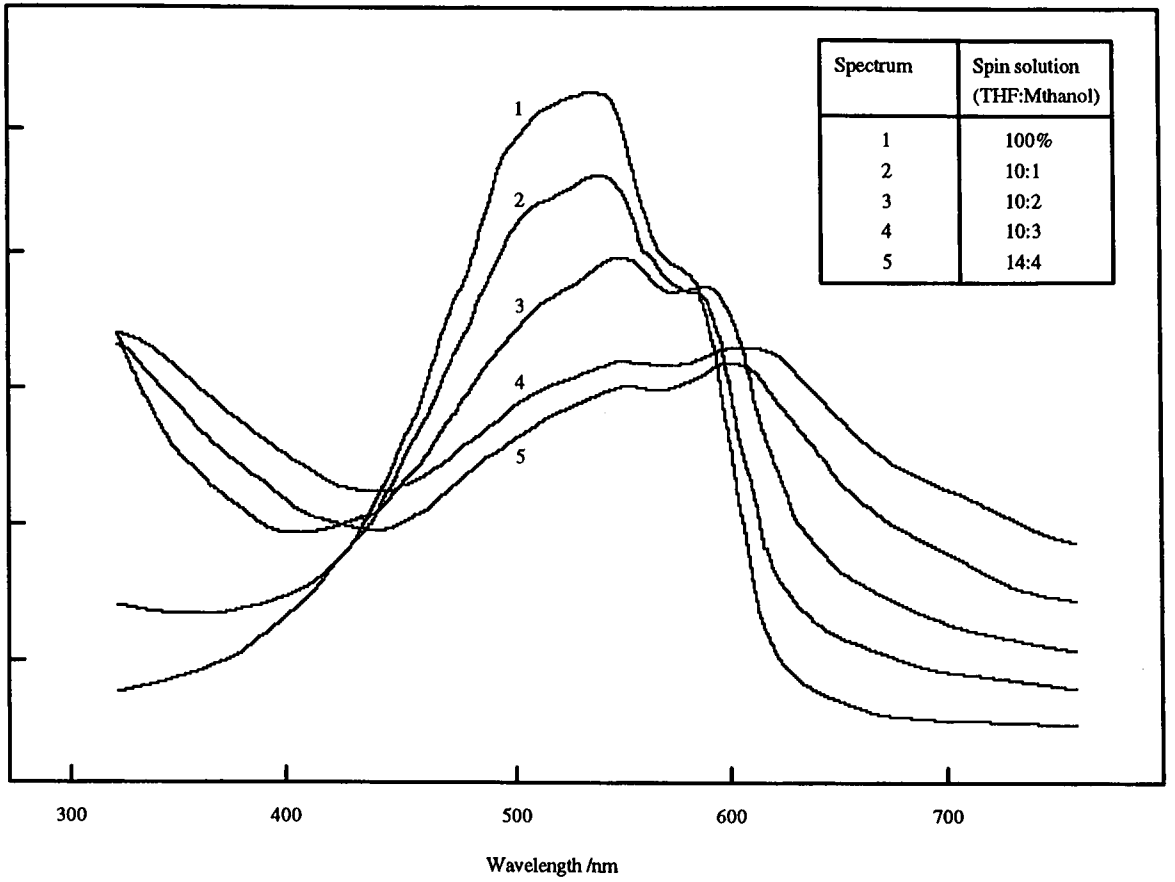

Fig. 5.5 Absorption spectra for films of PMBET spun from solutions of different concentrations of THF and methanol.

The shoulder in spectrum 1, and new peaks which are clearly evident in the subsequent spectra of fig. 3 are ascribed to vibronic bands. In all cases the lowest energy band is the 0-0 transition, with the first vibronic sideband being 190 meV higher in energy. This is very consistent with the electronic transition being strongly coupled to the C = C stretch of the polymer backbone. Typically for most thiophenes, the C = C stretch occurs at ≈1500 cm^{-1} or 185 meV. This energy separation is independent (to within a few meV) of chromic shift. The results from these films are consistent with those reported by Rughooputh et. al. [8] in solutions of polyalkylthiophenes.

5.4.2 FET Characterisation

As previously stated, all mobility measurements were performed with devices operating in accumulation mode in the linear regime [9] i.e. $|V_G| > |V_D|$. A set of typical results from a PMBET FET is presented in fig. 5.6. As predicted by theory (equation 5.3) the data sets, each of which correspond to a different value of V_D, are linear, thus allowing accurate determination of μ from their gradient.

The mobility data from MISFET devices formed by spinning films from the 5 PMBET solutions treated with methanol are presented in table 5.2. Sample 5 displayed no measurable modulation of the source-drain current with applied gate voltage. Along with the mobility data, the electrical conductivity of the polymer within each device was estimated. The film thickness, required for calculation of σ, was estimated at ≈100 Angstroms by comparison of the absolute absorption of the samples prepared for the spectroscopic study, to the absorption coefficient of PMBET. The conductivity of sample 3 appears to be somewhat low. This is ascribed to an overestimate of the film thickness, and the inherently low accuracy of two terminal conductivity measurements.

A correlation is found between the methanol content of the solution used to produce each film, the field effect mobility and electrical conductivity. In all cases an increased methanol content in the spinning solution yields lower carrier mobility and reduced bulk conductivity.

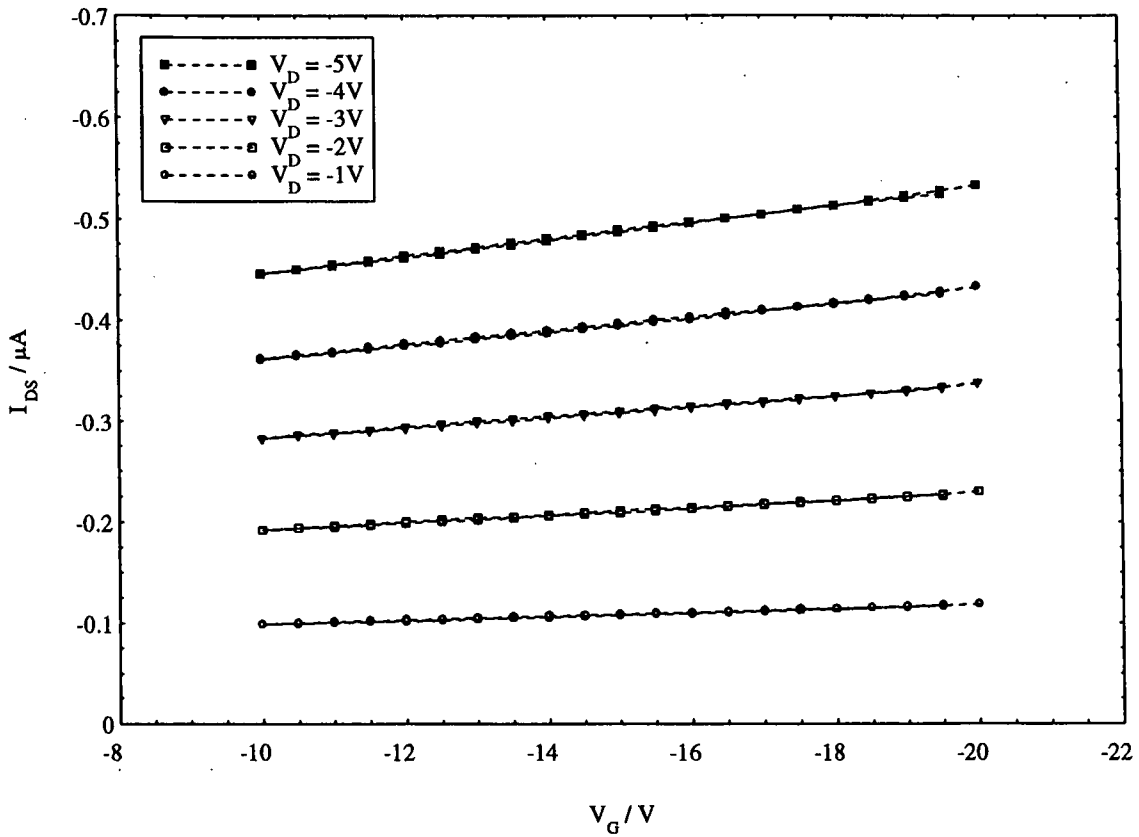

Fig 5.6 Electrical characteristics of a polymer field effect transistor device incorporating PMBET, deposited from solution in pure THF.

Sample	Conductivity Scm^{-1}	Mobility $cm^2V^{-1}s^{-1}$
1	1.7×10^{-5}	4.0×10^{-5}
2	7.3×10^{-6}	1.5×10^{-5}
3	6.1×10^{-9}	1.5×10^{-8}
4	3.0×10^{-8}	1.5×10^{-8}
5	9.5×10^{-9}	unmeasurable

Table 5.2 Conductivity and mobility data from PMBET films. For preparation details see table 5.1.

5.4.3 Discussion

From the optical absorption measurements, it can be seen that generally, as poor solvent is added to the solutions used to spin cast films of PMBET, the absorption of the resultant films is red shifted. This is accompanied by an increase in UV absorption ascribed to an increase in scattering. The shift in the absorption peak towards longer wavelengths is interpreted as an increase in the effective intrachain conjugation length. This arises in solution because the average length of rigid rod along the polymer chain increases as the concentration of methanol (nonsolvent) in the solution is increased. Similar effects are well documented in side chain substituted PDAs. In this case the addition of hexane to solutions of BCMU derivatives [7] causes solvatochromatic shifts in the absorption spectrum. Here chains occur as random wormlike coils in good solvent, the addition of bad solvent causes the individual chains to collapse down on themselves via intramolecular interactions such that sections of the polymer chain form into rigid rods [10]. These rigid chains readily aggregate, even in dilute solution. The driving force for their collapse is not hydrogen bonding [11], but an intramolecular attraction. In the

BCMUs, it is still not clear whether the aggregates are amorphous or fringed micelles which have partial crystallinity.

In good solvent the side chains of the PMBET molecules will have plenty of free volume, enabling them to move rapidly. This degree of side chain freedom will cause the polymer to take up a wormlike configuration [12]. This will in turn cause a twisting between neighbouring rings along the polymer backbone. This deviation from planarity of the conjugated structure will drive the system to a more localised geometry [13]. These effects are locked in when films are spun as the solvent evaporates rapidly (from the very thin films), not giving the chains and side groups time to reorient. As poor solvent is added to the solution, the degree of sidechain freedom is thought to be reduced, via an intramolecular interaction as in the case of the BCMUs, introducing order (rigid rod character) to the chains and allowing aggregation to occur. Thus the chains can return to a more planar and hence more conjugated form, shifting the π-π^* absorption to lower energy. Again after film spinning the chain configuration is locked in. At very high nonsolvent content, aggregation dominates, leading to the observed high degree of scattering from the films.

The appearance of spin cast films of PMBET, becoming progressively more cloudy as the nonsolvent content of the spinning solution was increased, suggests an increase in the crystalline fraction of the films or that aggregation of the polymer chains occurs in solution prior to (or during) the spinning process. This would explain the existence of the scattering tail on the low energy side of the of the π-π^* transition of the polymer. Further evidence for this comes from the gain in oscillator strength of the 0-0 and vibronic side bands, indicative of an increased number of one dimensional chains, which would be the case in the crystalline fractions.

The effects of the changes in chain configuration and aggregation in PMBET can clearly be seen in the mobility and conductivity data from cast films. At first sight the findings are counterintuitive, field effect mobility and hence conductivity fall markedly as nonsolvent is added to the spinning solution, but at the same time, the effective conjugation length of each chain in the film is increased. An enhancement in the

intrachain electrical transport might have been expected to reveal itself in the bulk properties of the polymer. However, within the more ordered regions of the film, the conjugated backbone will be more rigid. This rigidity will reduce the degree of freedom of the substituent side groups, causing them to order. This ordering of the side groups will, on average, increase the interchain separation of the conjugated backbones reducing the hopping probability of interchain charge carrier transport. It is this factor which contributes to the decrease of mobility and conductivity in the films prepared from solutions containing nonsolvent. These results are in good agreement with the report of Paloheimo et. al. [9] in which it is shown that increasing the size of the side substituent of polythiophene derivatives, thus increasing interchain separation, also leads to a decrease in the carrier field effect mobility.

On comparing our values of mobility with those quoted by Horowitz et. al. for various thiophene systems [14], nothing untoward is seen. The value $4x10^{-5}$ $cm^2V^{-1}s^{-1}$ obtained for the field effect mobility of PMBET films cast from purely good solvent is high for a substituted polymer, but not unduly so. Thus the observed effects on mobility must be caused by the effects of either order or aggregation or both. Recent work in the field of oligomeric thiophenes [14,15] has shown that interchain transport is all important. Compared to α substitution (end of chain), β substitution (side chain) drastically reduced carrier mobility, due in part to loss of crystallinity and because the adjacent, facing thiophene rings are much further apart. The electronic states that contribute to the electrical properties of this material are contained within the thiophene units. Reducing the communication between the electrically active parts of the polymer (the conjugated backbone) will decrease the ease of charge transport between chains and hence limit the mobility. Placing large substituent groups on the side of the polymer chain will have just this effect. β-substituted dodeca thiophene has a field effect mobility of $5x10^{-6}$ $cm^2V^{-1}s^{-1}$, a value approaching the maximum value obtained in PMBET. From these findings, we deduce that in the pristine films PMBET, there is a fair degree of order between the more closely spaced chains, as the optical absorption spectrum of such a film displays vibronic structure, hence interchain transport is high with a concomitant

high carrier mobility. As nonsolvent is added to the spinning solution chain rigidity increased conjugation ensues, corresponding to increased order within the film; aggregation occurs, as deduced from the increased optical scattering. The mobility of carriers within such films falls, however, this is ascribed to the effects of increased chain separation on a molecular scale and to the effects of grain boundaries on a macroscopic scale. The boundaries between individual aggregate particles disrupts the bulk mobility, which is the parameter probed by investigation of FET devices. Although, if particles contain regions of significant interchain order, the carrier mobility within them may be higher than the bulk (measured) value.

5.5 Conclusions

The MISFET structure has been used to measure the charge carrier mobility and electrical conductivities of thin films of PMBET, spun cast from solvent : nonsolvent mixtures. Optical characterisation of films spun from solutions containing varying ratios of THF (solvent) and methanol (nonsolvent) shows clear vibronic structure on the π-π^* electronic transition. Solvatochromatic shifts are maintained in the spun films due to the rapid evaporation of the solvent from the (thin) films during the spinning process. The rapid evaporation locks in the chain conformation established in solution. As the nonsolvent content of the spinning solution is increased, films show increased conjugation, i.e. red shift of the visible absorption. This is ascribed to increased rigidity, and hence longer conjugation lengths along the polymer chain. Accompanying this, films appear to scatter more strongly; this is ascribed to aggregation of polymer within the solutions, and the films produced from them.

The latter observation is very important when considering the charge carrier mobility and electrical conductivity data obtained from films incorporated into FET devices. As nonsolvent content increases, the mobility in films spun from these solutions decreases. This can be ascribed to effects on both the microscopic and macroscopic scales. On the microscopic level, increased chain rigidity will cause the side chain groups

on the polymer to order, increasing interchain separation and hence decreasing the ease of interchain charge transfer. The presence of macroscopic grain boundaries, associated with the aggregation particles in the films affects the bulk mobility within the films.

These results should be kept in mind when considering transistor devices made with high mobility oligomers, as again grain boundaries may be limiting the maximum attainable carrier mobility and thus compromising the ultimate device performance. Further experiments, perhaps including microwave measurements of the electrical conductivity are required to probe the intrinsic properties of ordered regions of the polymer. This might reveal whether the mobility is enhanced in these ordered regions, or if it is limited by increased interchain separation.

References

[1] R.H. Friend, J.H. Burroughes & K.E. Ziemelis, from "Science and Applications of Conducting Polymers", Adam Hilger, Bristol (1991) p. 35

[2] G. Horowitz, X.Z. Peng, D. Fichou & F. Garnier, *J. Mol. Electronics.* **7** (1991) p. 85 and *J. Appl. Phys.* **67** (1990) p. 528

[3] M.M. Bouman & E.W. Meijer, *Polymer* **35** (1994) p. 309

[4] E.R. Holland, D. Bloor, A.P. Monkman, A. Brown, D. DeLeeuw, M.M. Bouman & E.W. Meijer, *J. Appl. Phys.* **75** (1994) p. 7954

[5] S.M. Sze, from "Semiconductor Devices and Technology", Wiley, New York (1985) p. 200

[6] S.D.D.V. Rughooputh, D Philips, D. Bloor & D.J. Ando, *Polym. Commun.* **25** (1984) p. 242

[7] D. Bloor, D.J. Ando, J.S. Obhi, S. Mann & M.R. Worboys, *Makromol. Chem. Rapid commun* **7** (1986) p. 665

[8] S.D.D.V. Rughooputh, S. Hotta, A.J. Heeger & F. Wudl, *J. Polym. Sci. Polym. Phys.* **25** (1987) p. 1071

[9] J. Paloheimo, H. Stubb, P. Yli-Lahti & P. Kuivalinen, *Synth. Met.* **41-34** (1991) p. 563

[10] M.A. Taylor, J.A. Odell, D.N. Batchelder & A.J. Campbell, *Polymer*, **31** (1990) p. 1116

[11] M. Rawiso, J.P. Aime, J.L. Fava, M. Schott, M.A. Muller, M. Schmidt, H. Baumgartl & G. Wegner, *J. Phys (Paris)* **49** (1988) p. 861

[12] Alisdair J. Campbell, *Ph.D Thesis*, University of London 1992

[13] R. Lazaroni, S. Rachidi & J.L. Bredas, from "Science and Application of Conducting Polymers", Adam Hilger, Bristol (1981) p. 13

[14] G. Horowitz, F. Deloffre, F. Garnier, R. Hajlaoui, M. Huiyene & A. Yassar, *Synth. Met* **54** (1993) p. 435

[15] P.Ostoja, S. Guemi, S. Rossini, M. Serradori, C. Taliani & R. Zamboni, *Synth. Met.* **54** (1993) p. 447

CHAPTER 6

Summary

6.1 Review Of Research

6.2.1 Polyaniline

The electrical conductivity and thermopower of conductive polyaniline films, prepared by two alternative methods (PANi-NMP and PANi-CSA) have been measured as a function of temperature. The results indicate a stark contrast between the charge transport mechanisms in these two materials.

Conductivity data from free standing film samples of PANi-NMP in which there is no deliberate polymer chain orientation reveal that this material is a relatively poor conductor, σ <30 Scm^{-1} at 300 K. Stretch elongation of films, by 500% prior to protonation induces partial chain alignment, with the result that the material has a significant electrical anisotropy. Parallel to the axis of orientation, conductivity is enhanced to <250 Scm^{-1} whilst in the perpendicular direction σ is relatively unchanged from that of unstretched PANi-NMP. The magnitude of σ in all cases is found to reduce (typically by 80%) when moisture absorbed by the polymer is extracted on exposure to high vacuum conditions.

The monotonic increase of σ with temperature in the range 10 K to 300 K is indicative of a disordered conductor in which charge carriers are localised, perhaps upon the molecular scale. Curve fits to the data suggest that the mechanism of fluctuation induced tunnelling (FIT) provides a good, but not complete description of electrical transport in this system.

Thermopower measurements upon stretch aligned films have highlighted the anisotropic nature of chain oriented PANi-NMP. A metal-like behaviour, indicated by linear variation of the Seebeck coefficient with temperature is observed in parallel to the direction of chain alignment. Perpendicular to this axis the thermopower is similar to that measured in unoriented PANi-NMP. However it is difficult to ascribe these results to the influence of any particular charge transport mechanism.

It is argued that the anisotropic behaviour displayed in both the conductivity and thermopower of stretch oriented PANi-NMP arises from an anisotropy induced in the charge carrier mean free path as a result of polymer chain alignment. A longer mean free path is expected along the orientation axis because the polymer backbone provides a low resistance path for charge transport. Alignment of chains is thought to permit a far greater proportion of transport (along the common axis) by propagation along the chains. Therefore the frequency of carrier scattering by interchain transfer events is reduced. This is supported by the fact that the maximum conductivity of samples occurs in a direction parallel to the stretch axis. This is not the case in the direction perpendicular to chain alignment or for unoriented samples, where the frequency of interchain charge transfer processes is expected to be higher, thus limiting the mean free path. This might account for the similar trends which have been observed in conductivity and thermopower in these two cases.

Polyaniline prepared as PANi-CSA is capable of displaying far greater conductivity than PANi-NMP. For example, at nominal 60% doping, the conductivity of unstretched films can approach 300 Scm^{-1} and by stretch orientation of this material, values as high as 800 Scm^{-1} can be achieved. In addition, removal of volatile species under high vacuum results in only a 20% drop in the magnitude of σ. The metallic behaviour observed in 'highly doped' PANi-CSA, indicated by a negative temperature coefficient of the conductivity has been the subject of intense study. By variation of the dopant concentration, the onset and progression of this metallic response has been revealed using a range of samples, prepared with CSA contents sufficient to protonate 10, 20, 30, 40, 50 and 60% of the polymer chain nitrogen sites. At 10% and 20% doping, low conductivity is observed (0.6 Scm^{-1} and 7 Scm^{-1} respectively) and this has a temperature dependence similar to that observed for PANi-NMP. The metal-like response appears in samples doped at, and above 30%. In these cases σ has a positive temperature coefficient at low temperatures, but reaches a peak at a characteristic temperature T_p, above which conductivity falls in a manner akin to that of crystalline metals e.g. copper. In fact, regions of crystalline order have been identified within PANi-

CSA, by an independent x-ray diffraction analysis which is yet to be published. As the level of doping is increased beyond 30% conductivity increases and T_p shifts to lower temperatures, such that the metallic behaviour becomes more evident. The fall off in σ at low temperatures is also less pronounced. Thermopower data from PANi-CSA (at 30% 40% and 50% doping levels) has a linear dependence upon temperature which compliments the evidence for metallic charge transport provided by the conductivity data.

Estimates of the charge carrier mobility within samples were made from the value of σ at 300 K in each case. This revealed that the mobility increases sharply as a function of increased doping, until the transition to metal-like behaviour at 30% protonation is crossed e.g. at 10% doping $\mu = 4x10^{-3}$ $cm^2V^{-1}s^{-1}$, whilst for 60% doping $\mu = 0.3$ $cm^2V^{-1}s^{-1}$. This behaviour could be due to an increased overlap of conduction band electronic states as more chain sites are protonated, such that charge carrier localisation, occurring at low doping levels, is gradually eliminated. Alternatively, the change in μ could arise due to a growth in the number or size of metallic regions within the polymer as the level of protonation is increased.

6.1.2 PMBET Field Effect Transistors

The charge carrier mobility was investigated within thin films of 3[2(S2-methylbutoxy)ethyl]-polythiophene (PMBET) formed by spin coating the polymer from solution in tetrahydrofuran. This was achieved by incorporating the material as the active layer in a metal-insulator-semiconductor field effect transistor (MISFET) structure and measuring the device characteristics, during operation in enhancement mode. The influence of different states of molecular order within the polymer was investigated. By treating the spin casting solution with different quantities of methanol, a nonsolvent for PMBET, reorganisation of the polymer sidechain groups can be induced, which leads to an increased effective conjugation length in the chain backbone. This is indicated by a solvatochromatic shift upon addition of the nonsolvent. A spectroscopic study revealed

that the intramolecular order induced by the nonsolvent is preserved when thin films are cast from the solvent-polymer-nonsolvent mixtures.

However, the electrical conductivity and field effect mobility of thin films containing ordered polymer chains is far below that measured in films spun from simple solvent-polymer mixtures, where $\mu < 4x10^{-5}$ $cm^2V^{-1}s^{-1}$ and $\sigma < 1.7x10^{-5}$ Scm^{-1}. In the most extreme cases, the mobility was below measurable limits, in this case $< 1x10^{-8}$ $cm^2V^{-1}s^{-1}$. The conductivity was reduced to $<9x10^{-9}$ Scm^{-1}. The reduction in mobility and conductivity which accompanies the increase in intramolecular order within thin films PMBET is ascribed in part to an increased interchain separation resulting from an outward ordering of the side chain substituent species. This is thought to reduce the probability of interchain charge transfer. In addition, the presence of grain boundaries between aggregated regions of polymer, or small crystallites becomes more evident in films with more intramolecular order. This is expected to inhibit electrical transport within the bulk film.

6.2 Conclusions

It is clear that the nature of intermolecular order is a very important factor governing the bulk charge transport properties of the conductive polymer systems considered in this thesis. In the case of polyaniline, two very different conductors can be produced by the use of different methods, described in chapter one, of processing the unprotonated emeraldine base form. These are PANi-NMP and PANi-CSA.

Within PANi-NMP samples, there is no evidence for long range order on the molecular level. It is unsurprising therefore that the electrical conductivity has a temperature activated behaviour, indicating that charge carriers are not free to diffuse as they are in the structure of a crystalline conductor. Since there is little or no coherence between polymer chains in the amorphous structure of PANi-NMP a high probability of carrier scattering is expected at interchain charge transfer processes. The enhancement of the conductivity along one direction which can be induced by stretch elongation of this

material is ascribed to a reduction in the number of interchain scattering events due to the partial alignment of polymer chain backbones, along which charge transport is preferred.

The crystal structure revealed by an (independent) x-ray analysis of samples of PANi-CSA and the evidence, from conductivity data, that charge transport is limited by phonon scattering at high temperatures, e.g. above 130 K, for 60% doped films, suggest that this material is very close to the metal-insulator boundary. The conductivity of 'metallic' samples is in the region predicted for the minimum metallic conductivity of a disordered system described in chapter 2, and is almost ten times higher than that in samples of unoriented PANi-NMP. The conductivity of PANi-CSA is still limited, presumably by disordered regions, such that at lower temperatures (<100 K) conductivity is temperature activated. A combination of two charge transport mechanisms, fluctuation induced tunnelling and phonon scattering has been used to model the conductivity data obtained from PANi-CSA doped to levels at and above 30%, see chapter 3, section 3.3.2). It is also interesting to note that attempts to exceed the theoretical maximum protonation level, of 50% (see, section 1.6, chapter 1) by doping the polymer with CSA sufficient for 60% protonation resulted in improved conductivity and an enhanced 'metallic' response.

Most studies of conductive polymers are concerned with the value of electrical conductivity, because this property indicates the suitability of the material for real applications. Thermoelectric analysis, on the other hand, is useful only as a scientific tool. Since measurement of thermopower is (ideally) a zero current process, this technique can be used to identify the presence of 'hidden' metallic states, not revealed by analysis of the conductivity, for example in stretch oriented PANi-NMP (see chapter 4, section 4.3). However, in the case where data deviate from a linear dependence upon temperature, predicted for diffusion of carriers in a metal, the results are very difficult to interpret. It was hard therefore, to make anything other than a qualitative analysis from the thermoelectric measurements obtained from polyaniline samples, especially given the

limited range of temperature, 100 to 300 K, over which data could be acquired with the apparatus available.

The role of order and disorder is again revealed in the study of charge carrier mobility in PMBET. In this case it was revealed that although the intramolecular order within thin films of this polymer can be increased, a detrimental effect upon the interchain charge transfer resulted in decreased conductivity and mobility. This finding highlights one difficulty with conjugated polymers to which sidechain groups are added to increase the solubility of the material. Whilst the addition of these groups increases the ease of processability their presence also increases the average separation between polymer chain backbones. Since it is this part of the polymer which contains electronic states for mobile charge carriers, if the overlap between the π orbitals of adjacent chain backbones is reduced, the bulk electrical properties of the material will suffer.

The ideal conductive polymer is therefore a material which is easily processed, but has no bulky sidechain groups. In addition, it must contain a high degree of long range interchain order, i.e. crystallinity, to allow coherent charge transport with a high mobility.

6.3 Suggestions For Future Study

There are a number of questions raised by the work presented in this thesis, particularly concerning the nature of electrical transport within PANi-CSA. The balance of metallic and non-metallic charge flow mechanisms exhibited by this material deserves a more detailed investigation. Ideally, this would involve detailed x-ray diffraction analysis to determine the structural conformation and coherence length within the crystalline regions of the polymer. Microwave techniques of electrical conductivity measurement might succeed in revealing the intrinsic properties of these regions. A fine tuning of the polymer film production method is required to see if greater crystalline order can be achieved. In particular, the effects upon the chemical structure of including CSA at levels intended to exceed 50% protonation must be quantified, in order to

determine whether the polysemiquinone radical cation structure (described in chapter 1, section 1.7) is the ultimate conductive form of polyaniline. These factors and others must be addressed before polyaniline and other organic conductors are suitable for widespread use as reliable and easily processed electronic materials.

List Of Publications

1. "Thermoelectric power measurements in highly conductive stretch oriented polyaniline films."
E.R. Holland & A.P. Monkman., *Synthetic Metals*, **74** (1995) pp. 75-79.

2. "Effects of order and disorder on field effect mobility measured on conjugated polymer thin film transistors."
E.R. Holland, D. Bloor, A.P. Monkman, A. Brown, D. de Leeuw, M.M. Bouman & E.W. Meijer, *Journal of Applied Physics*, **75** (1994) pp. 7954-7958.

3. "Polyaniline, air stable metal, fact no longer fiction"
A.P. Monkman, P.N. Adams, P.J. Laughlin & E.R. Holland, *Synthetic Metals*, **69** (1993) p. 183

4. "A visible large area light emitting diode fabricated from porous silicon using a conducting polyaniline contact"
D.P. Halliday, J. Eggleston, P.N. Adams, E.R. Holland, & A.P. Monkman. *IEEE colloquium on materials for displays* 1995.

5. "Electroluminescence from porous silicon using a conducting polyaniline contact"
D.P. Halliday, E.Holland, J.M. Eggleston, P.N Adams, S.E., Cox & A.P.Monkman, EMRS Spring conference, 1995 *Thin Solid Films* (submitted)

6. "Aspects of the Camphor Sulphonic Acid Processing Route of Polyaniline"
L. Abell, S. Pomfret, E.R. Holland, P.N. Adams & A.P. Monkman, *Society of Plastic Engineers*, conference proceedings (1996) submitted for publication